

L-411

NATIONAL ADVISORY COMMITTEE FOR AERONAUTICS
JPL LIBRARY
CALIFORNIA INSTITUTE OF TECHNOLOGY

WARTIME REPORT

ORIGINALLY ISSUED
July 1942 as
Advance Restricted Report

WIND-TUNNEL STUDY OF THE EFFECTS OF PROPELLER OPERATION
AND FLAP DEFLECTION ON THE PITCHING MOMENTS AND
ELEVATOR HINGE MOMENTS OF A SINGLE-ENGINE
PURSUIT-TYPE AIRPLANE

By H. R. Pass

Langley Memorial Aeronautical Laboratory
Langley Field, Va.



WASHINGTON

NACA WARTIME REPORTS are reprints of papers originally issued to provide rapid distribution of advance research results to an authorized group requiring them for the war effort. They were previously held under a security status but are now unclassified. Some of these reports were not technically edited. All have been reproduced without change in order to expedite general distribution.



NATIONAL ADVISORY COMMITTEE FOR AERONAUTICS

ADVANCE RESTRICTED REPORT

WIND-TUNNEL STUDY OF THE EFFECTS OF PROPELLER OPERATION
AND FLAP DEFLECTION ON THE PITCHING MOMENTS AND
ELEVATOR HINGE MOMENTS OF A SINGLE-ENGINE
PURSUIT-TYPE AIRPLANE

By H. R. Pass

SUMMARY

A mock-up of a pursuit airplane has been tested in the NACA full-scale wind tunnel and the effects of propeller operation and flap deflection on the aerodynamic characteristics of the wing-fuselage combination and of the horizontal tail have been determined. The results of these tests have been compared with the results of previous tests and with available theories and, in general, satisfactory comparisons have been obtained. These results have also been used to develop empirical procedures for determining the effect of propeller operation on the lift and on the pitching moments of a flapped wing and to evaluate empirical factors for calculating the downwash angles at the tail with the propeller operating. The general applicability of these empiricisms has not been determined. The elevator hinge-moment characteristics have also been determined from tests on the mock-up and indicate the inadequacy of available data on the hinge-moment parameters. The procedure for calculating stick forces from wind-tunnel data has been outlined.

INTRODUCTION

Extensive longitudinal-stability and control tests have been conducted in the NACA full-scale wind tunnel on a mock-up of a pursuit airplane. The results have been analyzed to evaluate the various factors that effect the pitching moments of the airplane and the stick forces. A comparison of these results with the results of previous

work indicates the limitations of available information for preliminary design purposes.

The study is considered in four parts. In part I, the effect of the fuselage on the wing characteristics is considered. Part II is a study of the effect of the tail on the pitching moment and includes an estimate of the isolated tail characteristics and of the effective downwash and velocity acting on the tail. Surveys of air flow in the region of the tail are also included. The results of parts I and II are combined in part III in which the pitching-moment curves for the complete airplane are developed. Part IV deals with the elevator free-floating and stick-force characteristics of the airplane and indicates the interdependence of the various factors previously considered. The effects of flap deflection and propeller operation are considered in all sections.

SYMBOLS

W	gross weight
C_L	lift coefficient
C_D	drag coefficient
C_N	normal-force coefficient
M	pitching moment
C_m	pitching-moment coefficient
Ch_e	elevator hinge-moment coefficient $\left(\frac{\text{hinge moment}}{qS_e \bar{c}_e} \right)$
C_P	power coefficient $\left(\frac{P}{\rho n^3 D^5} \right)$
c_m	section pitching-moment coefficient
c_l	section lift coefficient
P	power input to propeller
T	axial propeller thrust

F	stick force
D	propeller diameter
V	airspeed
β	propeller blade angle
n	propeller rotational speed, revolutions per second; also, distance from center of gravity forward to aerodynamic center of wing-fuselage combination (measured parallel to thrust line)
η	propulsive efficiency
ρ	air density
T_c	thrust coefficient $\left(\frac{T}{\rho V^2 D^2}\right)$
C_T	absolute thrust coefficient $\left(\frac{T}{\rho n^2 D^4}\right)$
q	local dynamic pressure $\left(\frac{1}{2}\rho V^2\right)$
q_0	free-stream dynamic pressure
$(q/q_0)_{\text{eff}}$	effective dynamic-pressure factor, ratio of measured $dC_m/d\delta_e$ to value corresponding to free-stream dynamic pressure at tail
$(q/q_0)_{\text{av}}$	ratio of average dynamic pressure at tail, as found from air-flow surveys, to free-stream dynamic pressure; the average is weighted according to chord
$(q/q_0)_{\text{aa}}$	ratio of arithmetical-average dynamic pressure at tail, as found from air-flow surveys, to free-stream dynamic pressure
ϵ	local downwash angle
ϵ_{eff}	effective downwash angle at tail, as found by comparison of pitching moments with various tail settings and without tail

ϵ_{av}	average downwash angle at tail, as found from air-flow surveys; the average is weighted according to both chord and local dynamic pressure
ϵ_{aa}	the arithmetical average of downwash angle across tail, as found from air-flow surveys
s	velocity-increment factor back of propeller disk
a_0	lift-curve slope for infinite aspect ratio
S	area
b	span
c	chord
\bar{c}	mean geometric chord
l_1	distance from propeller disk to center of gravity of airplane (measured parallel to thrust line)
l_2	distance from center of gravity to elevator hinge line (measured parallel to thrust line)
l_3	distance from trailing edge of root chord to elevator hinge line (measured parallel to thrust line)
α_T	angle of attack of thrust axis
α_t	angle of attack of tail
i_t	angle of tail setting relative to thrust axis
δ	control-surface deflection
τ	relative elevator effectiveness factor
λ	empirical factor in formula for determining increase in lift due to slipstream velocity
λ_t	theoretical factor used in determining increase in tail lift due to slipstream

L-411

l_s stick length
 u, v hinge-moment parameters
 $\Delta\epsilon_1, \Delta\epsilon_2$ empirical corrections used to obtain effective downwash angles at tail from calculated values
 Δ denotes change, usually due to propeller operation

Subscripts:

o propeller-removed condition
 p propeller-operating condition
 P propeller
 w wing
 f flap
 $f + w$ wing-fuselage combination
 fw flapped wing
 t horizontal tail
 A airplane
 e elevator, back of hinge
 i portion immersed in slipstream
 is isolated
 s slipstream
 b balance
 tr trim
 ff free floating
 $a.c.$ aerodynamic center
 cal calculated

TESTS

The tests were made in the NACA full-scale wind tunnel (reference 1). The usual wind-tunnel corrections to the angle of attack and the drag, obtained from reference 2, and the additional correction due to the "blocking effect" (reference 3) have been applied to the experimental data. The pitching moments have not been corrected for the wind-tunnel interference on the downwash at the tail (reference 4); the interference was, however, considered in the discussion of the results.

The mock-up represented a single-engine, tractor-type, low-midwing airplane design (fig. 1). All parts of the cooling system and the carburetor scoop were removed for the tests. The elevator was controllable from the cockpit during the runs. The wing flap was of the slotted type and was deflected 40° for all flap-deflected conditions. A 25-horsepower electric motor installed in the mock-up operated a Curtiss electric controllable-pitch propeller whose blade-angle setting could be controlled and determined during the runs.

The force tests consisted of measurements of lift, drag, and pitching moment on the mock-up without the tail surfaces and with the tail surfaces with various settings of the stabilizer and the elevator. For the elevator-effectiveness and hinge-moment tests an operator in the cockpit manipulated the elevator control stick and, using a conventional NACA control-force indicator, measured the stick forces. All tests included the effects of flap deflection and propeller operation. The propeller characteristics (fig. 2) were determined from propulsive-efficiency tests of the complete mock-up. The accuracy of the stabilizer and elevator settings was estimated to be within $\pm 0.25^\circ$. In the analysis of the data, extensive cross fairing was performed.

With the horizontal and vertical tails removed, air-flow surveys were made in the region of the tail. The surveys were made by means of a survey rack consisting of 15 pitch-yaw tubes.

At each angle of attack the propeller was operated over a range of blade angles and advance-diameter ratios to obtain a range of thrust coefficients. A large range

1171
of possible operating conditions was thereby covered; the greater part of the measurements, however, were made for conditions that approximated full-power operation of the mock-up as a typical pursuit airplane with 1000 brake horsepower (fig. 3). Propeller charts for a nearly similar propeller were used for the preliminary calculations. In order to obtain desired values of V/nD , the tunnel speed was varied between 30 and 60 miles per hour.

As previously noted in reference 5, it was found that the lift and the pitching moments were relatively unaffected by reasonable variations of the propeller blade angle β if the same thrust coefficient T_c was maintained. The results of reference 5 indicate that, for the cases with flaps retracted, the use of the lift coefficient for the propeller-removed condition in determining the propeller-operating conditions is barely satisfactory as a first approximation. For the cases with flaps deflected, however, this procedure is entirely unsatisfactory and the effect of propeller operation on the lift must be estimated. The propeller-operating conditions must then be recalculated, the new lift coefficient being used.

I. WING-FUSELAGE COMBINATION

The addition of a fuselage to an isolated wing generally shifts the aerodynamic center forward (reference 6); the lift and the pitching moments for a conventional combination, however, are practically the same as those of the isolated wing (the pitching moments being taken about the corresponding aerodynamic centers). The wing and the fuselage can therefore be conveniently treated as a unit.

Lift-Curve Slope

Lift, drag, and pitching-moment curves for the tailless mock-up with flaps both retracted and deflected are presented in figure 4. For the retracted flap the experimental slope of the lift curve is 0.071 per degree. The slope for the isolated wing as calculated by the methods of reference 7, estimated section characteristics being used, is 0.073 per degree. The results of previous tests of similar wing-fuselage combinations (reference 6)

also show practically negligible effect of the fuselage on the slope of the wing lift curve.

The experimental slope of the lift curve for the case with flaps deflected is 0.072 per degree. Reference 8 also indicates only a slight change, in general, in the slope of the lift curve due to flap deflection.

Aerodynamic-Center Location

The experimental aerodynamic-center locations have been determined for the wing-fuselage combination from figure 4 following the methods of reference 9.

Retracted flaps.- With the flaps retracted the aerodynamic center is 0.32 foot in front of and 0.89 foot below the center of gravity. The calculated location for the wing alone, by reference 7, is 0.10 foot in front of the center of gravity. The forward shift of the aerodynamic center caused by the fuselage is, therefore, $\Delta n = 0.040\bar{c}_w$, which is in approximate agreement with the experimental results of reference 6. This value is also in excellent agreement with the theoretical value of $0.043\bar{c}_w$ for Δn calculated from the formulas given in reference 10.

The vertical location of the aerodynamic center is primarily a function of the drag characteristics of the mock-up.

Deflected flaps.- The position of the aerodynamic center for the wing-fuselage combination with flaps deflected is 0.60 foot in front of and 1.55 feet below the center of gravity. This position is considerably forward of the location with retracted flaps. The theory of reference 10 indicates that part of this additional forward shift is probably due to an increase in the effect of the fuselage when the flaps are deflected. The further downward movement of the aerodynamic center is due to the increased wing drag.

Effect of Propeller Operation

Propeller operation has two separate effects on the lift and the pitching moments of the wing-fuselage combination. The first, designated the direct effect, arises

from the forces on the propeller itself and may be estimated from the results of tests of isolated propellers in yaw. The second, designated the slipstream effect, results from the increased velocity and the change in the direction of the air flow at that part of the wing immersed in the slipstream.

Retracted flaps.- The experimental effect of propeller operation at various angles of attack and thrust conditions on the lift and on the pitching moments of the wing-fuselage combination with flaps retracted are presented in figures 5 and 6, respectively. For comparison, the effects calculated by the methods of reference 5 are also shown in the figures. The agreement between the experimental and the calculated lift values is considered satisfactory. The agreement for the values of pitching moment, however, although satisfactory, is not quite so good as for the lift values; the effects of the slipstream on the wing and the fuselage pitching moments, which have been neglected in reference 5, may possibly account for part of the discrepancy.

Deflected flaps.- The experimental effects of propeller operation on the lift and the pitching moments of the wing-fuselage combination with deflected flaps are presented in figures 7 and 8, respectively. The lift increments due to propeller operation are much larger than those obtained for the corresponding condition with flaps retracted and the pronounced diving moments indicate the considerable effect of the slipstream on the wing pitching moments for the flap deflected. An attempt was made to apply the methods of reference 5, heretofore used only for unflapped wings, to the present case, in order to indicate, if possible, the applicability of these methods to flapped wings. It was found that, except for the necessity of changing one parameter, the effect on the lift calculated by these methods was in reasonably satisfactory agreement with the experimental results. These methods are summarized as follows:

The calculated lift values (fig. 7) were obtained from

$$C_{Lp} = C_{L_0} + \Delta C_{Lp} + \Delta C_{Lw} \quad (1)$$

where ΔC_{Lp} was determined from the formulas and charts of reference 5 and

$$\Delta C_{L_w} = \frac{b_{wi} \bar{c}_{wi}}{S_w} s (\lambda c_{l_0} - 0.6 a_0 \Delta \epsilon) \quad (2)$$

This formula is similar to the corresponding formula (reference 5) for the plain wing; it was found, however, that λ should be 1.6 instead of 1.0. According to reference 11, this value indicates the marked effect of the slipstream on the flapped-wing-vortex system. The term c_{l_0} is the estimated local lift coefficient, without slipstream, at the center of the flapped wing rather than the average lift coefficient of the wing.

The calculated pitching-moment coefficients, presented in figure 8, have been obtained by consideration of the direct effect of the propeller forces and of the slipstream effect on the wing pitching moment. The slipstream effect is much larger than the direct effect of the propeller forces, as indicated in figure 9, in which the direct effect has been calculated from the formula of reference 5.

The slipstream effect on the wing pitching moment has been taken as the sum of two components. The first component is due to the wing-lift increment, which is assumed to act at the fuselage-wing aerodynamic center. The second, and largest, component is the increase in the actual pitching moment of the wing center sections about their aerodynamic centers. The second component is a function of the increase in velocity of the slipstream and of the immersed wing area. If it is assumed that the section pitching-moment coefficients are not affected by the slipstream, this increment may be expressed as follows:

$$\Delta M_{a.c.} = c_{m_{a.c.}} (q - q_0) S_{wi} \bar{c}_{wi} \quad (3)$$

The factor $c_{m_{a.c.}}$ is the pitching-moment coefficient of the flapped sections and is assumed constant across the flapped portion S_{fw} of the wing area. It is closely approximated, from the data for the propeller removed, as

$$c_{m_{a.c.}} = C_{m_{a.c.}} \frac{S_w}{S_{fw}}$$

Dividing equation (3) by $S_w q_0 \bar{c}_w$ gives

$$\Delta C_{m_{a.c.}} = c_{m_{a.c.}} \frac{\bar{c}_{wi}}{c_w} \frac{S_{wi}}{S_w} (q/q_0 - 1) = c_{m_{a.c.}} \frac{\bar{c}_{wi}}{c_w} \frac{S_{wi}}{S_w} \frac{8}{\pi} T_c \quad (4)$$

The final expression for the effect of the slipstream on the wing pitching moment is

$$\Delta C_{m_w} = c_{m_{a.c.}} \frac{\bar{c}_{wi}}{c_w} \frac{S_{wi}}{S_w} \frac{8}{\pi} T_c + \frac{n}{c_w} \Delta C_{L_w} \quad (5)$$

If the effect of the slipstream on the fuselage pitching moment is neglected, the total calculated effect of propeller operation is given by

$$\Delta C_{m_p} = \Delta C_{m_p} + \Delta C_{m_w} \quad (6)$$

The value of ΔC_{m_p} is, as for the condition with flap retracted, determined by the charts of reference 5.

II. TAIL CONTRIBUTION

The study of the tail contribution to the pitching moment of the airplane involves consideration of the isolated-tail parameters and of the effective dynamic pressures and effective downwash angles at the tail. The characteristics of the isolated tail, although an important link in the analysis, were not available, because no tests were made of the tail alone. For purposes of this development, these characteristics were estimated by analysis of the data for the propeller removed; methods that have received some verification in previous studies (reference 12) were followed. The effective dynamic pressure at the tail is defined by the elevator effectiveness $dC_m/d\delta_e$ and is equal to the average local dynamic pressure at the tail for the low-angle propeller-removed conditions but, for the propeller-operating conditions, it is less than the average local dynamic pressure mainly because of the finite extent of the slipstream. The effective downwash angle is

defined by the tail incidence for which the contribution of the tail to the pitching moment is zero.

The data on the elevator effectiveness was found to be in good agreement with the theory of reference 5; the data on the downwash angles appeared, in general, to be less satisfactory and exhibited some apparent inconsistencies.

As a check on the over-all applicability of the various assumptions, empirical factors, and formulas, the total tail contribution to the pitching moment has been calculated with their aid and compared with the experimental values.

Air-Flow Surveys

Some surveys of air flow in the region of the horizontal tail are presented in figures 10 to 25. With the propeller removed, the wing wake is considerably below the horizontal tail but approaches it with increasing angle of attack. The fuselage boundary layer is clearly evident in all cases. With the propeller operating, the limits of the slipstream and the effects of propeller rotation are readily determined. As is apparently characteristic for single-engine airplanes (references 5 and 12), the slipstream is not circular. The marked increase in dynamic pressure, especially evident at the high angles of attack and the large thrust coefficients, on the side of the downward-moving propeller blade has been attributed to a shifting of the centroid of the thrust, as discussed in reference 13. The very strong local downwash fields for the case with flaps deflected should be noted. It should also be observed that the downwash angles do not appreciably vary with distance from the elevator hinge line.

All the surveys were evaluated to determine the average dynamic pressure and the downwash of the air flow at the horizontal tail. The results are presented in table I for the case with flaps retracted and in table II for the case with flaps deflected. Two different types of average are shown in the tables. The values with the subscript aa are straight arithmetic averages, defined as

$$(q/q_0)_{aa} = \frac{1}{b_t} \int_{-b_t/2}^{b_t/2} (q/q_0) dx \quad (7)$$

$$e_{aa} = \frac{1}{b_t} \int_{-b_t/2}^{b_t/2} e \, dx \quad (8)$$

L-411
The values with the subscript av are weighted averages, the local dynamic pressure being weighted according to the local chord and the local downwash angle being weighted according to both local dynamic pressure and local chord:

$$(q/q_0)_{av} = \frac{1}{S_t} \int_{-b_t/2}^{b_t/2} (q/q_0) \, c \, dx \quad (9)$$

$$e_{av} = \frac{1}{S_t (q/q_0)_{av}} \int_{-b_t/2}^{b_t/2} e (q/q_0) \, c \, dx \quad (10)$$

Tables I and II indicate that, in most instances, either method may be used to evaluate surveys. Weighted surveys have been used exclusively herein.

Isolated-Tail Parameters

The isolated-tail parameters are the slope of the normal-force curve $dC_{N_t}/d\alpha_t$ and the relative elevator-effectiveness factor τ . From tests with the propeller removed and with the horizontal tail at various settings (fig. 26) and from the formula

$$\frac{dC_{N_t}}{d\alpha_t} = \frac{(dC_m/di_t) S_w \bar{c}_w}{(q/q_0)_0 S_t l_2} \quad (11)$$

the average experimental value for $dC_{N_t}/d\alpha_t$ was found to be 0.051. (Values of $(q/q_0)_0$ were taken from surveys.) This value is in excellent agreement with the value of 0.052 taken from figure 21 of reference 14. The average value of τ , determined in this report by the ratio

$dC_m/d\delta_e/dC_m/di_t$, is 0.59 and is in excellent agreement with the value of 0.53 obtained from figure 26 of reference 14.

It should be mentioned that previous comparisons of experimental data with figures 21 and 26 of reference 14 have not always given such excellent agreements as indicated in the foregoing paragraph.

Elevator Effectiveness and Effective Dynamic Pressure

The experimental variation of the elevator effectiveness with thrust coefficient with the flaps retracted and with the flaps deflected, is shown in figures 27 and 28, respectively. With the propeller removed, the elevator effectiveness is approximately proportional to the average dynamic pressure at the tail; accordingly, for these conditions, the effective dynamic pressure approximately equals the average dynamic pressure; that is,

$$(dC_m/d\delta_e)_o = (dC_{N_t}/d\alpha_t) \tau (q/q_o)_o \frac{S_t}{S_w} \frac{l_a}{c_w} \quad (12)$$

The proportionality no longer exists at the higher thrust coefficients; for such conditions the effective dynamic pressure is less than the average found from the surveys (tables I and II).

The difference is due mainly to the finite extent of the slipstream, which is taken into account in the following equation (simplified from reference 5):

$$\left(\frac{dC_m}{d\delta_e}\right)_p = \left[(q/q_o)_o + \frac{b_{t_i} \bar{c}_{t_i}}{S_t} \lambda_t s_s \right] \left(\frac{dC_m}{d\delta_e}\right)_{is} \quad (13)$$

where

$$\left(\frac{dC_m}{d\delta_e}\right)_{is} = \frac{(dC_m/d\delta_e)_o}{(q/q_o)_o} \quad (14)$$

and b_{t_i} is the span of the tail immersed in the slipstream, λ_t is a function of this immersion and may be

1-11

obtained from reference 5, and

$$s_s = -1 + \sqrt{1 + 8/\pi T_c}$$

The effective dynamic pressure is thus given by the factor

$$(q/q_0)_{\text{eff}} = (q/q_0)_0 + \frac{b_{t_i} \bar{c}_{t_i}}{S_t} \lambda_t s_s \quad (14a)$$

For comparison with the experimental results, the elevator effectiveness was calculated by formula (13) for a range of conditions. Experimental values of $(dC_m/d\delta_e)_0$ and $(q/q_0)_0$ were used. For the condition with the flaps retracted, the surveys and also the computations made by the methods of reference 5 indicate practically complete immersion of the tail in the slipstream; accordingly, a value of 2 for λ_t , as indicated by the analysis of reference 15, was used for these cases. For the condition with the flaps deflected, the tail immersion was calculated to vary between 8.5 and 9.0 feet (also approximately verified by the surveys), giving an average value of 1.64 for λ_t (fig. 41 of reference 5). The values of elevator effectiveness calculated with these two values of λ_t are shown, together with the experimental results, in figures 27 and 28. Satisfactory agreement is observed in both cases.

Downwash

As previously mentioned, the average downwash at the tail ϵ_{av} has been evaluated from the air-flow surveys. For these same conditions, the effective downwash ϵ_{eff} has been determined from figures 29 and 30. The disagreement between these two experimental downwash angles (shown in figs. 31 and 32 and in tables I and II), especially in the lower angles, has been previously observed, notably in reference 12. The reasons are uncertain. The discrepancy, $\Delta\epsilon_1 = \epsilon_{\text{eff}} - \epsilon_{av}$, is apparently mainly a function of ϵ_{av} and is independent of flap deflection and propeller operation, as shown in figure 33. The curve of this figure was used to supply a downwash-angle correc-

tion in the calculations to be given later; its general applicability, however, is obviously very questionable.

Propeller removed.- The average downwash angle of the air stream at the tail for all propeller-removed conditions has been calculated following the methods of references 16 and 17. The agreement between the calculated and the experimental average downwash angles, indicated in figures 31 and 32, is considered satisfactory, especially for retracted flaps. The calculated values include the effects of wing twist (references 16 and 18) and the wind-tunnel corrections.

Propeller operating.- The average downwash at the tail with the propeller operating has been calculated by the procedure given in reference 5. Briefly,

$$\epsilon_p = \epsilon_{wp} + \epsilon_p = \epsilon_{cal} \quad (15)$$

where ϵ_p is obtained from charts in reference 5 and

$$\epsilon_{wp} = \epsilon_{w_0} \frac{C_{L_0} + \Delta C_{L_w}}{C_{L_0}}$$

This rather elementary procedure gives fairly satisfactory checks with the average experimental values (tables I and II). A comparison of these results with the results of some recent British tests indicates that the methods used give values of ϵ_p that, for the flap-deflected conditions, are too large. Inasmuch as even small increments of downwash may considerably affect the pitching moment contributed by the tail, the discrepancy, $\Delta\epsilon_2 = \epsilon_{av} - \epsilon_{cal}$, was computed and plotted as a function of ϵ_{cal} in figure 34. Different curves were found for the cases with flaps deflected and with flaps retracted; propeller operation, however, had no definite effect. Without further experimental study, the general applicability of the specific values given in figure 34 is very questionable.

III. COMPARISON OF CALCULATED WITH EXPERIMENTAL PITCHING MOMENTS

L-111

Parts I and II have summarized the available methods for calculating the pitching moments of single-engine airplanes and have derived the necessary parameters. The purpose of part III is to compare the pitching moments calculated by these methods with experimental pitching moments, in order to show the general applicability over the entire range of operating conditions of parameters derived as average values from particular sets of tests. The comparison is first given for the contribution of the fixed tail (tail-setting angle, 1.2° ; elevator angle, 0°) to the pitching moment; the comparison is then extended to the complete mock-up.

Tail Contribution

The experimental tail contribution has been obtained as the difference between pitching moments of the mock-up with the tail attached and with the tail removed. The calculated tail contribution is obtained by the following formula:

$$C_{m_{t_p}} = -\left(\frac{dC_{N_t}}{d\alpha_t}\right) \frac{S_t}{S_w} \frac{l_2}{c_w} \left[(q/q_0)_0 + \frac{b_{t_i} \bar{c}_{t_i}}{S_t} \lambda_t s_s \right] (\alpha_T + i_t - \epsilon_{eff}) \quad (16)$$

In equation (16)

$$\epsilon_{eff} = \epsilon_{cal} + \Delta\epsilon_1 + \Delta\epsilon_2 \quad (17)$$

in which

ϵ_{cal} obtained from theory of reference 5

$\Delta\epsilon_1$ and $\Delta\epsilon_2$ given by figures 33 and 34

$dC_{N_t}/d\alpha_t = 0.051$

$(q/q_0)_0$ values obtained from surveys

λ_t 1.64 for flaps extended and 2.0 for flaps retracted

$s_s = \sqrt{1 + \frac{8}{\pi} T_c} - 1$ (zero for propeller removed)

The experimental and calculated tail contributions for the condition with propeller removed are in satisfactory agreement (figs. 35 and 36). For comparative purposes, the tail contribution has also been calculated with experimental values of ϵ_{eff} and with $\epsilon_{eff} = \epsilon_{cal}$ (figs. 35 and 36).

For the propeller-operating condition, the agreement between the experimental and the calculated values is not entirely satisfactory (figs. 37 and 38). Calculations of the tail contribution using experimental values of ϵ_{eff} (as obtained from cross plots of tables I and II) are given in figures 39 and 40. These calculations indicate that a large part of the discrepancy in figures 37 and 38 occurs because the methods used in the estimation of the downwash angles are inadequate. The discrepancies at low thrust coefficients for the higher angles of attack may be, at least partly, attributed to the fact that few experimental data in this range were taken and to the fact that at zero thrust, with the propeller operating, the conditions are not quite equivalent to the conditions with the propeller removed. Calculated values of the tail contribution with $\epsilon_{eff} = \epsilon_{cal}$ are also included for comparative purposes in figures 39 and 40.

Pitching-Moment Curves for Complete Mock-Up

The experimental and the calculated pitching-moment curves for the complete mock-up are presented in figure 41 for the case with retracted flaps and in figure 42 for the case with deflected flaps. The calculated curves were obtained by the following formulas:

For retracted flaps,

$$C_{m_A} = C_{m(f+w)_0} + C_{m_{tp}} + \Delta C_{m_P} \quad (18)$$

For deflected flaps,

$$C_{m_A} = C_{m(f+w)_0} + C_{m_{tp}} + \Delta C_{m_P} + \Delta C_{m_w} \quad (19)$$

Experimental values of $C_{m(f+w)_0}$ were taken from figure 4; the other terms have been previously evaluated. As

expected, the agreement is not entirely satisfactory; the disagreement is merely due to the accumulation of errors incurred in estimating the various components.

The effect of the landing gear on the pitching moment is presented in figure 43. As the landing gear is located outside the slipstream, the increment of pitching moment due to the landing gear is probably unaffected by propeller operation.

IV. ELEVATOR HINGE-MOMENT CHARACTERISTICS

The stick-force data have been analyzed with regard to the hinge-moment parameters of the tail surface, the elevator free-floating angles, and the stick forces required to trim the airplane.

Hinge-Moment Parameters

Some typical curves of the variation of hinge-moment coefficient with angle of elevator deflection are shown in figure 44. These coefficients are based on free-stream dynamic pressure. The increase in slope at a value of δ_e of approximately $\pm 8^\circ$ occurs for all conditions and is probably due to the projection of the leading edge of the elevator. The following analysis applies only to elevator angles within the linear range that, although limited, includes most flight conditions. Extending the methods to the larger elevator angles that are used in certain maneuvers may serve to show no more than the order of magnitude of the hinge moment.

The basic equation for hinge moment, taken from reference 19, is

$$C_{h_e} = u C_{N_t} + v \delta_e \quad (20)$$

where the coefficients C_{h_e} and C_{N_t} are based on the local dynamic pressure acting at the tail. The hinge-moment parameters u and v should be functions mainly of the area ratios S_e/S_t and S_b/S_e .

The values of u and v were determined experimentally by using the following relations, based on equation (20):

$$\left. \begin{aligned} u &= \left(\frac{\partial C_{h_e}}{\partial C_{N_t}} \right)_{\delta_e} \\ v &= \left(\frac{\partial C_{h_e}}{\partial \delta_e} \right)_{C_{N_t}} \end{aligned} \right\} \quad (21)$$

The parameter u was obtained as the mean slope of the curve obtained by plotting C_{h_e} against C_{N_t} for an elevator angle of 0° ; v was similarly obtained from an interpolated curve of C_{h_e} (based on local dynamic pressure) against δ_e for $C_{N_t} = 0$. Specifically, the factors were obtained as follows:

$$\left(C_{h_e} \right)_{\delta_e=0} \quad \text{from curves similar to those shown in figure 44}$$

$$\left(C_{N_t} \right)_{\delta_e=0} \quad \text{from the experimental values given in figures 37 and 38 by equation } C_{N_t} = -C_{m_t} \frac{\bar{c}_w}{l_2} \frac{S_w}{St}$$

$$\left(\delta_e \right)_{C_{N_t}=0} \quad \text{from figures 37 and 38 and figures 27 and 28 by the equation } \delta_e = \frac{C_{m_t}}{dC_m/d\delta_e}$$

$$\left(C_{h_e} \right)_{C_{N_t}=0} \quad \text{from curves similar to those shown in figure 44 for values corresponding to } \left(\delta_e \right)_{C_{N_t}=0}$$

$$\left(q/q_0 \right)_{av} \quad \text{by cross-fairing the values given in tables I and II}$$

The average experimental value of u is -0.022 and of v is -0.0043 . The generalized charts of reference 20, which were based on tests of a large number of isolated tail surfaces, indicate a value of $u = -0.067$ and $v = -0.0084$ for the horizontal tail surface.

The disagreement between the values of u and v determined from these tests and from the generalized charts of reference 20 is considerable. References 21 and 22 indicate, however, that details of elevator plan form and trailing-edge profile may considerably affect u and v ; other factors, such as scale effect and the cut-out, probably affect the pressure distribution over the elevator. For these reasons it is not unlikely that charts based on a large number of tests with various uncontrolled factors would be unsatisfactory for any particular tail.

The Rate of Change of Hinge Moment with Elevator Deflections

The rate of change of hinge moment with elevator deflection at constant angle of attack $dC_{he}/d\delta_e$ has been determined by measuring the slope at $\delta_e = 0^\circ$ of curves similar to those shown in figure 44. The experimental variation of this factor with angle of attack and with thrust coefficient is given in figure 45(a) for the case with retracted flaps and in figure 45(b) for the case with deflected flaps. It should be mentioned that the hinge-moment coefficient C_{he} is based on free-stream dynamic pressure.

The formula for calculating $dC_{he}/d\delta_e$ may be obtained by differentiating equation (20). If the difference between the effective and the average dynamic pressures at the tail is neglected, the final expression is

$$dC_{he}/d\delta_e = \left[u_T \left(\frac{dC_{ht}}{d\alpha_t} \right) + v \right] \left(\frac{q}{q_0} \right)_{av} \quad (22)$$

where, if desired, $(q/q_0)_{av}$ for the propeller-operating conditions may be calculated from

$$\left(\frac{q}{q_0} \right)_{av} = \left(\frac{q}{q_0} \right)_o + 2s_s \frac{b_{ti} \bar{c}_{ti}}{St} \quad (23)$$

For comparison, $dC_{he}/d\delta_e$ values were calculated, experimental values being used for all factors, and are also presented in figure 45.

1-411

The experimental and the calculated values are in excellent agreement for the case with flaps retracted. The agreement, however, is not entirely satisfactory for the case with flaps deflected; the discrepancy probably arises from the very marked variation in dynamic pressure across the elevator span.

Elevator Free-Floating Angle

The elevator free-floating angle is important with regard to stick-free stability characteristics of an airplane. The formula for calculating it is derived by simultaneously solving equation (20), with $C_{he} = 0$, and the normal-force equation. If the difference between the effective and the average dynamic pressure at the tail is neglected, the solution is

$$\delta_{eff} = - \frac{u \left(\frac{dC_{Nt}}{d\alpha_t} \right) (\alpha_T + i_t - \epsilon_{eff})}{u \left(\frac{dC_{Nt}}{d\alpha_t} \right) \tau + v} \quad (24)$$

By the substitution into this equation of values previously derived, the elevator free-floating angles were computed for a number of conditions. The results are plotted in figure 46, together with experimental values for the same conditions. There appears to be an almost constant difference of about 2° in δ_{eff} between the two sets of curves. The discrepancy is possibly due to dissymmetry of the tail surface. Measurements showed that the elevator hinge line was slightly above the chord line; it is uncertain, however, whether this error in construction can account for the entire observed discrepancy.

Stick Forces

The stick forces required to trim the airplane at any given condition can be determined from these tests after the corresponding elevator hinge-moment coefficients have been evaluated. The usual method of determining these coefficients is to use the basic equation for hinge moment

$$C_{h_{etr}} = (u C_{N_t} + v \delta_{etr}) \left(\frac{q}{q_0} \right)_{av} \quad (25)$$

where

$$\delta_{etr} = \frac{(C_{m_A})_{\delta_e=0}}{\frac{dC_m}{d\delta_e}}$$

and

$$C_{N_t} = \left(\frac{dC_{N_t}}{d\alpha_t} \right) (\alpha_T + i_t - \epsilon_{eff} + \tau \delta_{etr})$$

Inasmuch as the elevator free-floating angles and the rates of change of hinge-moment coefficient with elevator deflection have been experimentally determined (figs. 45 and 46), the hinge-moment coefficient at trim has been obtained more simply from

$$C_{h_{etr}} = (\delta_{etr} - \delta_{eff}) \frac{dC_{h_e}}{d\delta_e} \quad (26)$$

Values of $C_{h_{etr}}$ are presented in figures 47 and 48 for the conditions with flaps retracted and with flaps deflected, respectively. Experimental values of C_{m_A} and $(dC_m/d\delta_e)$ have been taken from figures 29 and 30 (for $i_t = 1.2^\circ$) and figures 27 and 28.

Neglecting the effects of friction in the control system allows the stick forces for trim to be calculated from

$$F_{tr} = \frac{C_{h_{etr}} q_0 S_e \bar{c}_e}{l_s} \quad (27)$$

where

$$q_0 = \frac{W}{C_{LAp} S_w} \quad (28)$$

or, if the airplane is climbing or diving at a large angle,

$$q_0 = \frac{W \cos \left(\tan^{-1} \frac{\frac{2D^2}{S_w} T_c \cos \alpha - C_D}{C_{LAp}} \right)}{C_{LAp} S_w} \quad (29)$$

At high angles of attack and large thrust coefficients equation (28) gives values of q_0 that are about 12 percent greater than those obtained from equation (29). Sufficiently accurate values of C_{LAp} may be obtained from figures 5 and 7 and values of C_D may be obtained from figure 4.

SUMMARY OF FINDINGS

The following remarks, although applying directly to the mock-up tested, probably possess varying degrees of general applicability.

1. For cases with flaps deflected, the propeller-operating conditions cannot be directly determined from the propeller-removed lift coefficient.

2. The slope of the lift curve of the tailless mock-up can be accurately calculated by the use of references 7 and 8.

3. The forward shift of the aerodynamic center of the plain wing caused by the fuselage can be estimated by the use of references 6 and 10.

4. The effect of propeller operation on the lift and on the pitching moment of the tailless mock-up with retracted flaps can be satisfactorily estimated from the procedures given in reference 5.

5. With the flaps deflected, the increments of lift due to propeller operation are much larger than those obtained for the corresponding condition with the flaps retracted. The difference is probably due to the effect of the slipstream on the flapped-wing vortex system.

6. The slipstream markedly increases the flapped-wing diving moment.

7. The isolated-tail parameters, as determined from these tests, compare satisfactorily with those given by the charts of reference 14.

8. The effective dynamic pressure at the tail for the propeller-operating conditions can be accurately estimated from references 5, 11, and 15.

9. The downwash angles at the tail determined from different tail settings are not equal to those determined from air-flow surveys, especially at low angles of attack.

10. The average downwash angles of the air flow at the tail, with the propeller removed, can be closely calculated from references 16, 17, and 18.

11. The methods of calculating the propeller-operating downwash angle at the tail from reference 5 are barely satisfactory as first approximations unless empirical correction factors are used. It is believed that most of the discrepancy, for the flap-deflected condition, may be attributed to the methods of calculating the downwash due to the propeller.

12. Pitching-moment curves for very nearly similar airplanes can probably be satisfactorily estimated by the use of the propeller-removed pitching moment of the tailless airplane and the empirical downwash correction factors.

13. The use of the charts of reference 20 for determining u and v , which are based on the results of a large number of tests of horizontal tails, is unsatisfactory. References 21 and 22 indicate that details of the elevator plan form and trailing-edge profile are important considerations.

14. The climb or the dive angle of an airplane in powered flight should be considered in calculating the free-stream dynamic pressure.

CONCLUDING REMARKS

Most of the basic factors affecting the pitching moments and the stick forces of an airplane can be satisfactorily estimated by use of the available theories and procedures; further systematic experiments and related theories, however, are necessary before the downwash at the tail with propeller operating may be reliably predicted. Experimental data and charts of the hinge-moment parameters should be used with extreme care, and due consideration should be given to the various factors affecting these parameters.

Langley Memorial Aeronautical Laboratory,
National Advisory Committee for Aeronautics,
Langley Field, Va.

REFERENCES

1. DeFrance, Smith J.: The N.A.C.A. Full-Scale Wind Tunnel. Rep. No. 459, NACA, 1933.
2. Silverstein, Abe, and White, James A.: Wind-Tunnel Interference with Particular Reference to Off-Center Positions of the Wing and to the Downwash at the Tail. Rep. No. 547, NACA, 1935.
3. Theodorsen, Theodore, and Silverstein, Abe: Experimental Verification of the Theory of Wind-Tunnel Boundary Interference. Rep. No. 478, NACA, 1934.
4. Silverstein, Abe, and Katzoff, S.: Experimental Investigation of Wind-Tunnel Interference on the Downwash behind an Airfoil. Rep. No. 609, NACA, 1937.
5. Goett, Harry J., and Pass, H. R.: Effect of Propeller Operation on the Pitching Moments of Single-Engine Monoplanes. NACA A.C.R., May 1941.
6. Jacobs, Eastman N., and Ward, Kenneth E.: Interference of Wing and Fuselage from Tests of 209 Combinations in the N.A.C.A. Variable-Density Tunnel. Rep. No. 540, NACA, 1935.
7. Anderson, Raymond F.: Determination of the Characteristics of Tapered Wings. Rep. No. 572, NACA, 1936.
8. Pearson, Henry A., and Anderson, Raymond F.: Calculation of the Aerodynamic Characteristics of Tapered Wings with Partial-Span Flaps. Rep. No. 665, NACA, 1939.
9. Thompson, M. J.: A simple Method for Determining the Aerodynamic Center of an Airfoil. Jour. Aero. Sci., vol. 5, no. 4, Feb. 1938, pp. 138-140.
10. Multhopp, H.: Aerodynamics of the Fuselage. NACA TM No. 1036, 1942.
11. Smelt, R., and Davies, H.: Estimation of Increase in Lift due to Slipstream. R. & M. No. 1788, British A.R.C., 1937.

12. Katzoff, S.: Longitudinal Stability and Control with Special Reference to Slipstream Effects. Rep. No. 690, NACA, 1940.
13. Glauert, H.: Airplane Propellers. Vol. IV, div. L, sec. 5, ch. XII of Aerodynamic Theory, W. F. Durand, ed., Julius Springer (Berlin), 1935, pp. 351-357.
14. Silverstein, Abe, and Katzoff, S.: Aerodynamic Characteristics of Horizontal Tail Surfaces. Rep. No. 688, NACA, 1940.
15. Koning, C.: Influence of the Propeller on Other Parts of the Airplane Structure. Vol. IV, div. M of Aerodynamic Theory, W. F. Durand, ed., Julius Springer (Berlin), 1935, pp. 361-430.
16. Silverstein, Abe, Katzoff, S., and Bullivant, W. Kenneth: Downwash and Wake behind Plain and Flapped Airfoils. Rep. No. 651, NACA, 1939.
17. Silverstein, Abe, and Katzoff, S.: Design Charts for Predicting Downwash Angles and Wake Characteristics behind Plain and Flapped Wings. Rep. No. 648, NACA, 1939.
18. Pearson, Henry A., and Jones, Robert T.: Theoretical Stability and Control Characteristics of Wings with Various Amounts of Taper and Twist. Rep. No. 635, NACA, 1938.
19. Glauert, H.: Theoretical Relationships for an Aerofoil with Hinged Flap. R. & M. No. 1095, British A.R.C., 1927.
20. Pass, H. R.: Analysis of Wind-Tunnel Data on Directional Stability and Control. T. N. No. 775, NACA, 1940.
21. Jones, Robert T., and Cohen, Doris: Determination of Optimum Plan Forms for Control Surfaces. NACA Rep. No. 731, 1942.
22. Jones, Robert T., and Ames, Milton B., Jr.: Wind-Tunnel Investigation of Control-Surface Characteristics. V - The Use of a Beveled Trailing Edge to Reduce the Hinge Moment of a Control Surface. NACA A.R.R., March 1942.

COMPARISON OF EXPERIMENTAL AND CALCULATED
DOWNWASH ANGLES FOR MOCK-UP WITH FLAPS RETRACTED

α_T (deg)	T_c	β (deg)	$(q/q_0)_{aa}$	$(q/q_0)_{av}$	ϵ_{aa} (deg)	ϵ_{av} (deg)	ϵ_{eff} (deg)	ϵ_{cal} (deg)
-0.2	(a)	(a)	0.87	0.84	1.2	1.2	2.5	0.9
3.1	(a)	(a)	.83	.79	2.6	2.6	4.2	2.4
6.9	(a)	(a)	.84	.81	4.6	4.7	5.6	4.2
10.9	(a)	(a)	.82	.79	6.6	6.6	6.4	6.3
-2.8	0	41	.94	.91	.1	.1	1.0	-.5
-2.5	.02	34	.93	.92	.4	.4	1.1	-.3
-1.5	0	36	.93	.90	.8	.9	1.7	.2
-1.5	.02	41	.99	.96	.7	.6	1.7	.2
-.2	.01	53	.87	.85	1.3	1.3	2.5	.9
-.2	.04	50	.97	.95	1.3	1.4	2.5	.9
1.0	.08	29	1.08	1.07	2.8	2.8	3.5	1.9
3.1	.03	30	.93	.91	3.1	3.0	4.5	2.6
3.1	.09	37	1.04	1.03	3.3	3.3	4.7	2.8
5.0	.16	26	1.29	1.26	5.2	5.3	6.1	4.5
5.1	.01	26	.96	.93	5.2	4.6	5.3	3.8
6.8	.11	30	1.09	1.07	5.9	6.0	7.1	5.5
6.8	.18	37	1.44	1.46	5.1	5.4	7.1	6.1
8.9	.05	26	1.02	1.00	6.8	7.0	7.8	6.3
10.7	.31	35	1.62	1.63	8.7	9.1	9.9	9.9
14.5	.46	29	2.01	2.01	12.6	12.9	12.7	14.2
14.7	.12	29	1.17	1.15	10.7	11.1	11.7	10.9

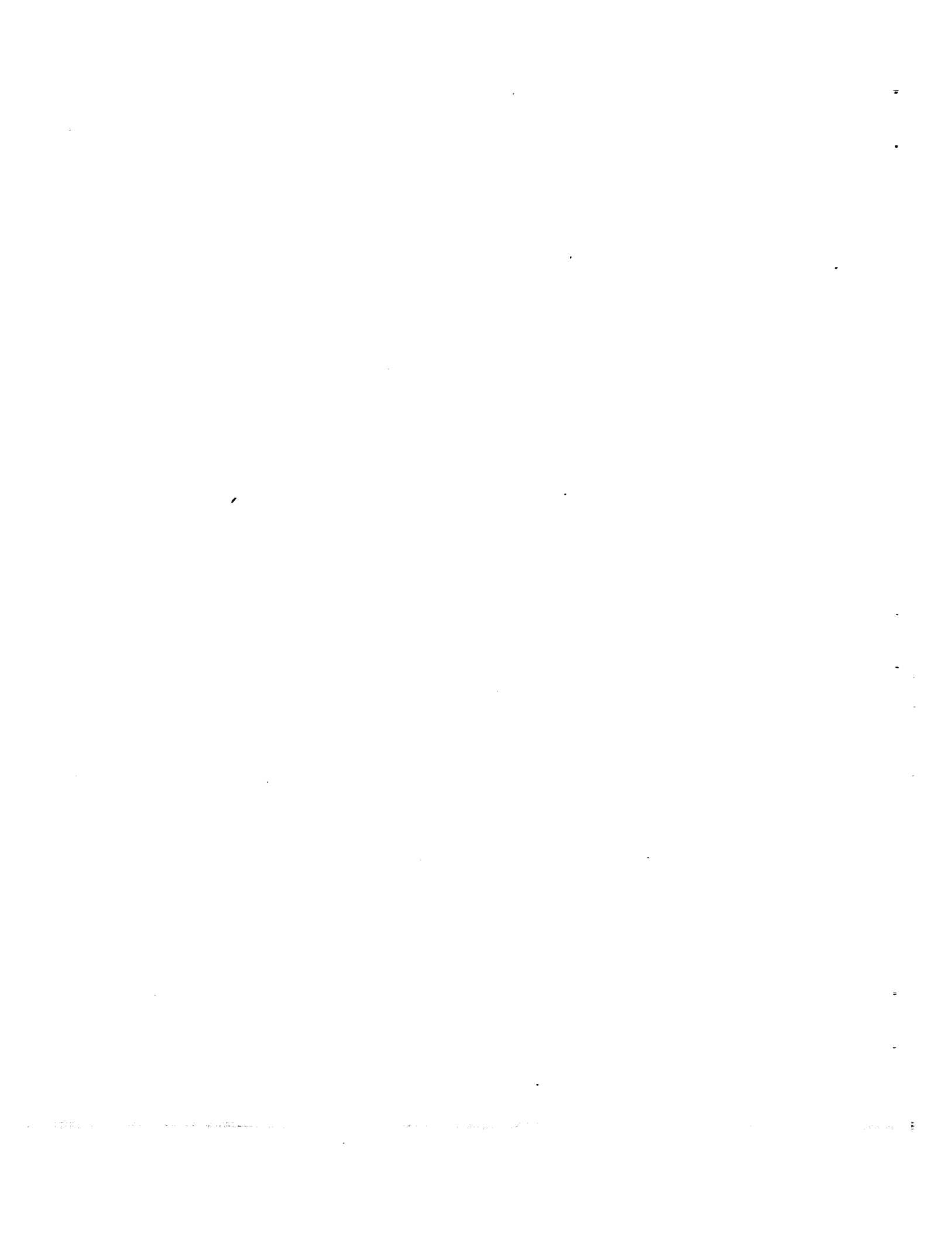
^aPropeller removed

TABLE II

COMPARISON OF EXPERIMENTAL AND CALCULATED
DOWNWASH ANGLES FOR MOCK-UP WITH FLAPS DEFLECTED

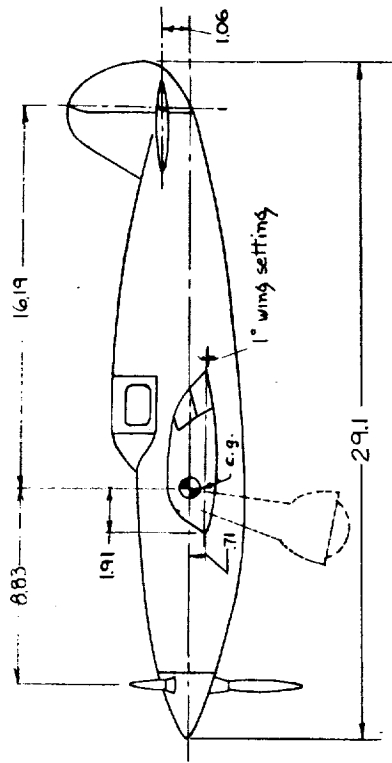
α_T (deg)	T_c	β (deg)	$(q/q_0)_{aa}$	$(q/q_0)_{av}$	ϵ_{aa} (deg)	ϵ_{av} (deg)	ϵ_{eff} (deg)	ϵ_{cal} (deg)
7.8	(a)	(a)	0.88	0.85	10.7	11.8	11.2	10.5
15.1	(a)	(a)	.83	.81	13.0	13.9	13.0	14.6
5.8	0.22	23	1.55	1.61	14.0	13.2	14.9	12.7
6.1	.07	18	1.28	1.27	13.0	12.6	12.3	11.0
7.3	.52	28	1.92	2.03	16.3	15.6	18.9	16.4
8.6	.34	23	1.67	1.72	16.6	16.7	17.2	16.5
9.6	.35	32	1.60	1.66	16.6	16.5	17.5	17.6
9.7	.17	18	1.34	1.36	15.2	15.2	15.6	14.9
9.7	.19	18	1.36	1.38	16.3	16.6	15.8	15.3
12.8	.46	23	1.80	1.89	19.4	19.9	19.3	21.9
13.1	.21	18	1.35	1.35	18.0	17.4	17.1	18.4
14.2	.58	28	2.00	2.01	21.4	20.1	20.8	24.8
15.0	.08	28	1.03	1.03	16.5	16.7	16.4	18.1

^aPropeller removed



NACA

Fig 1



Principal dimensions of mock-up

W	6500 lb	Wing aspect ratio	5.69
S_w	170 sq ft	Tail aspect ratio	3.46
S_t	30.1 sq ft	\bar{c}_w	5.47 ft
S_e	10.4 sq ft	l_1	8.83 ft
S_b	1.6 sq ft	l_2	16.19 ft
S_b/S_e	0.15	l_3	11.12 ft
S_e/S_t	0.35		

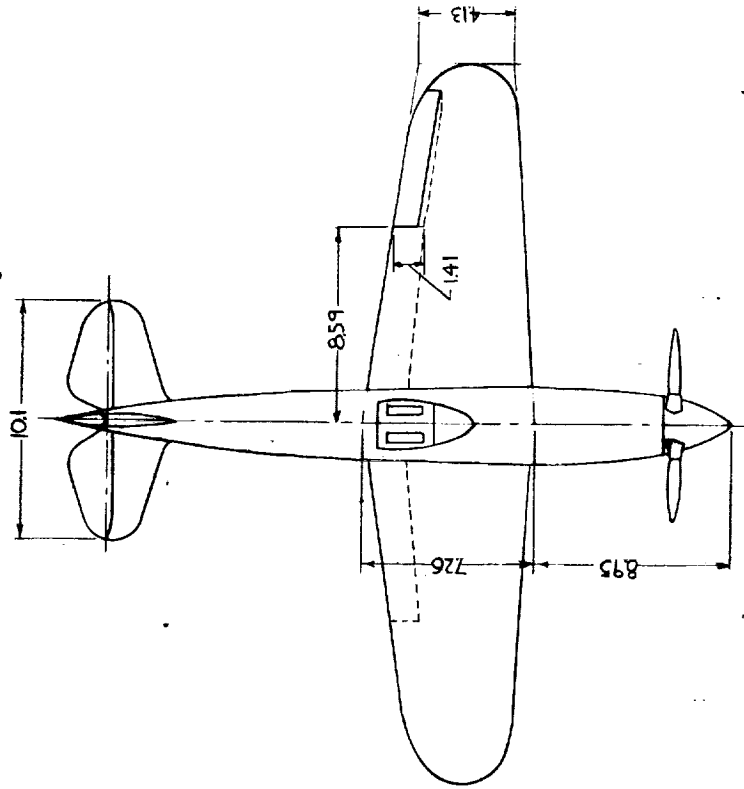
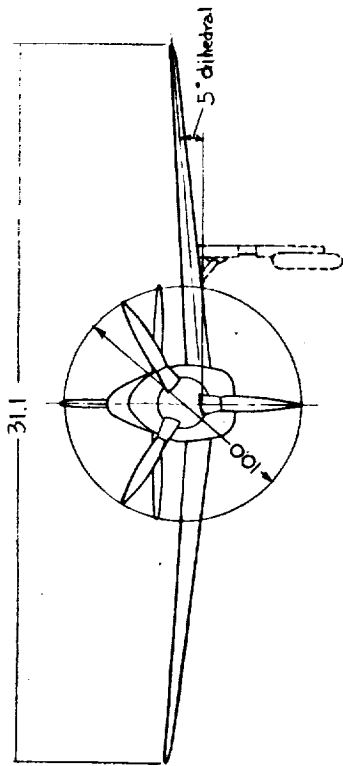
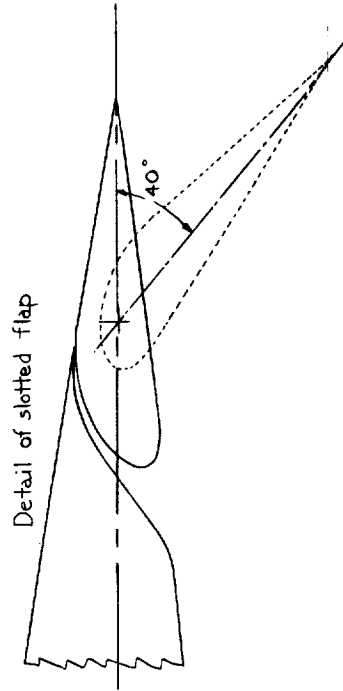
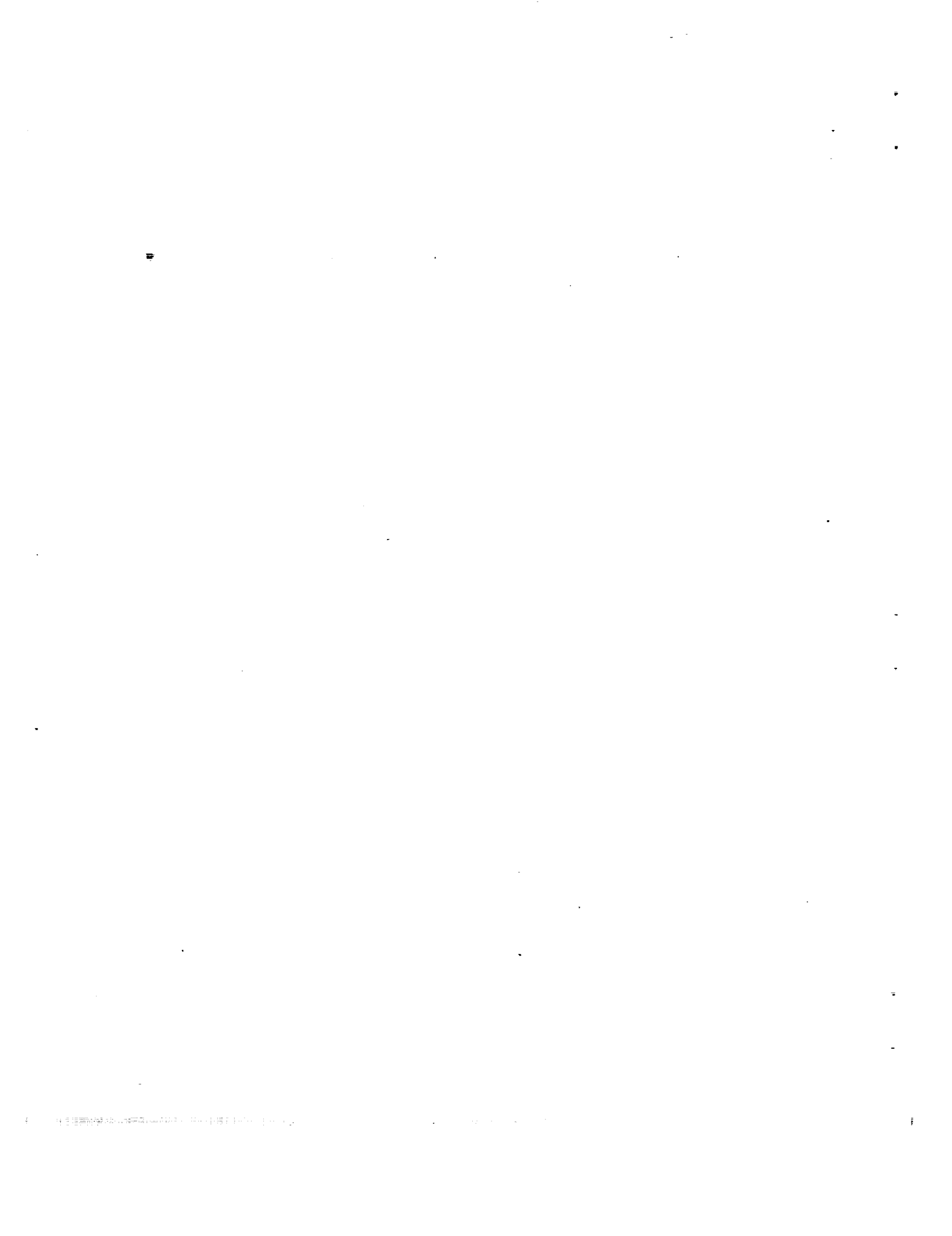


Figure 1. Three-view drawing of mock-up. All dimensions are in feet.



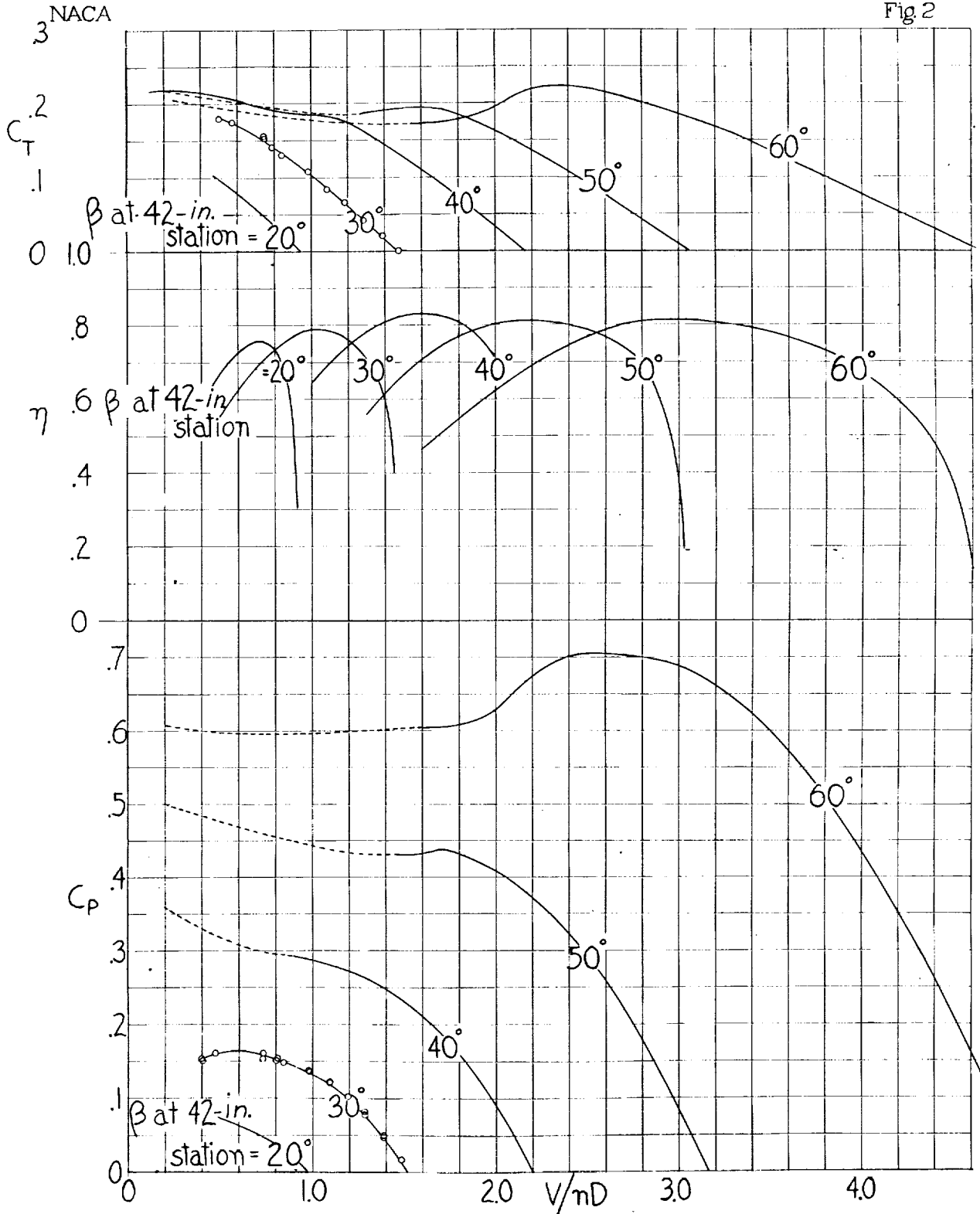
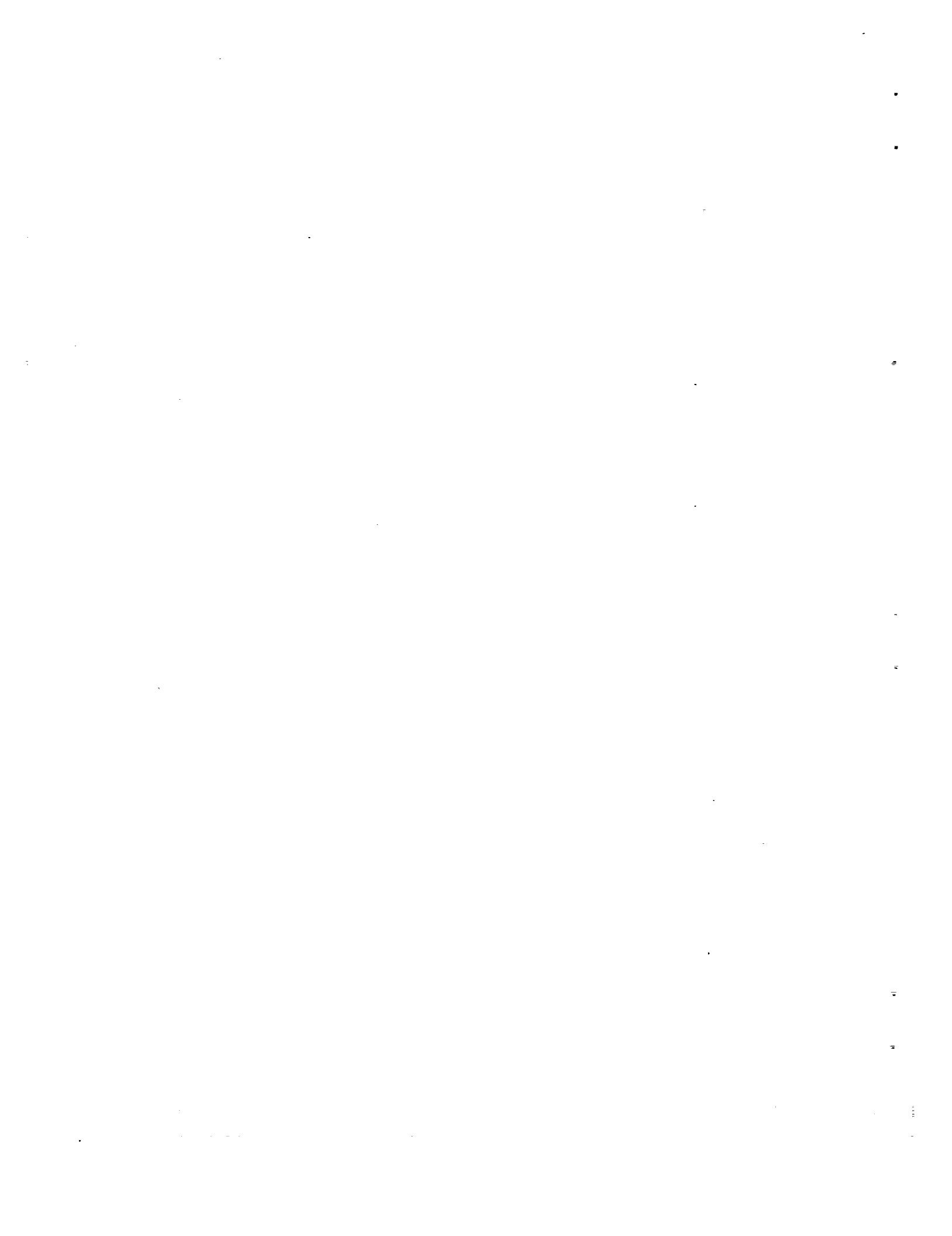


Figure 2.- Propeller characteristics as determined from tests of the complete mock-up in the NACA full-scale wind tunnel. Three-blade Curtiss electric propeller, blade 614Ccl.5-24, hollow steel.



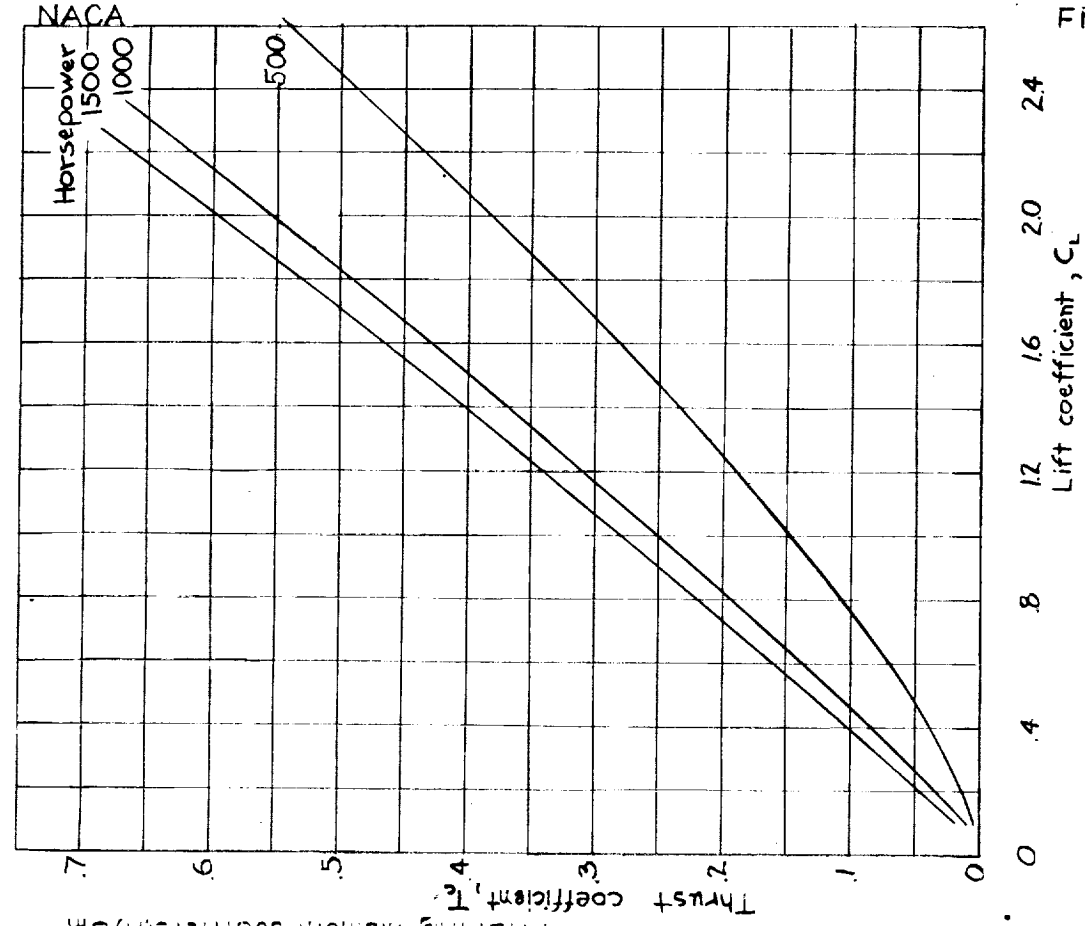


Figure 3. - Variation of thrust coefficient with lift coefficient for constant speed ($n=2165$) propeller operation at various horsepower levels.

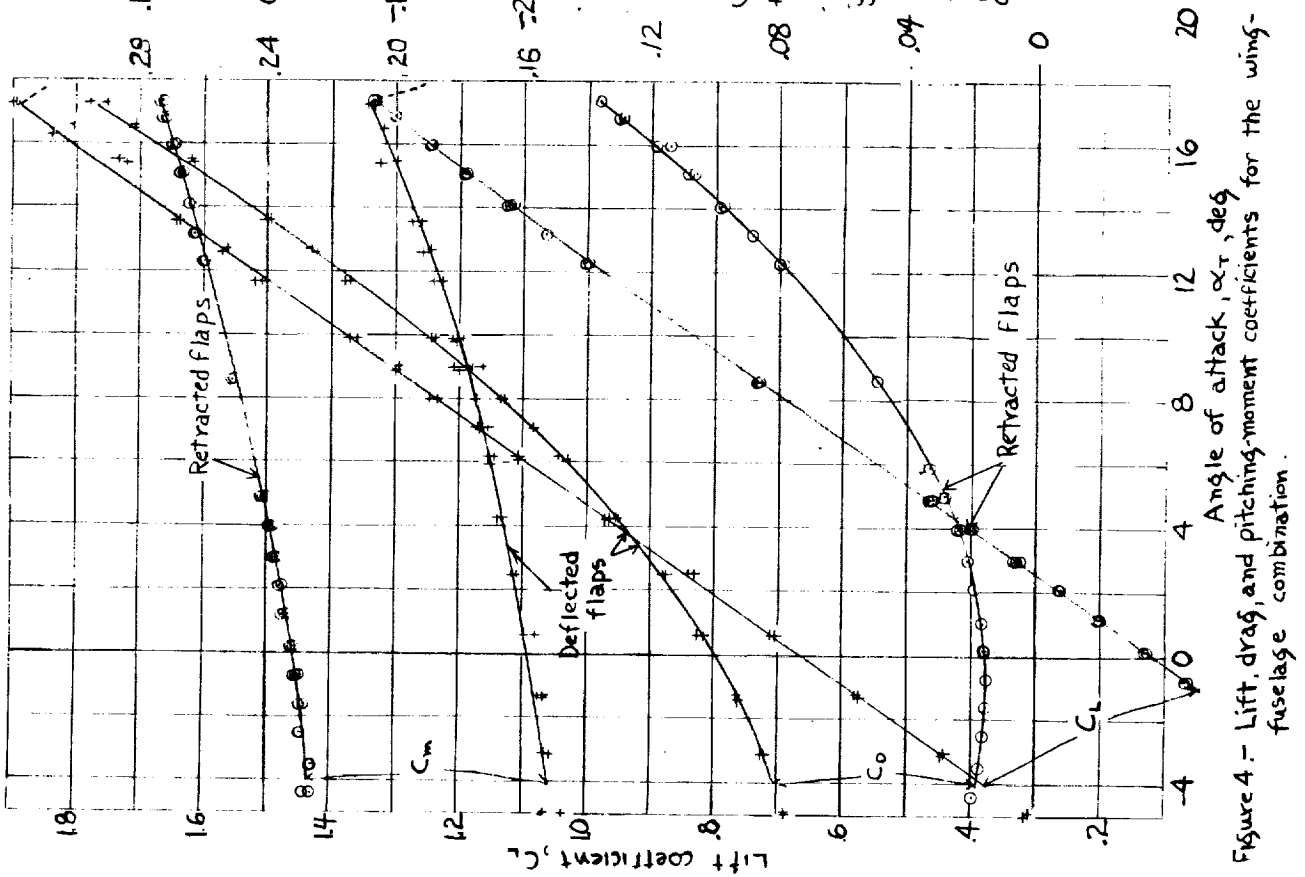
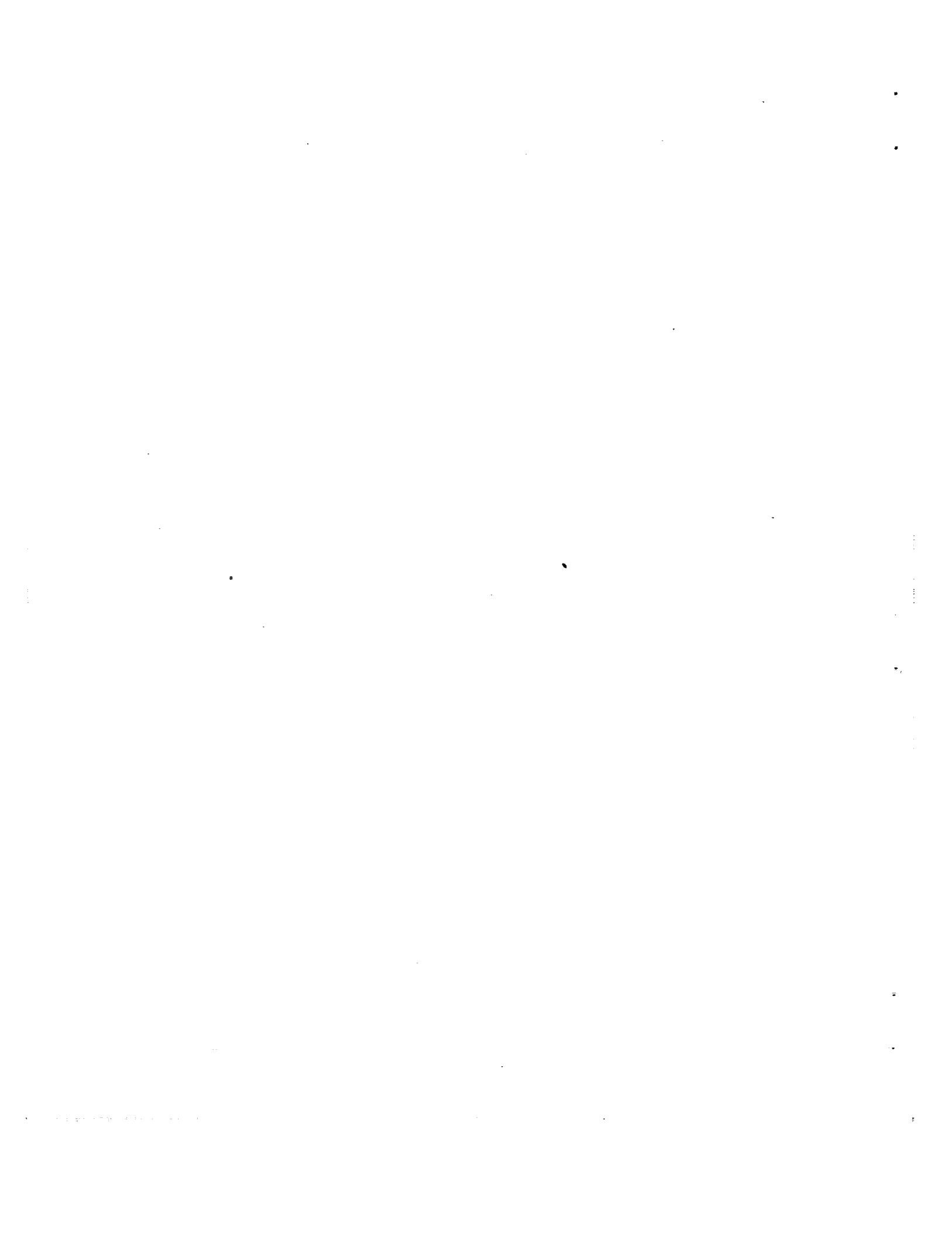


Figure 4. - Lift, drag, and pitching-moment coefficients for the wing-fuselage combination.



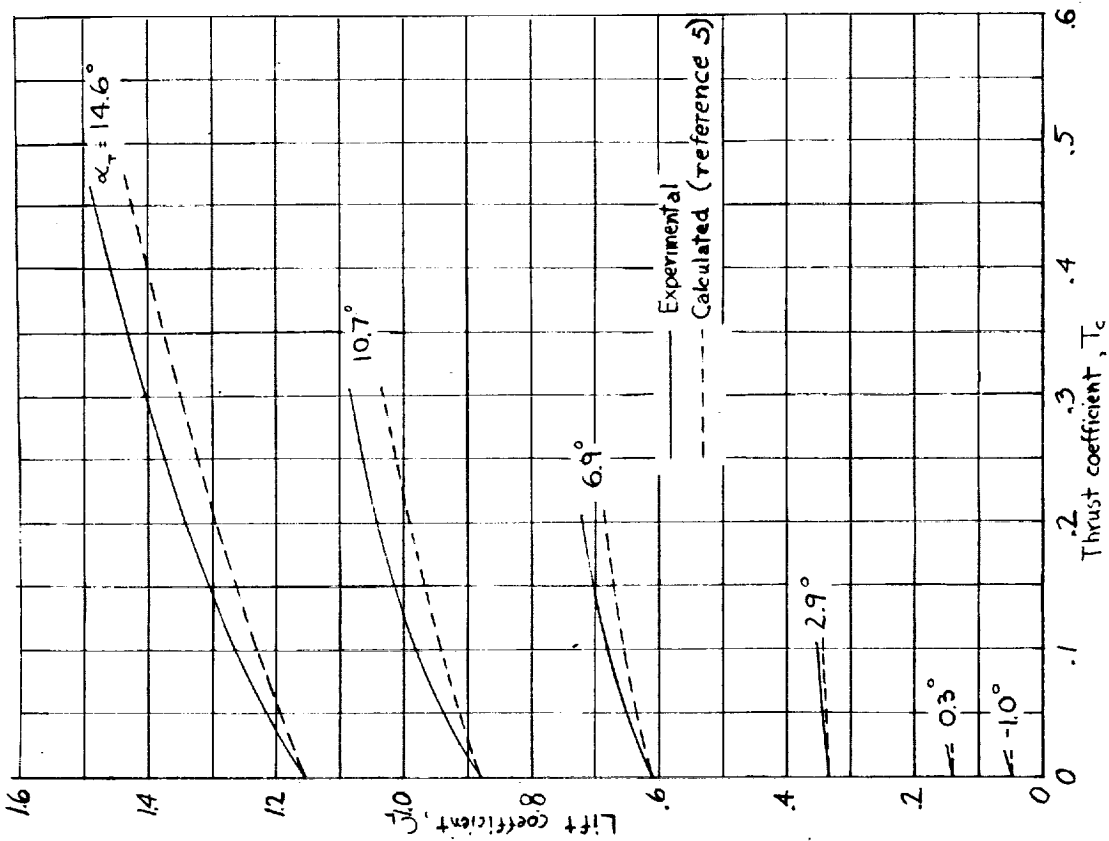


Figure 5.- Experimental and calculated effect of propeller operation on the lift coefficient of the wing-fuselage combination with retracted flaps.

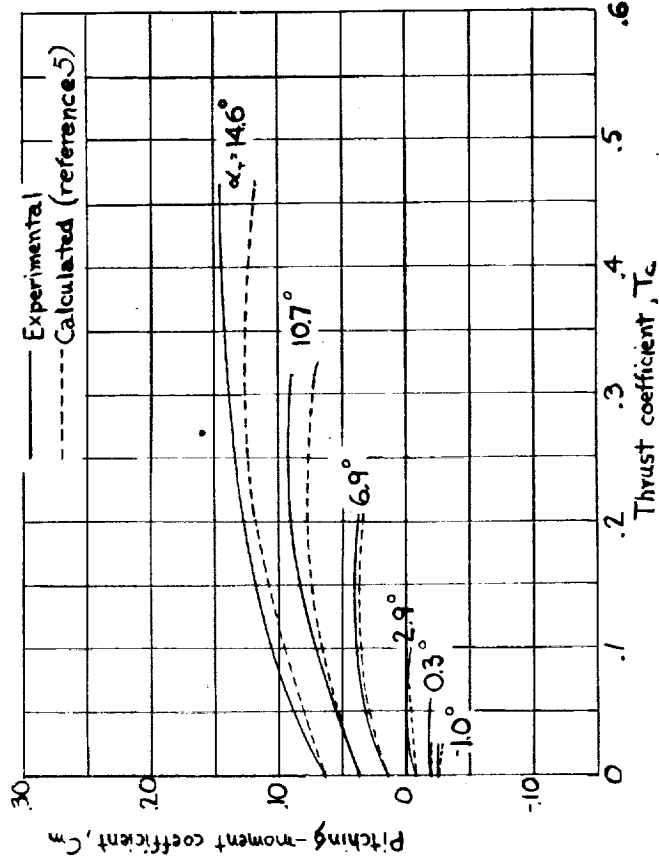


Figure 6.- Experimental and calculated effect of propeller operation on the pitching-moment coefficient of the wing-fuselage combination with retracted flaps.

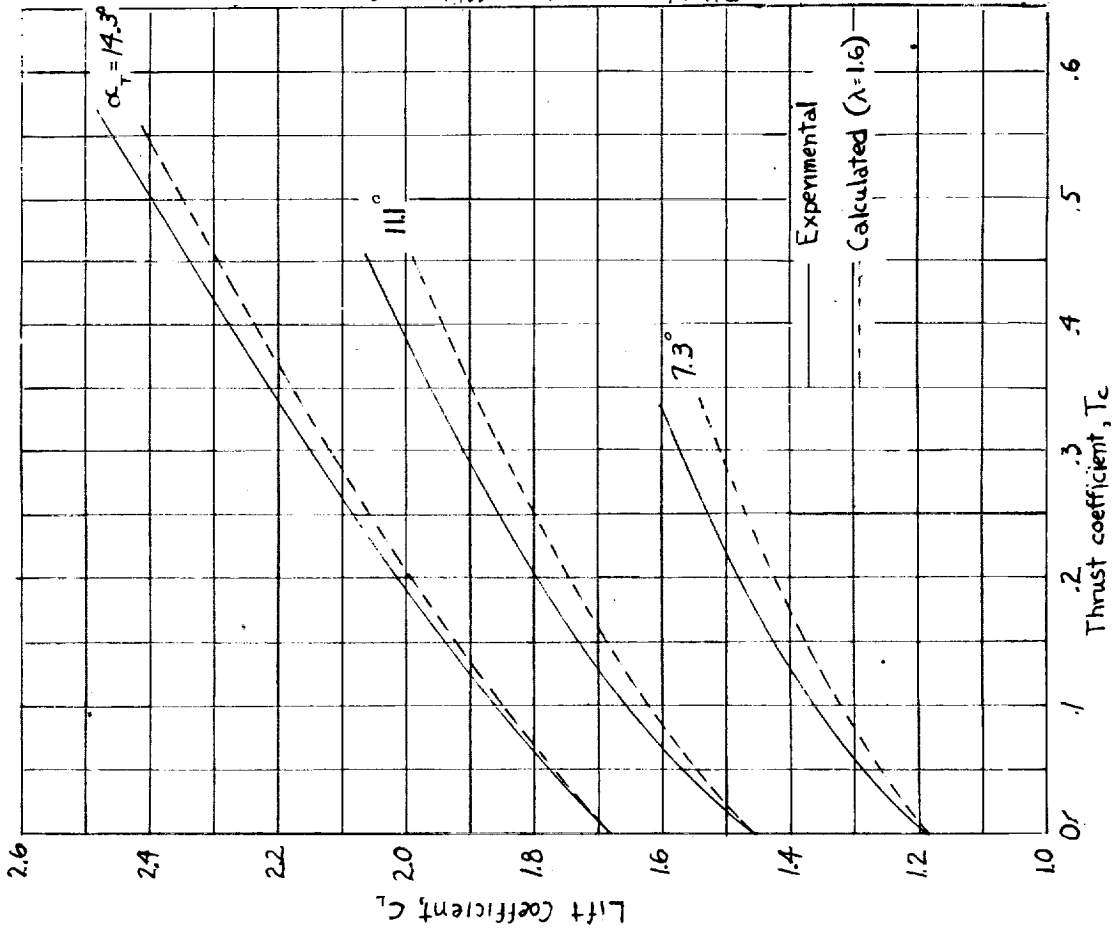


Figure 7.- Experimental and calculated effect of propeller operation on the lift coefficient of the wing-fuselage combination with deflected flaps.

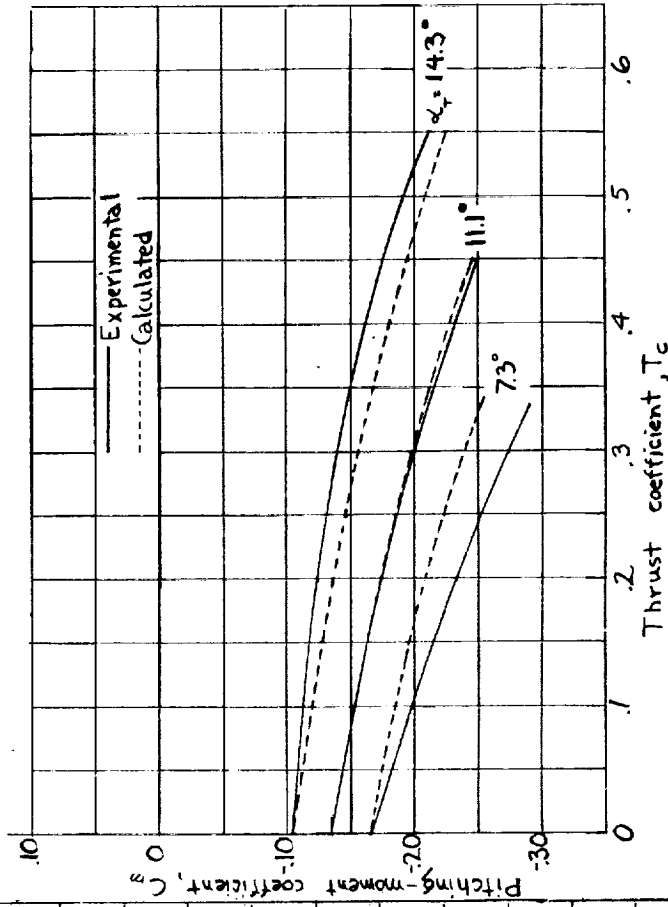


Figure 8.- Experimental and calculated effect of propeller operation on the pitching-moment coefficient of the wing-fuselage combination with deflected flaps.

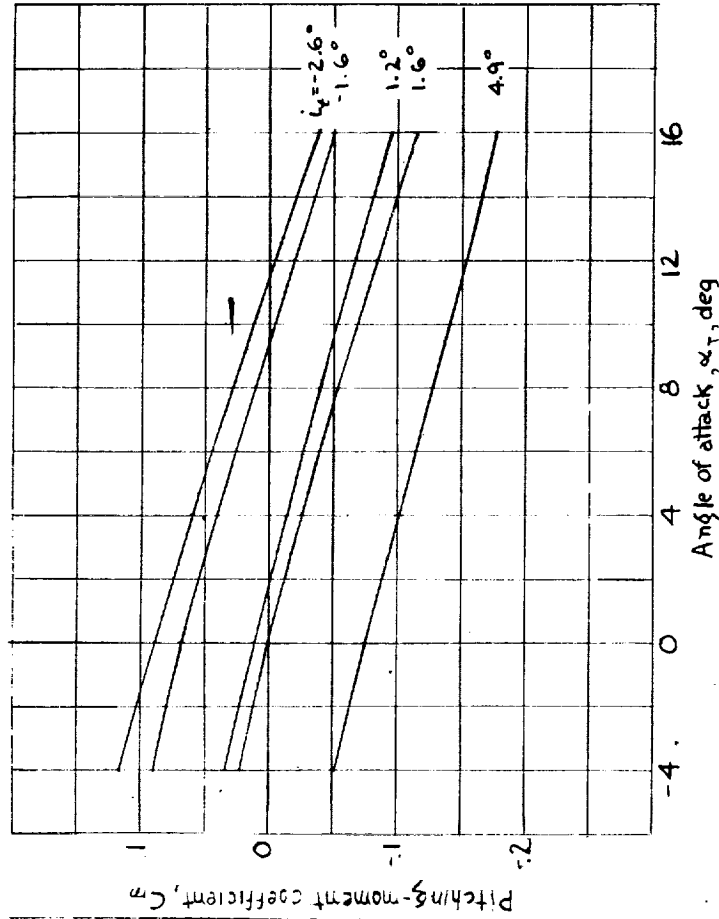


Figure 26. - Effect of tail setting on the pitching-moment coefficients of the mockup with retracted flaps, propeller removed.

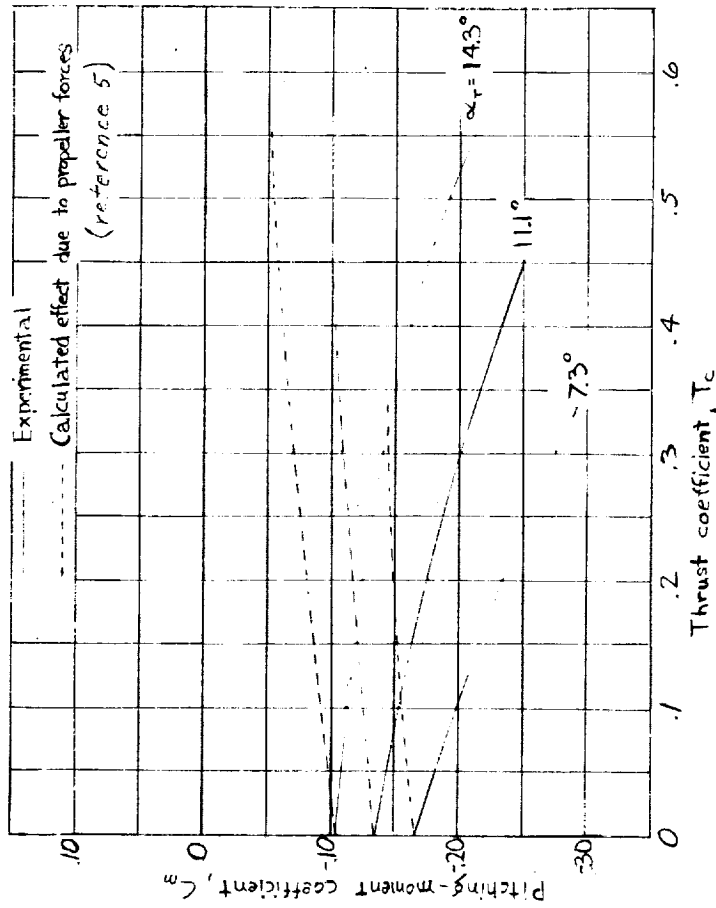
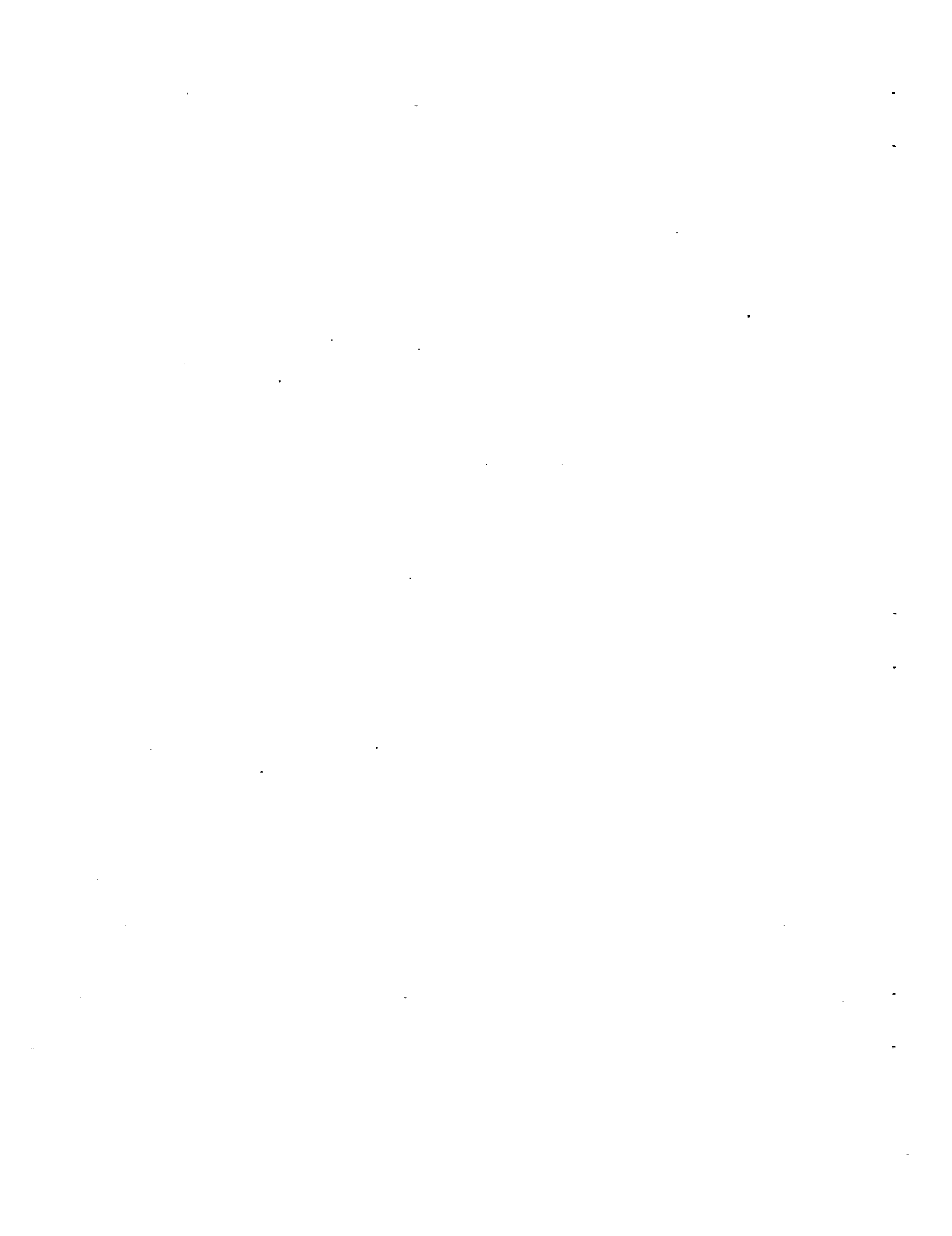
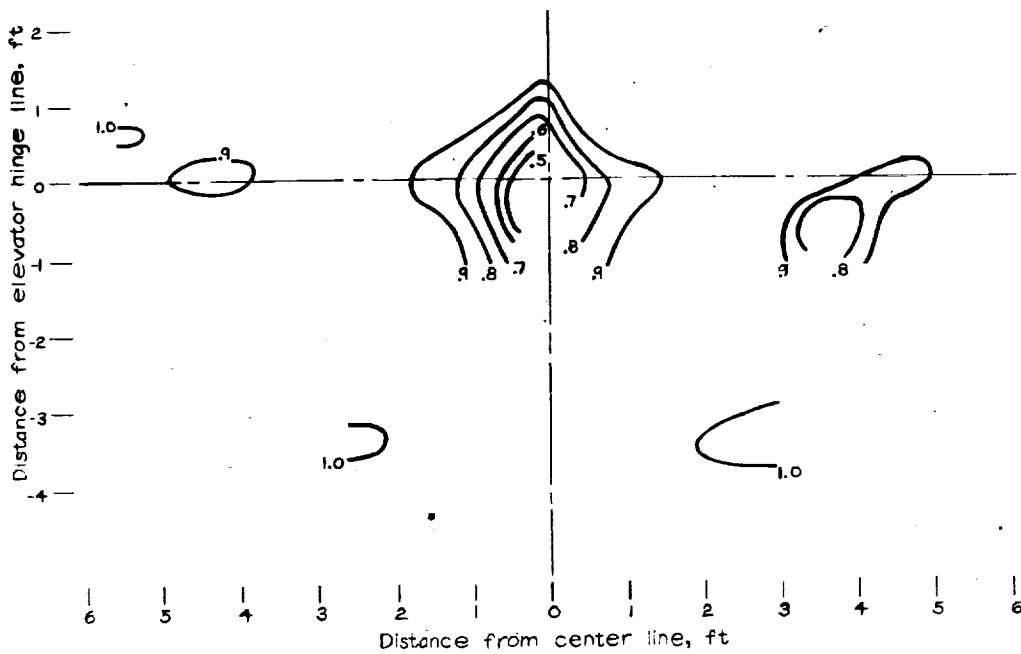


Figure 9. - Comparison of the calculated effect of propeller forces alone with the experimental effect of propeller operation on the pitching-moment coefficients of the wing-fuselage combination with deflected flaps.





(a) Dynamic-pressure (q/q_0) contours.

Figure 10. — Air flow in the plane of the elevator hinge line.
View looking forward; $\alpha_T, -0.2^\circ$;
 $\delta_T, 0^\circ$; propeller removed.

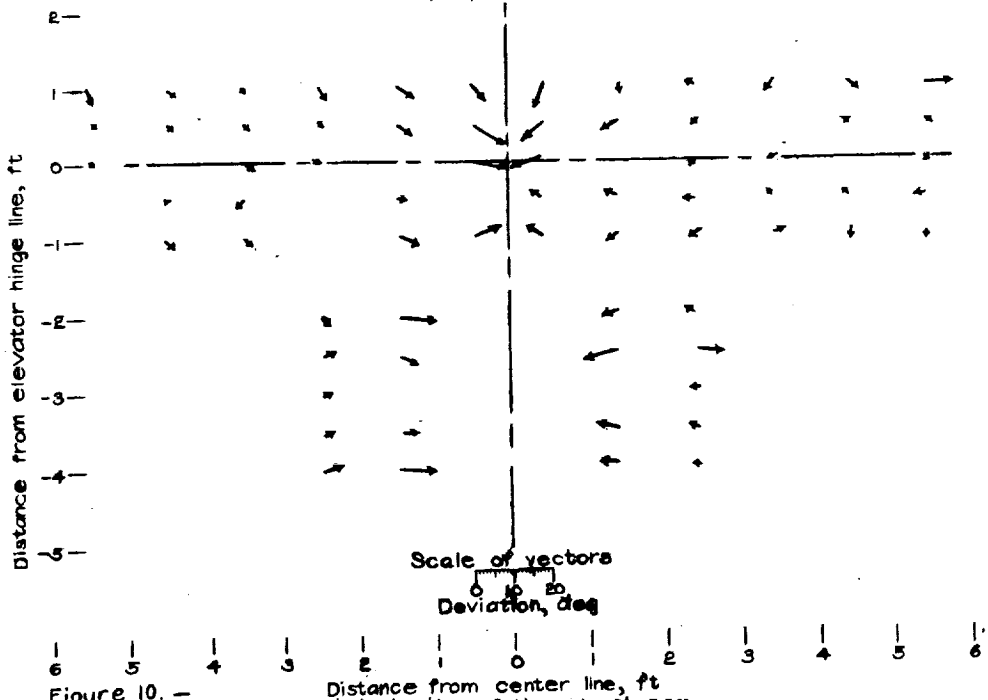
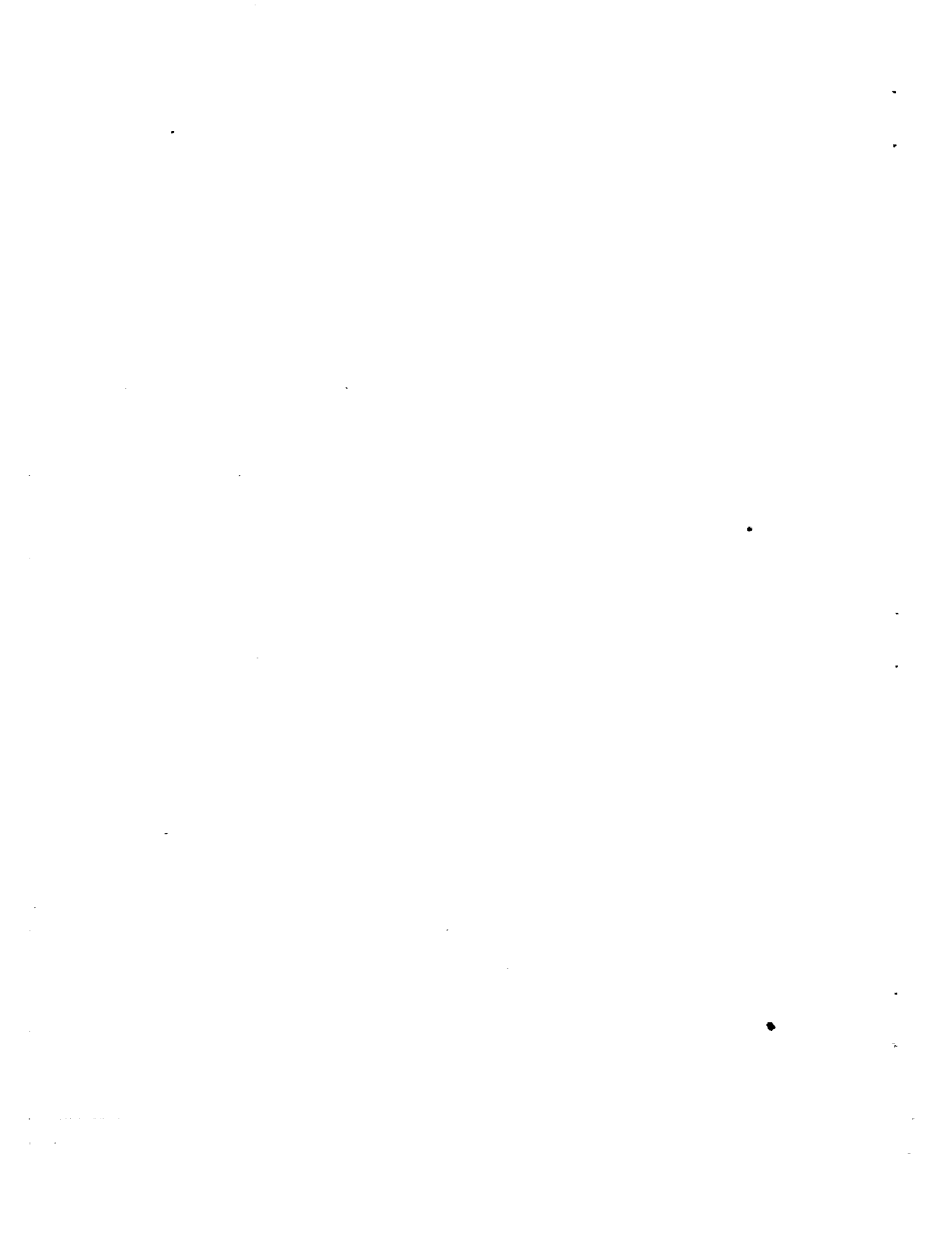
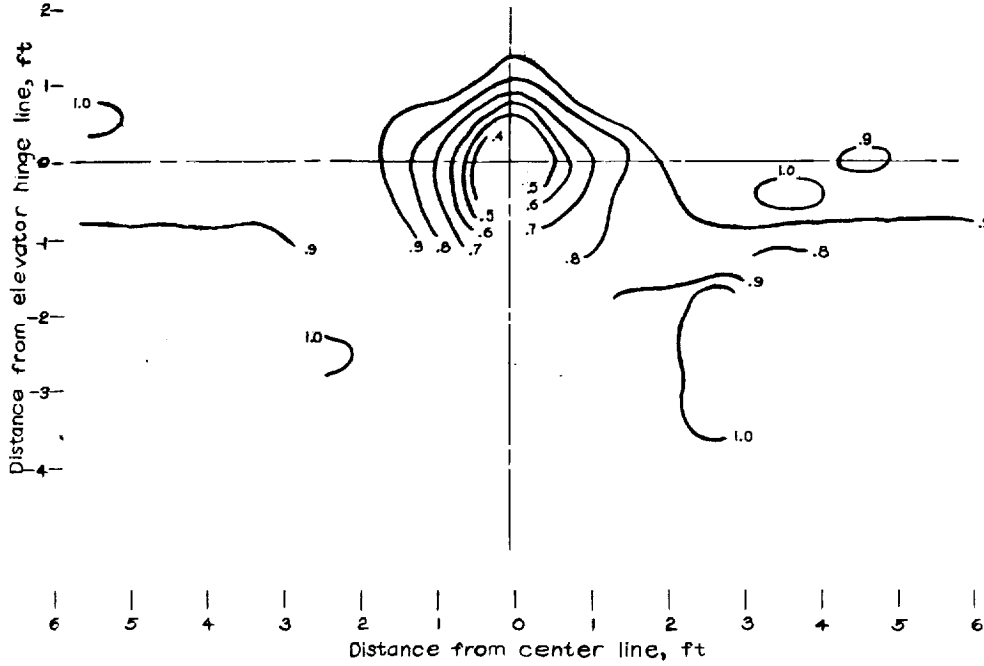


Figure 10. —
Concluded

(b) Inclination of the air stream.



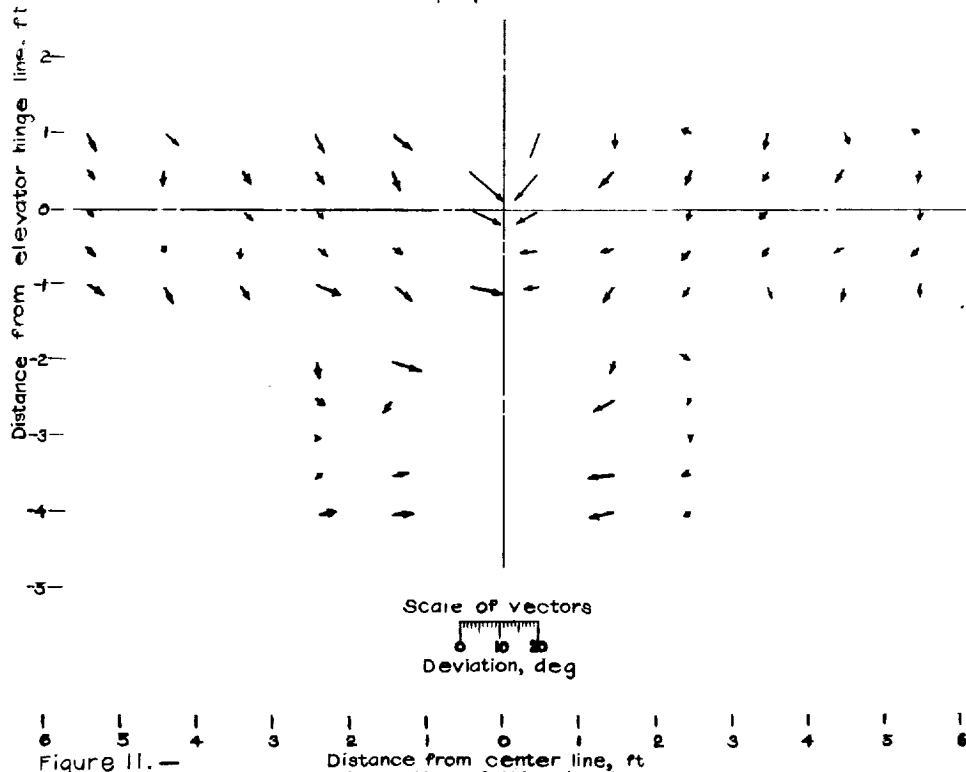


(a) Dynamic-pressure (q/q_0) contours.

Figure 11.—Air flow in the plane of the elevator hinge line.

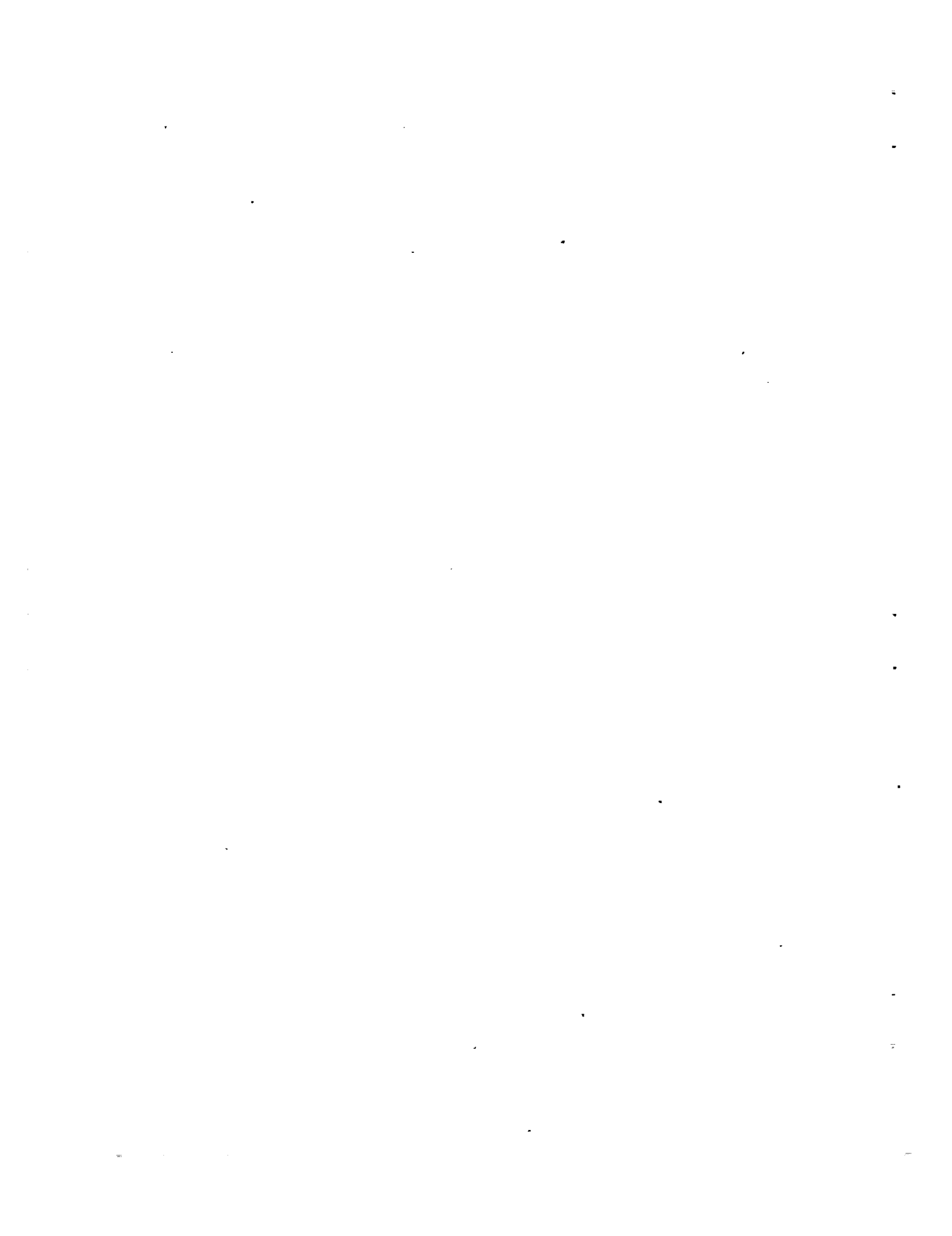
View looking forward; $\alpha_T, 3.1^\circ$;

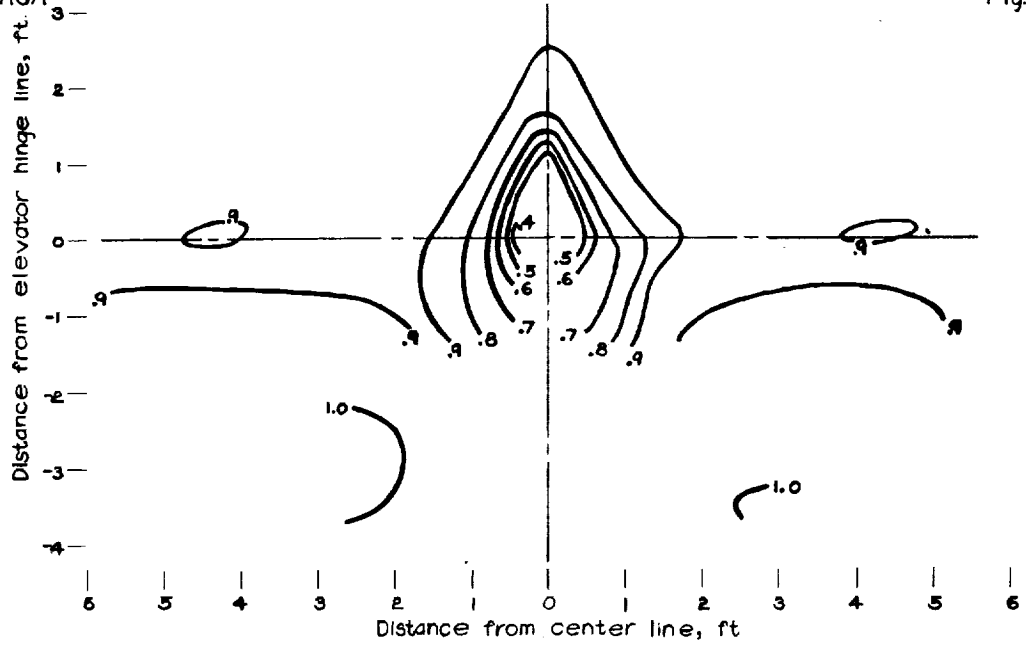
$\alpha_f, 0^\circ$; propeller removed.



(b) Inclination of the air stream.

Figure 11.—
Concluded





(a) Dynamic-pressure (q/q_0) contours.

Figure 12.—Air flow in the plane of the elevator hinge line.

View looking forward; $d_f, 6.9'$;

$\delta_f, 0'$; propeller removed.

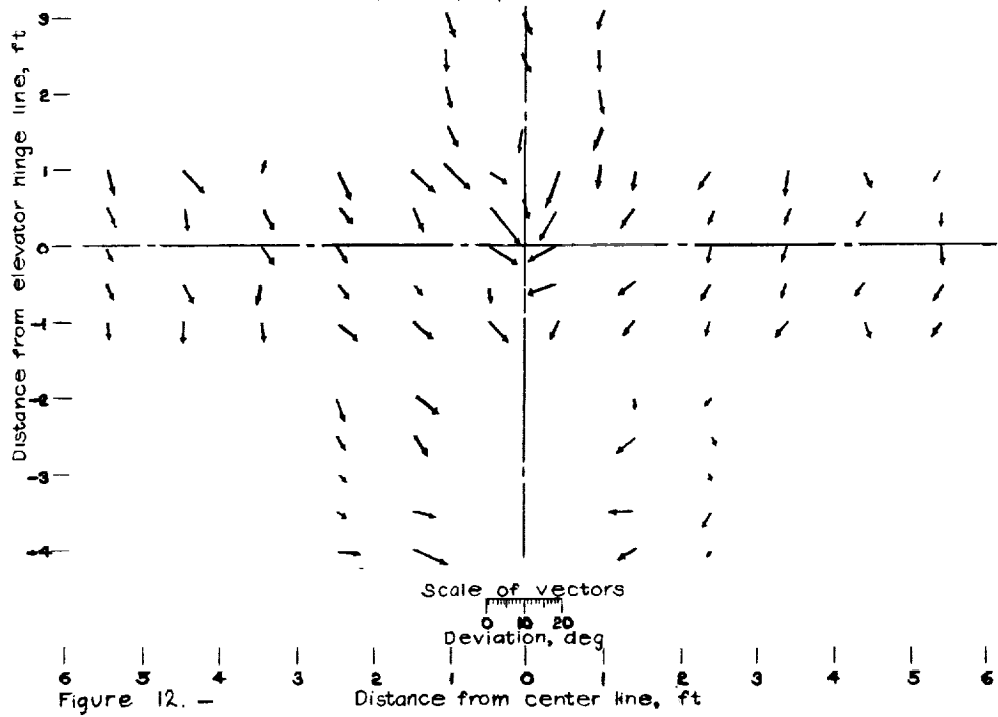
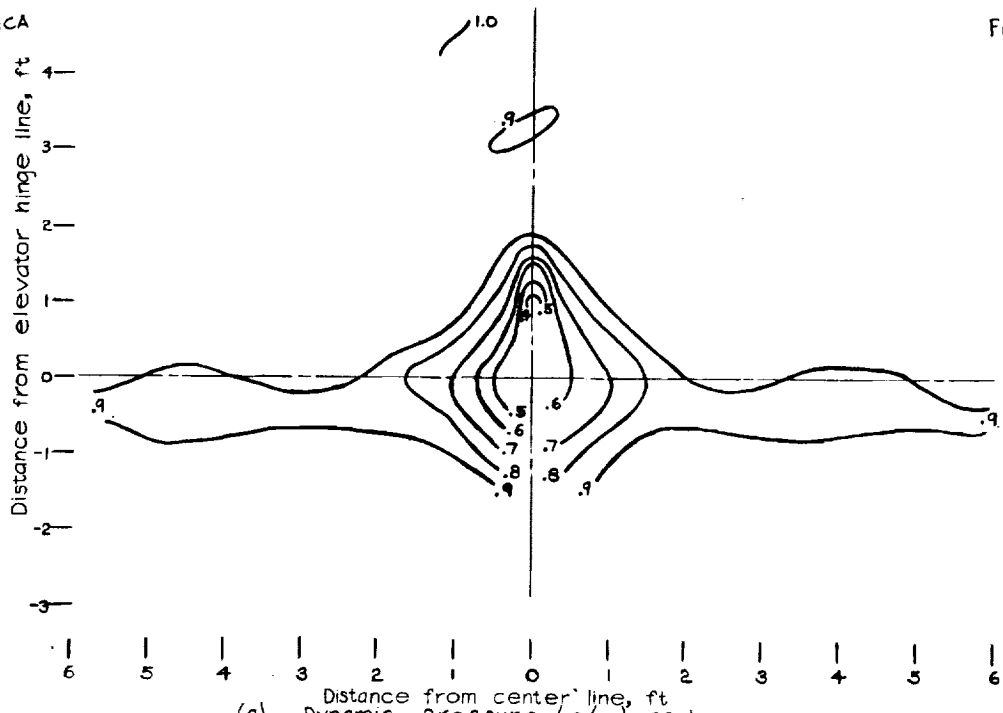
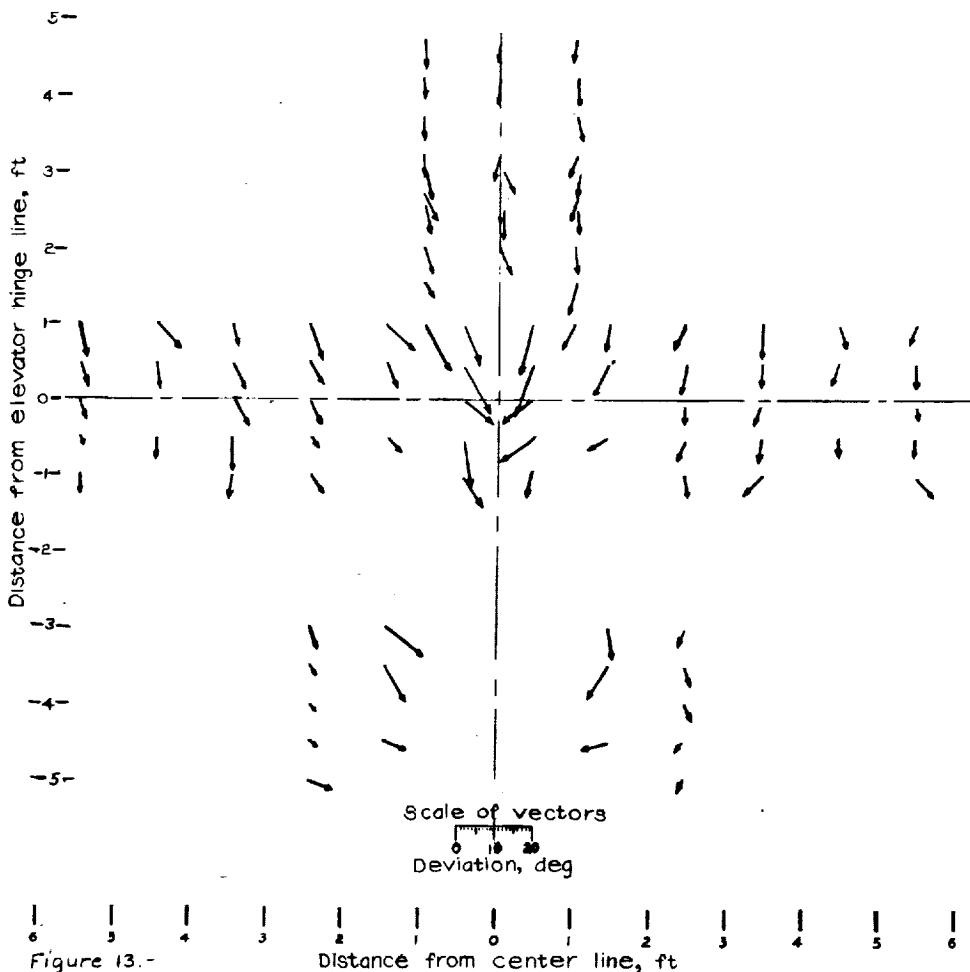


Figure 12. — Concluded.

(b) Incination of the air stream.

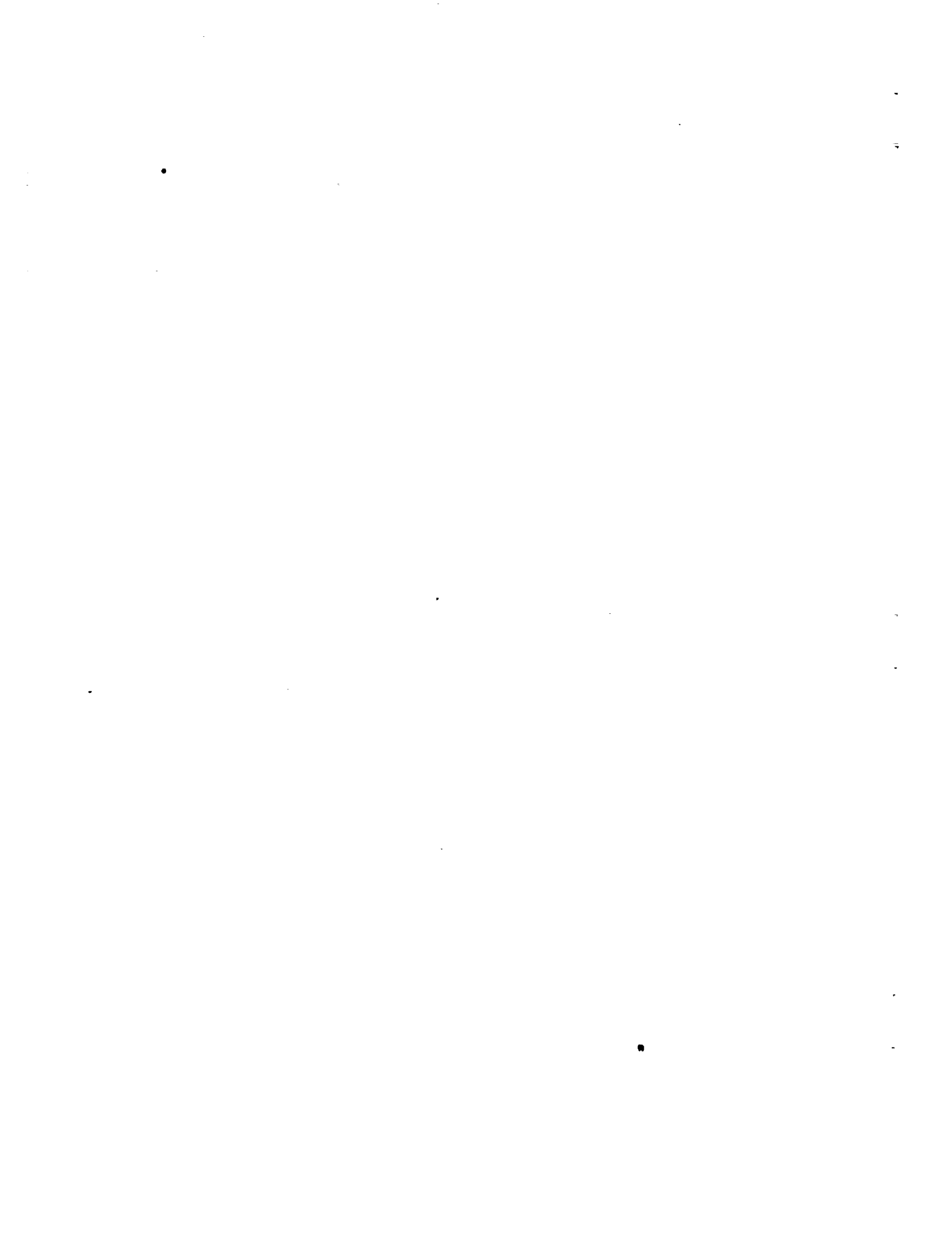


(a) Dynamic-pressure (q/q_0) contours.
 Figure 13. - Air flow in the plane of the elevator hinge line. View looking forward; $\alpha_T, 10.9^\circ$; $d_f, 0$; propeller removed.



(b) Inclination of the air stream.

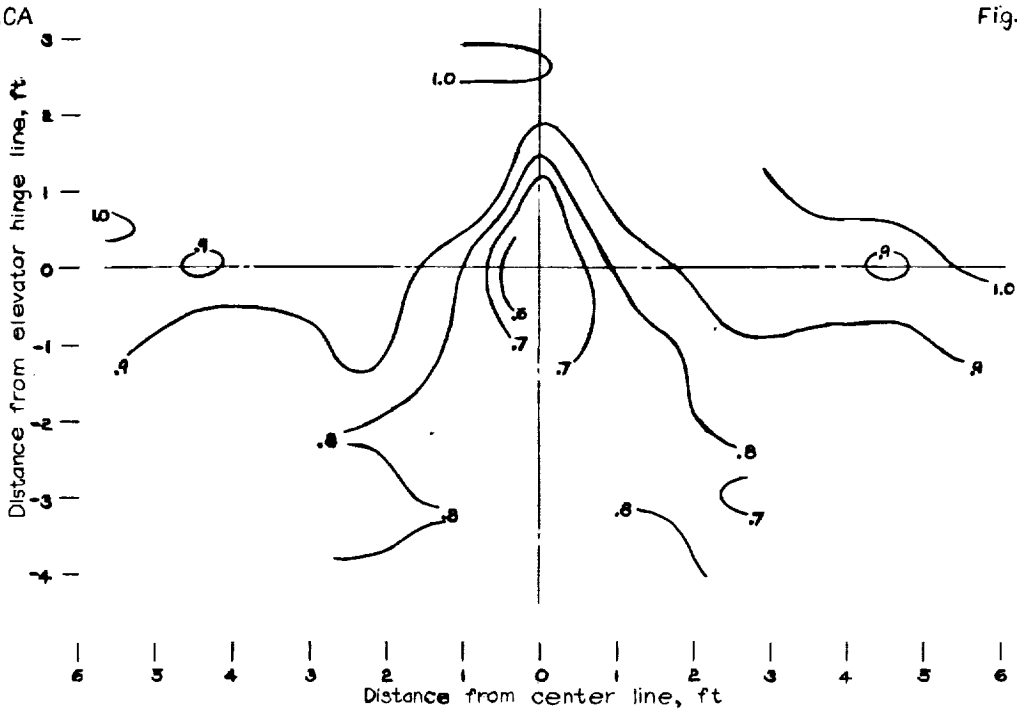
Figure 13.-
 Concluded.



L-444

NACA

Fig. 14



(a) Dynamic-pressure (q/q_0) contours.

Figure 14.—Air flow in the plane of the elevator hinge line.

View looking forward; $d_T, 7.8^\circ$;

$\alpha_f, 40^\circ$; propeller removed.

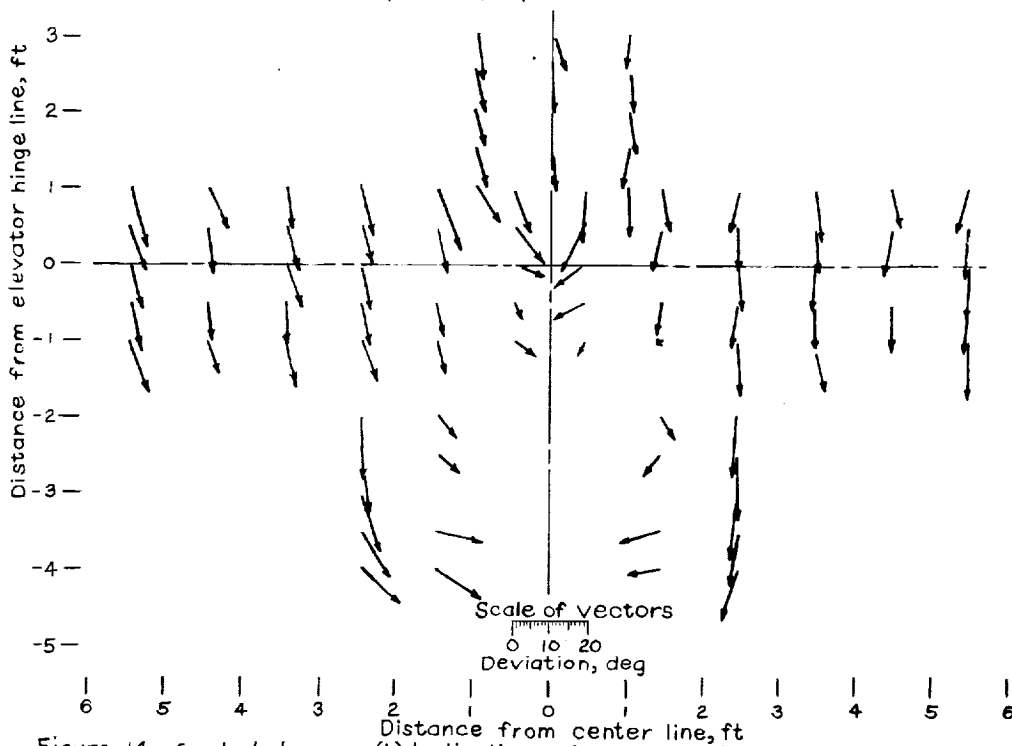
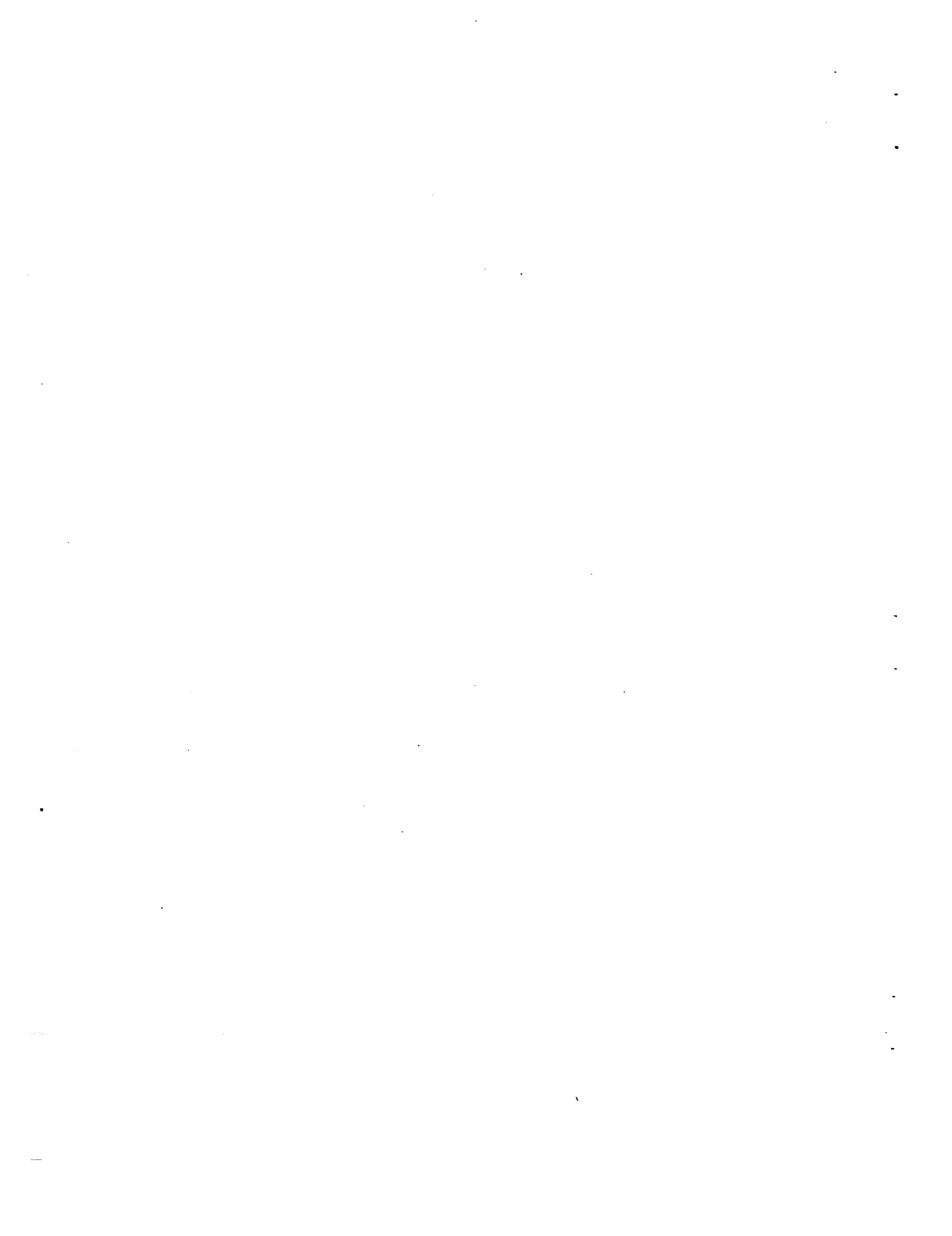
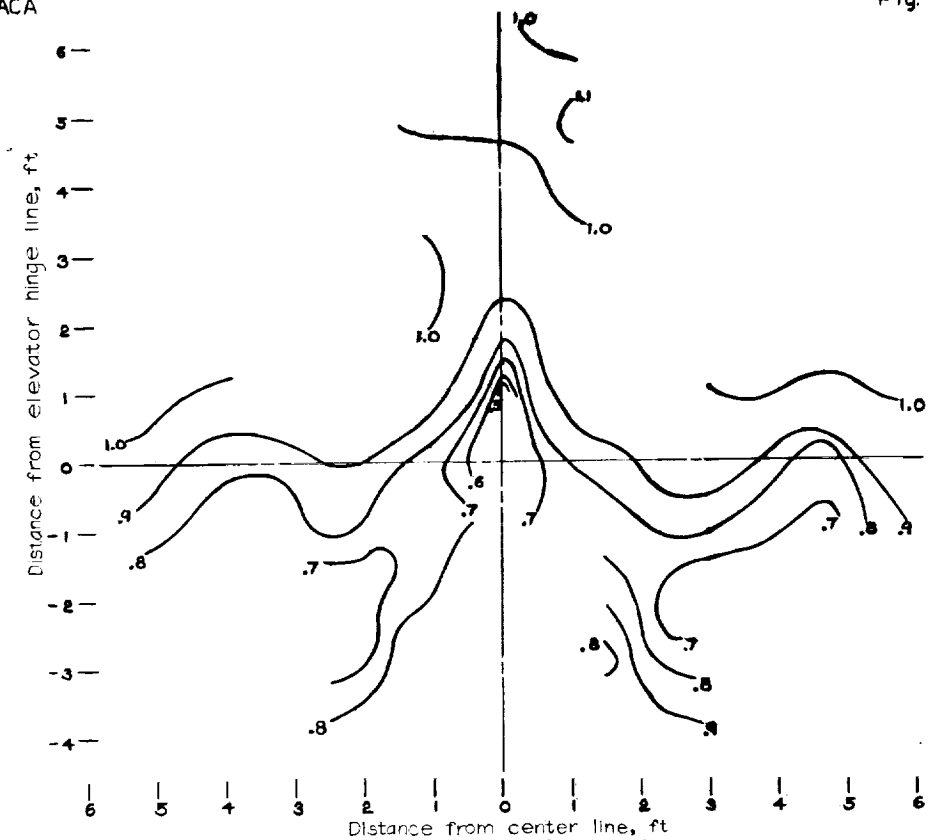


Figure 14.— Concluded.

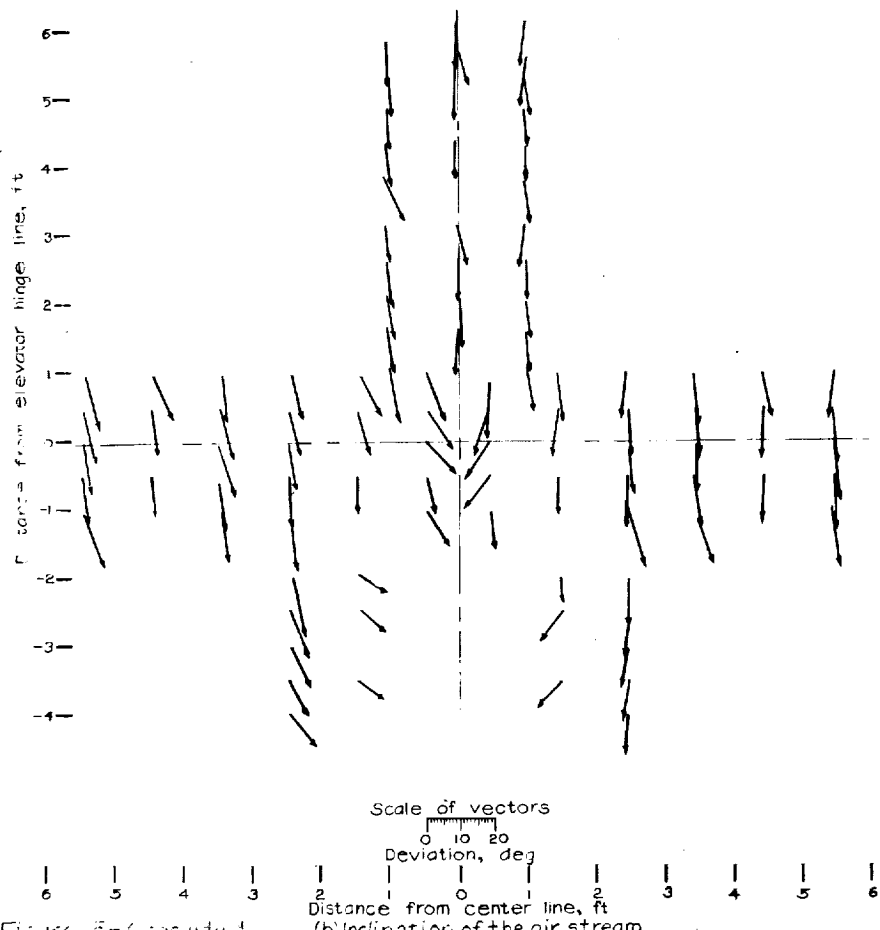
(b) Inclination of the air stream.





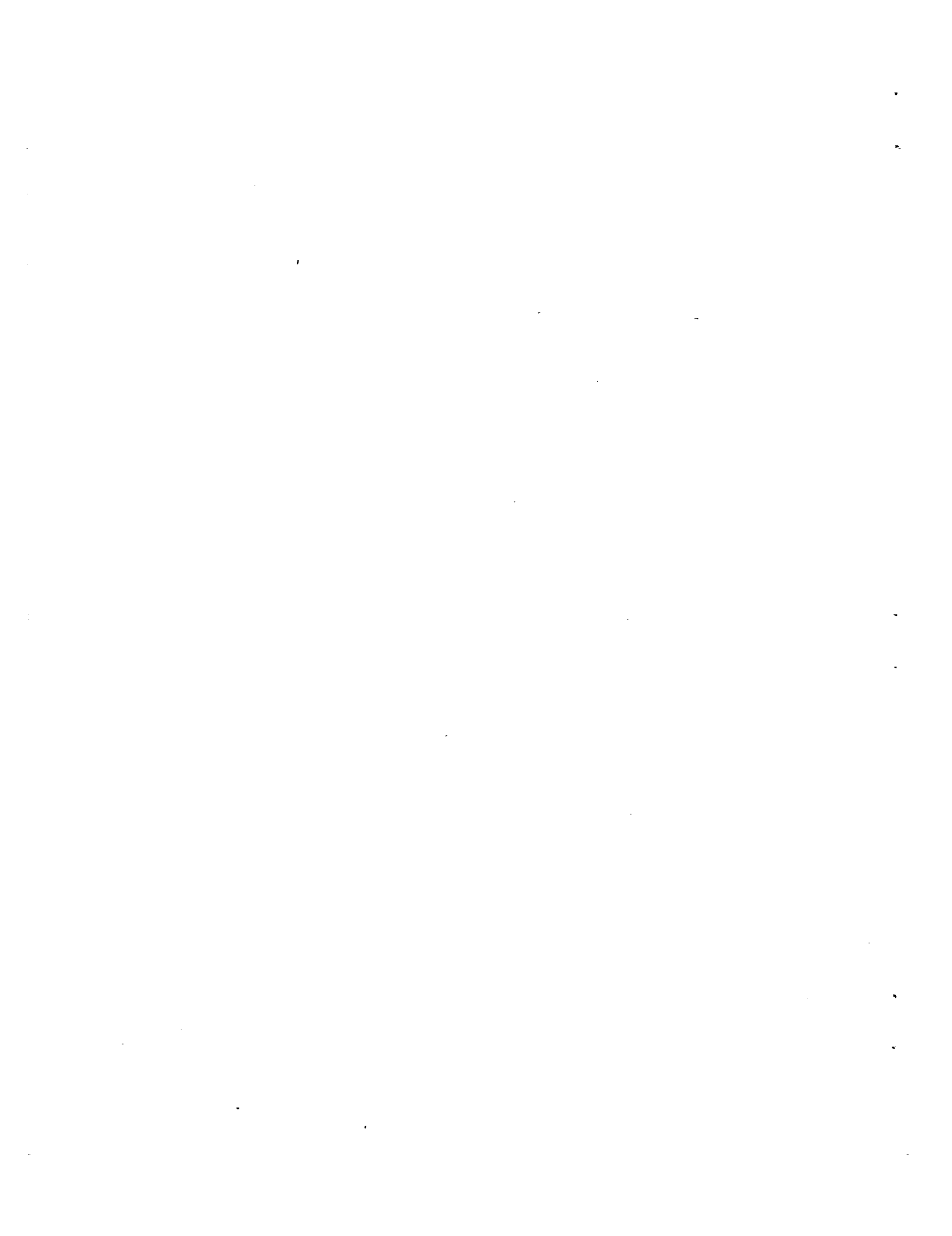
(a) Dynamic pressure (q/q_0) contours.

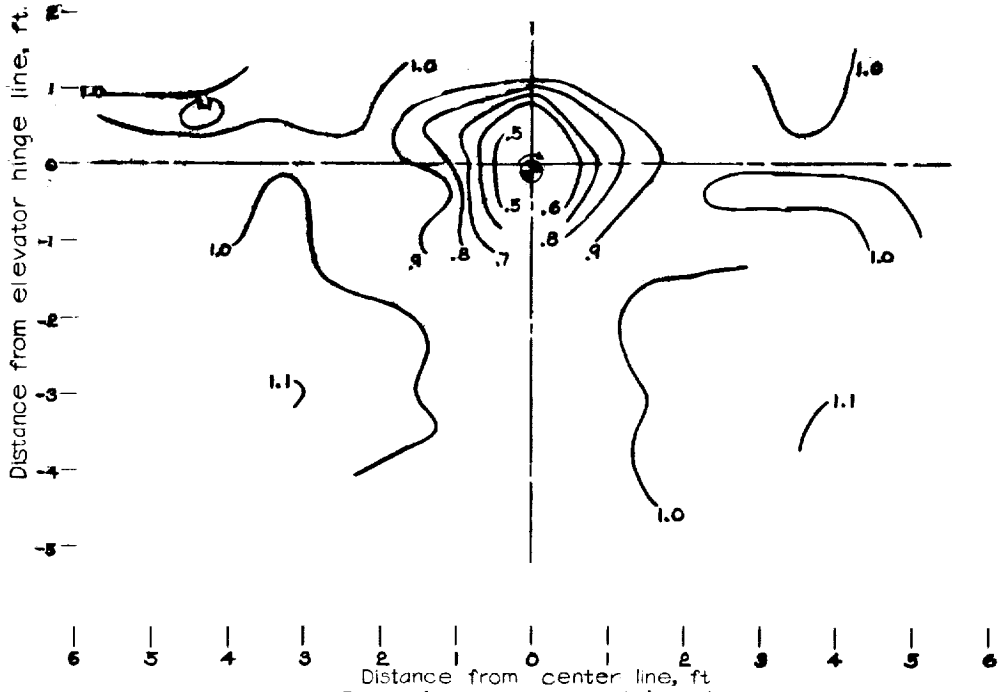
Figure 15. Air flow in the plane of the elevator hinge line. View looking forward; $d_T, 15.1^\circ$; $d_f, 40^\circ$; propeller removed.



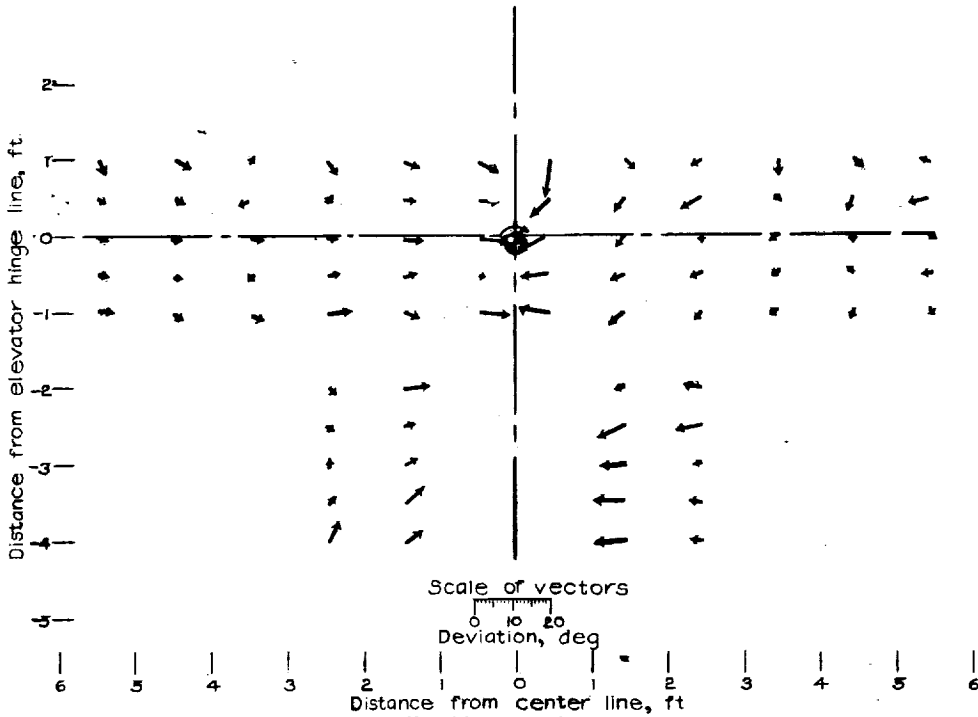
(b) Inclination of the air stream

Figure 15-Cont'd

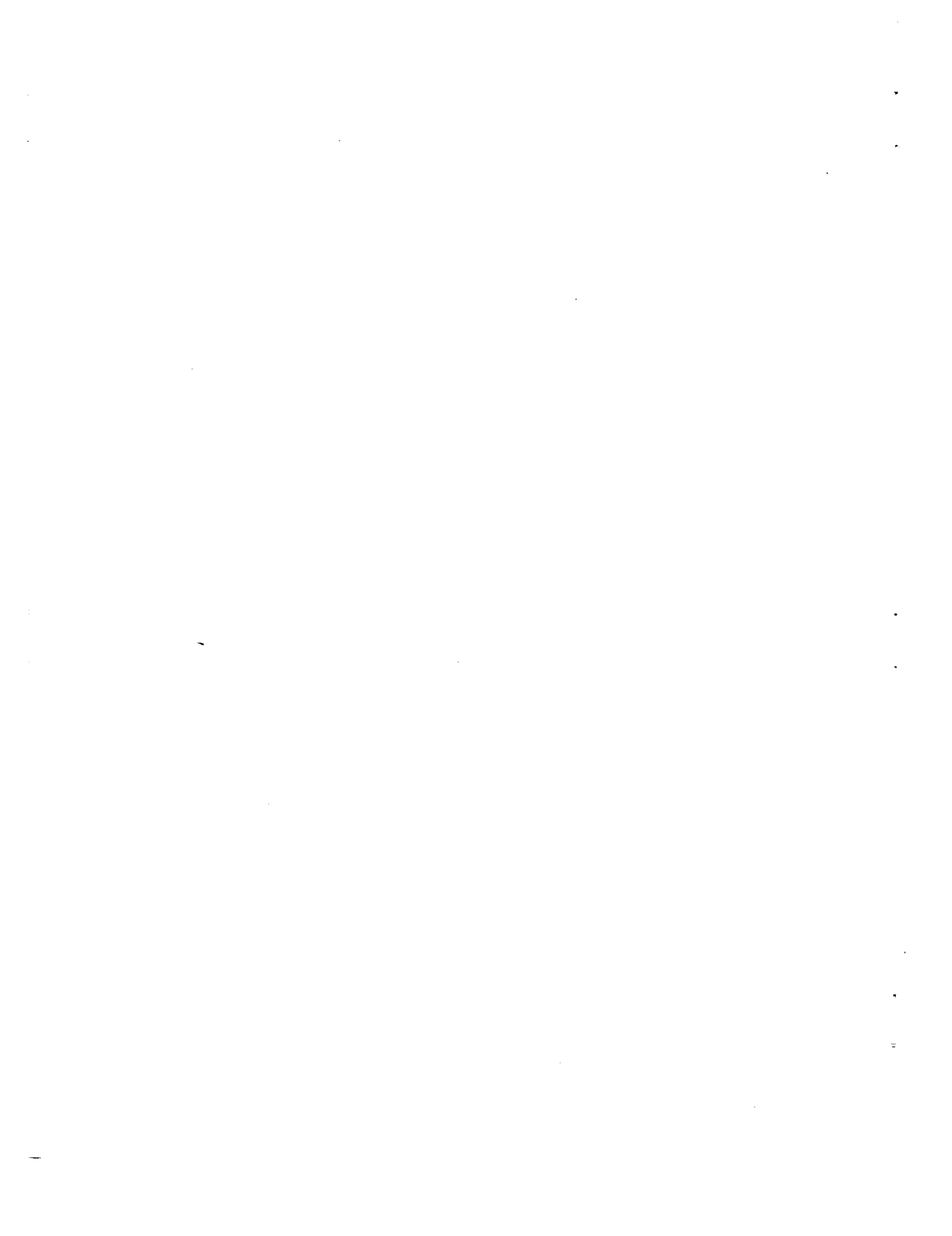


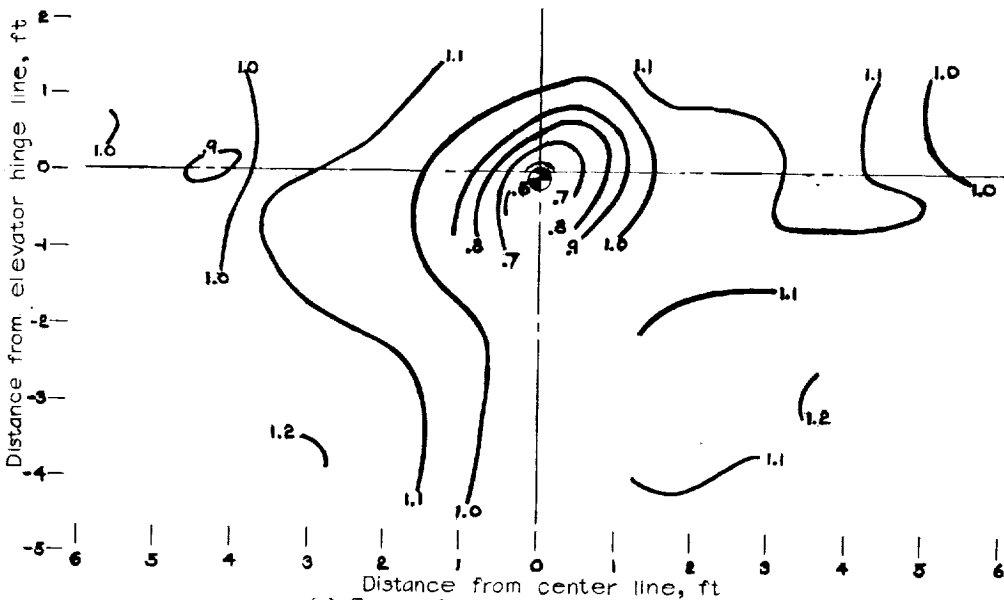


(a) Dynamic-pressure (q/q_0) contours.
Figure 16.- Air flow in the plane of the elevator hinge line. View looking forward; $\alpha_T, -0.2^\circ$; $\delta_f, 0^\circ$; $T_c, 0.014$.



(b) Inclination of air stream.
Figure 16.- Concluded





(a) Dynamic-pressure (q/q_0) contours.
 Figure 17.- Air flow in the plane of the elevator hinge line. View looking forward; $\alpha_T, -0.2^\circ$; $\delta_f, 0^\circ$; $T_c, 0.04$.

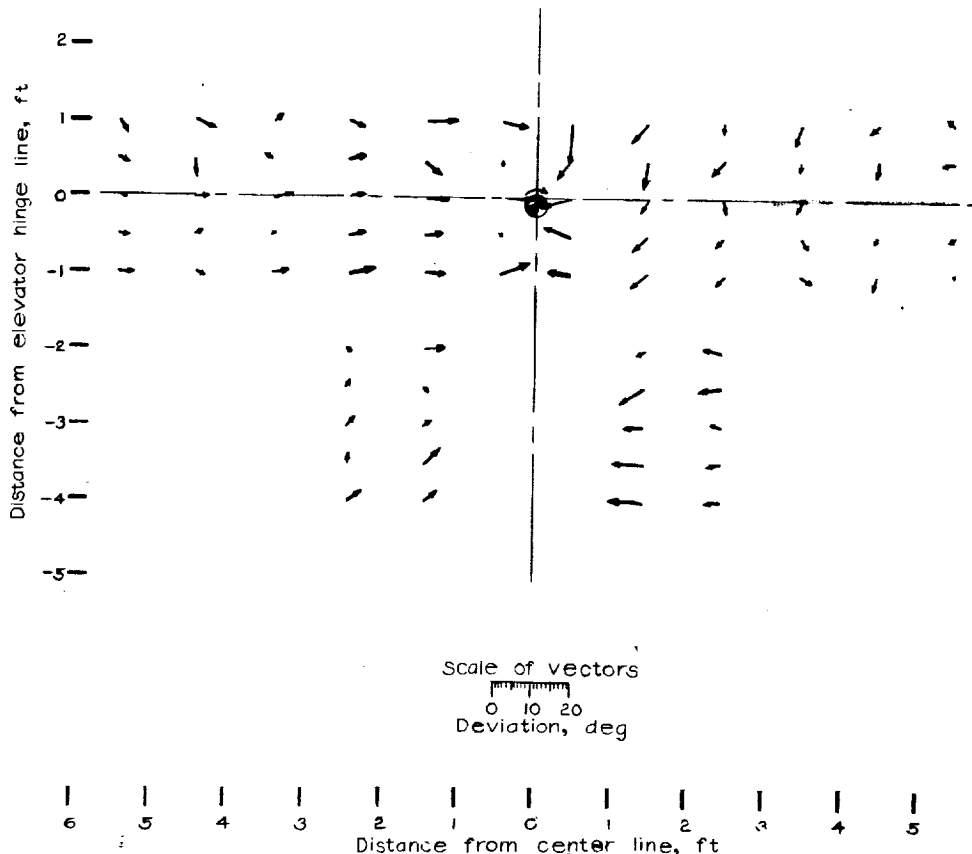
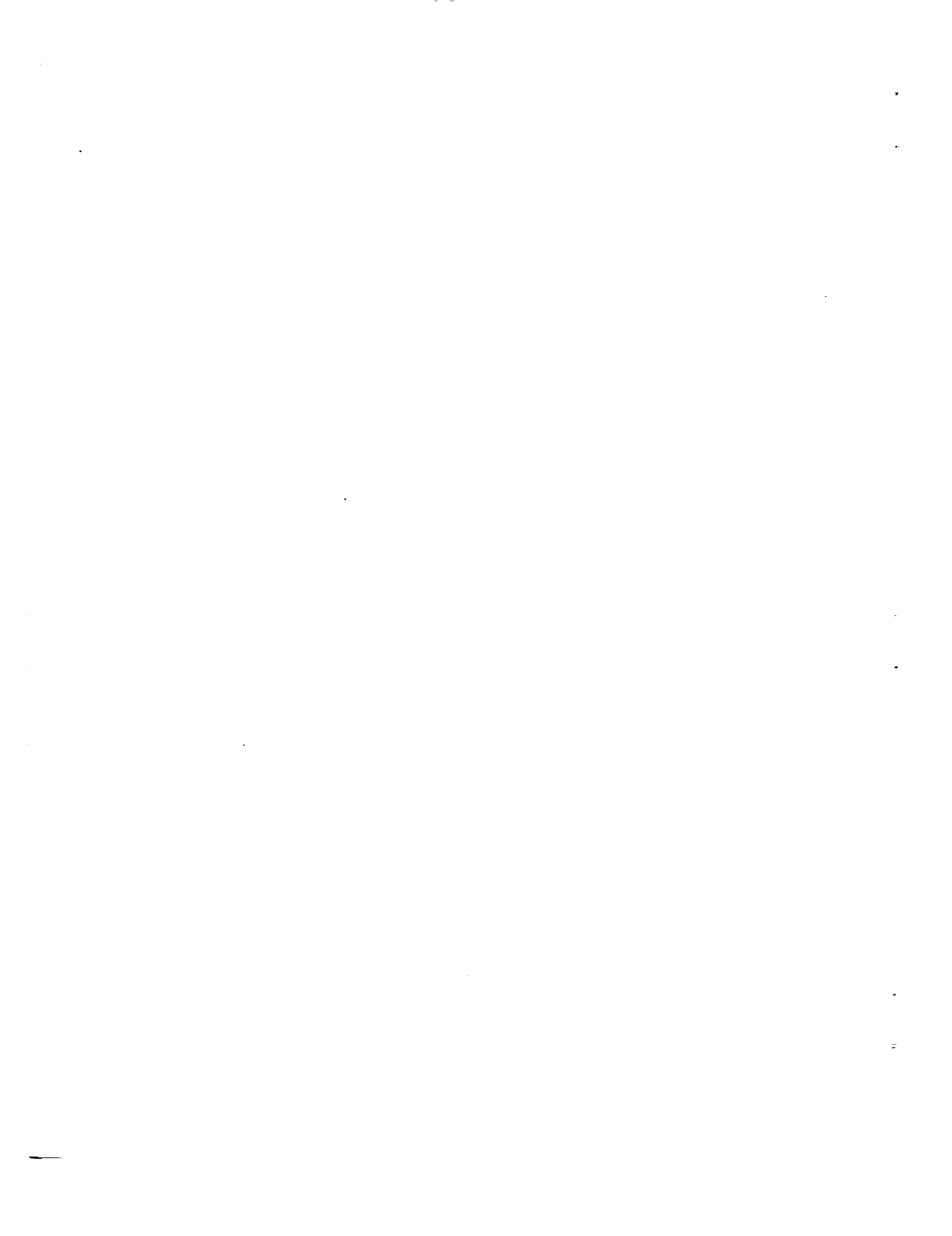


Figure 17.-Concluded.

(b) Inclination of the air stream.



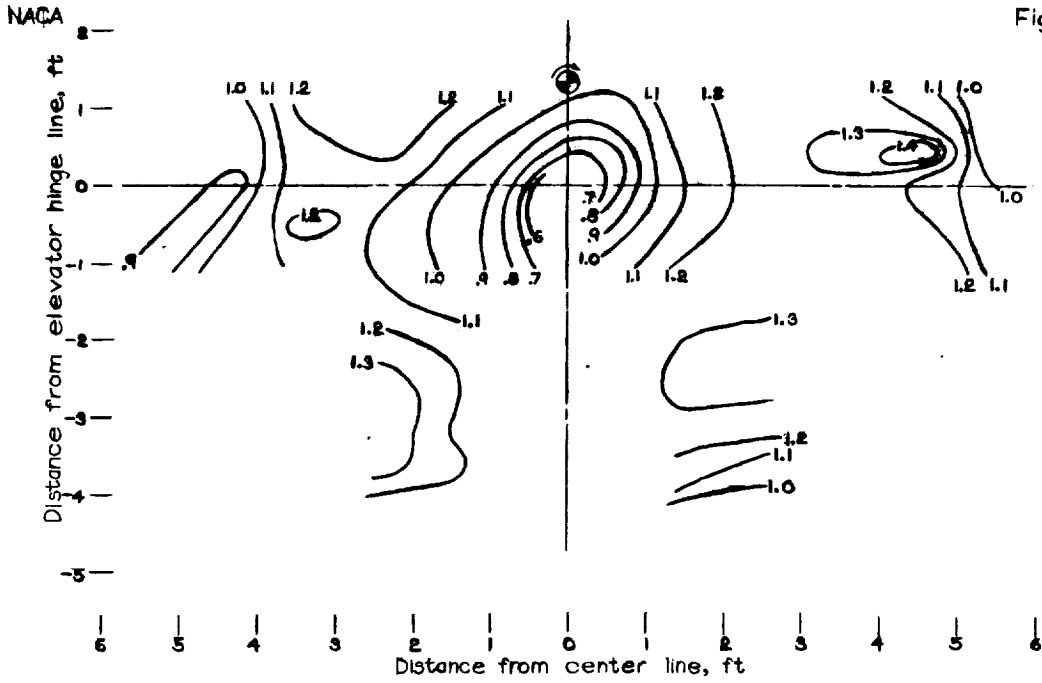


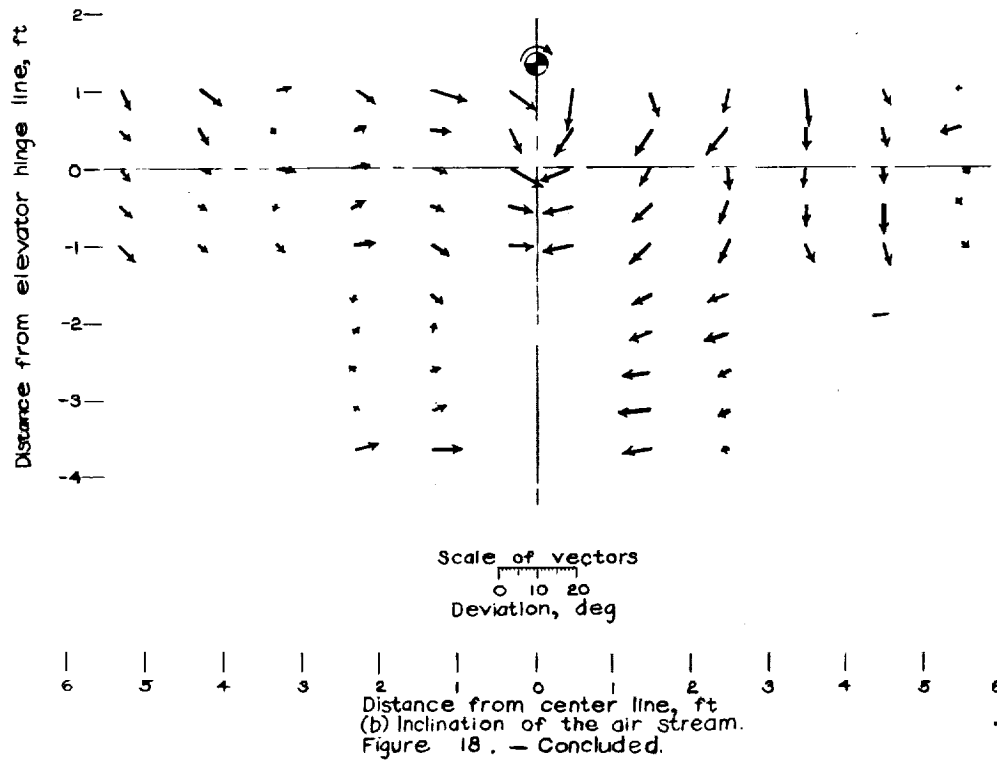
Fig. 18

(a) Dynamic-pressure (q/q_0) contours.

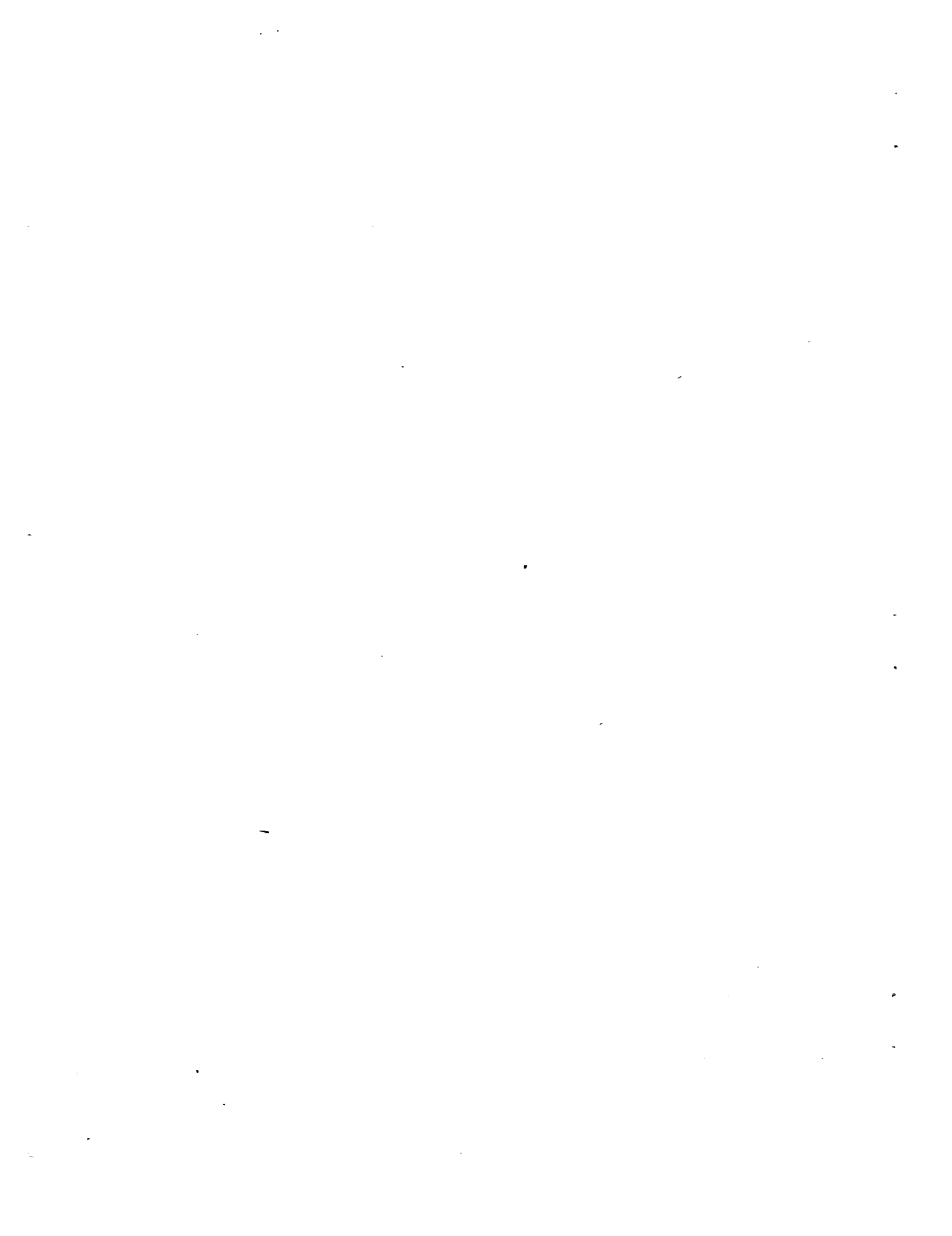
Figure 18. -Air flow in the plane of the elevator hinge line.

View looking forward; $\alpha_T, 3.1^\circ$

$\delta_f \sigma: T_c, 0.09.$



(b) Inclination of the air stream.
Figure 18. - Concluded.



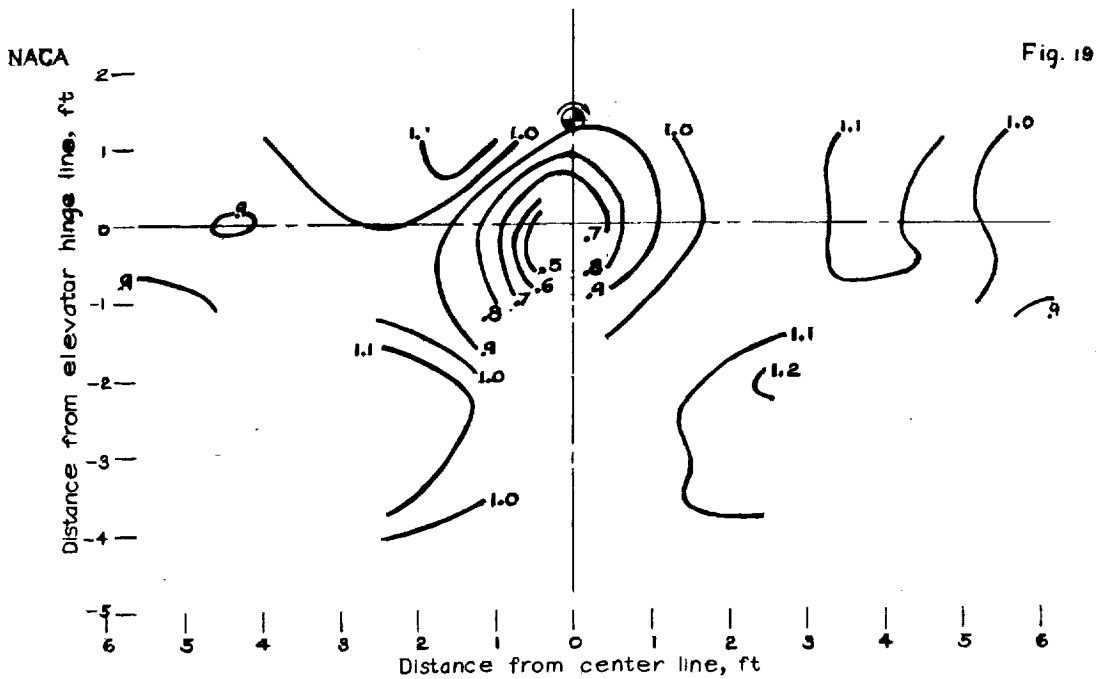


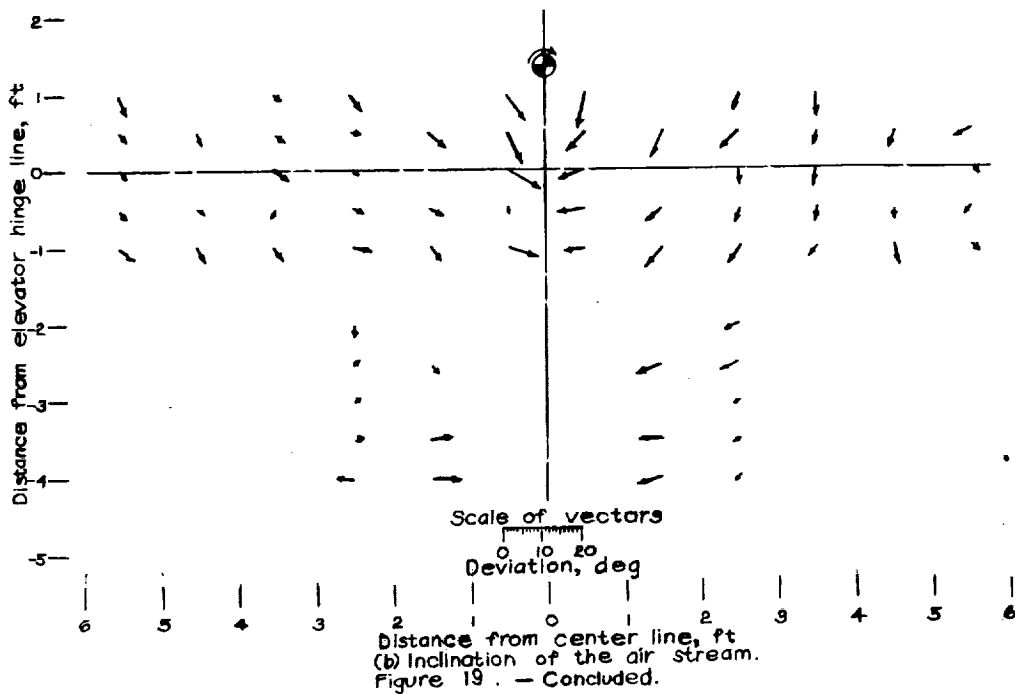
Fig. 19

(a) Dynamic-pressure (q/q_0) contours.

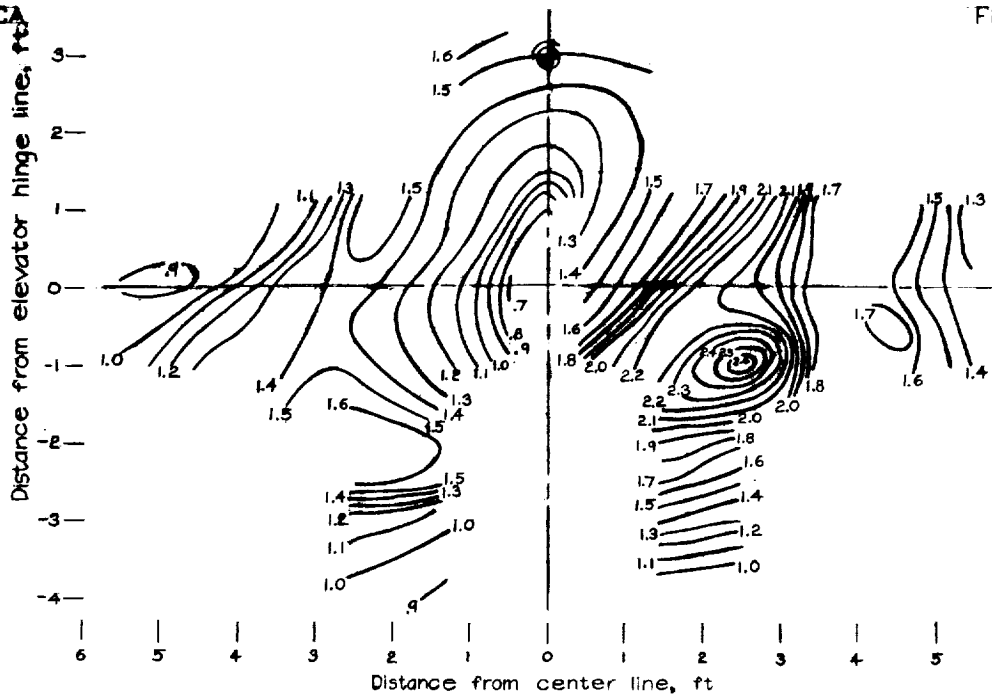
Figure 19. - Air flow in the plane of the elevator hinge line.

View looking forward; $\alpha_T, 3.1^\circ$

$\alpha_f, 0^\circ$; $T_c, 0.03$.



(b) Inclination of the air stream.
Figure 19. - Concluded.

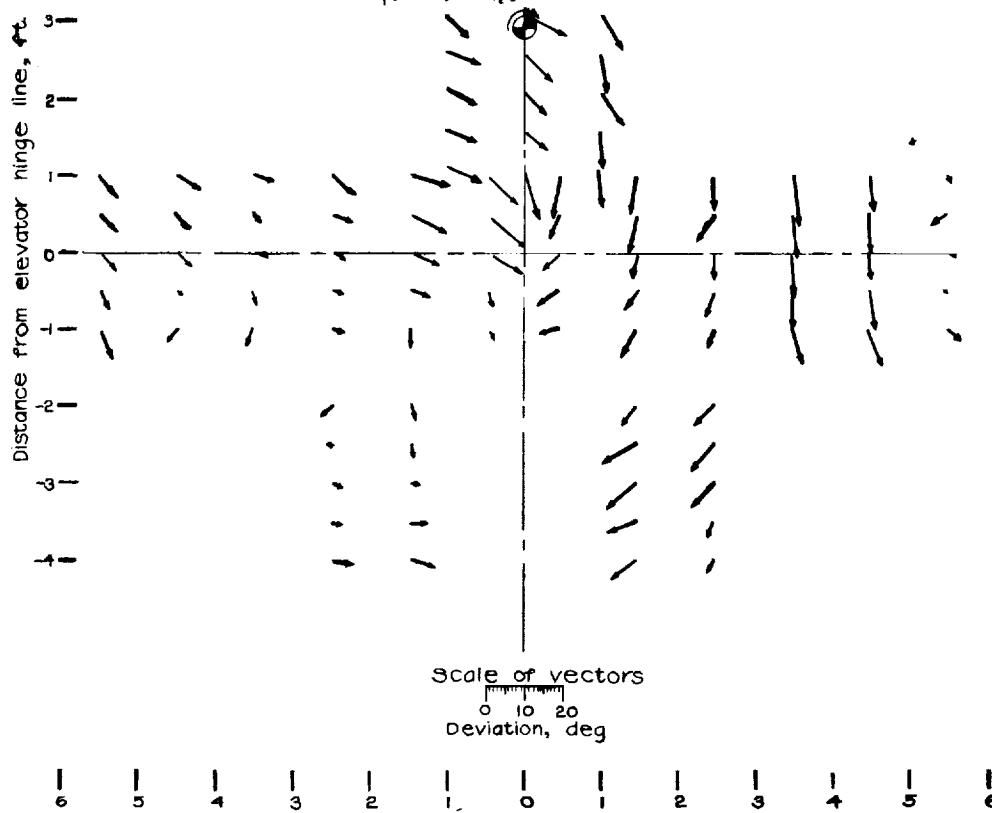


(a) Dynamic-pressure (q/q_0) contours.

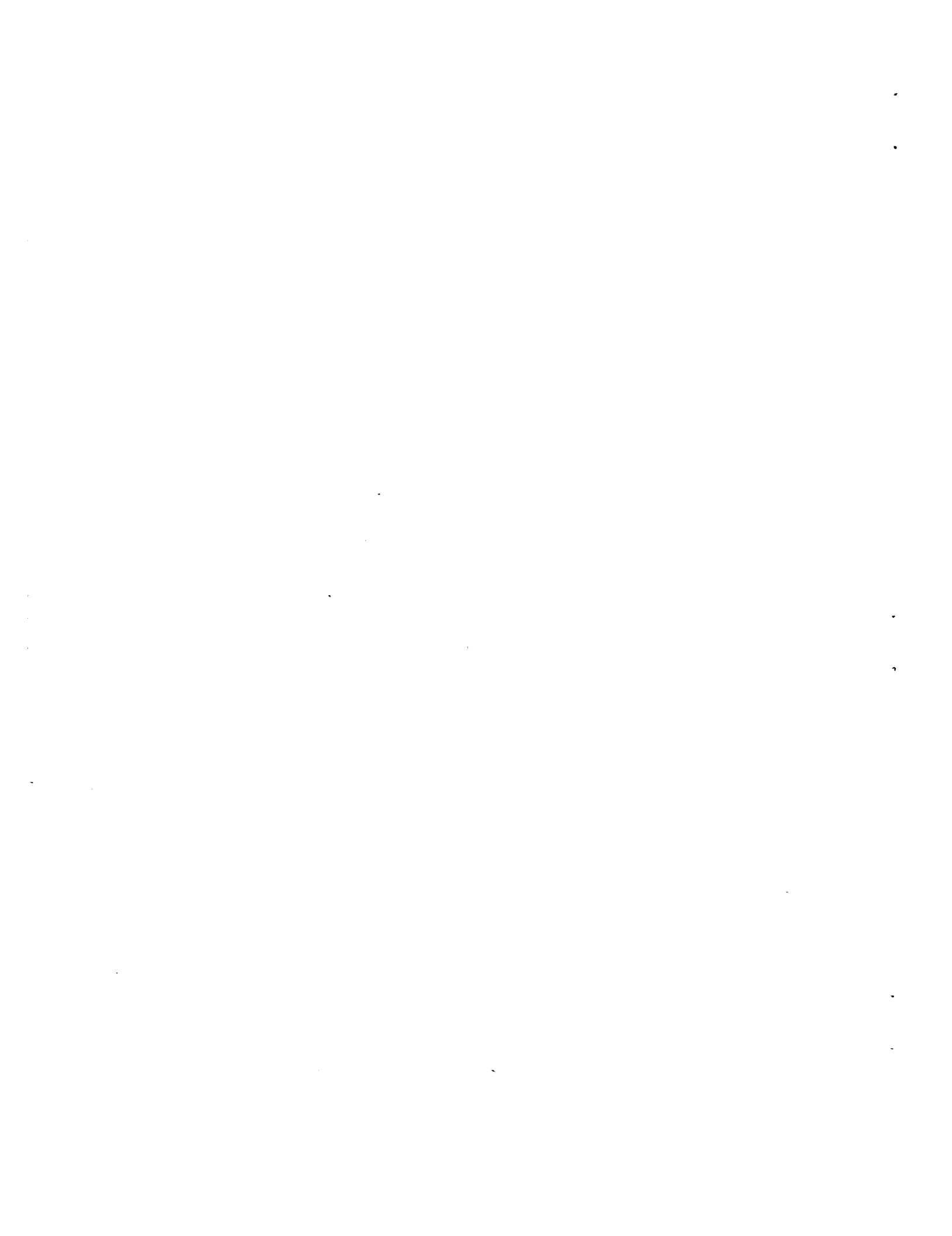
Figure 20. —Air flow in the plane of the elevator hinge line.

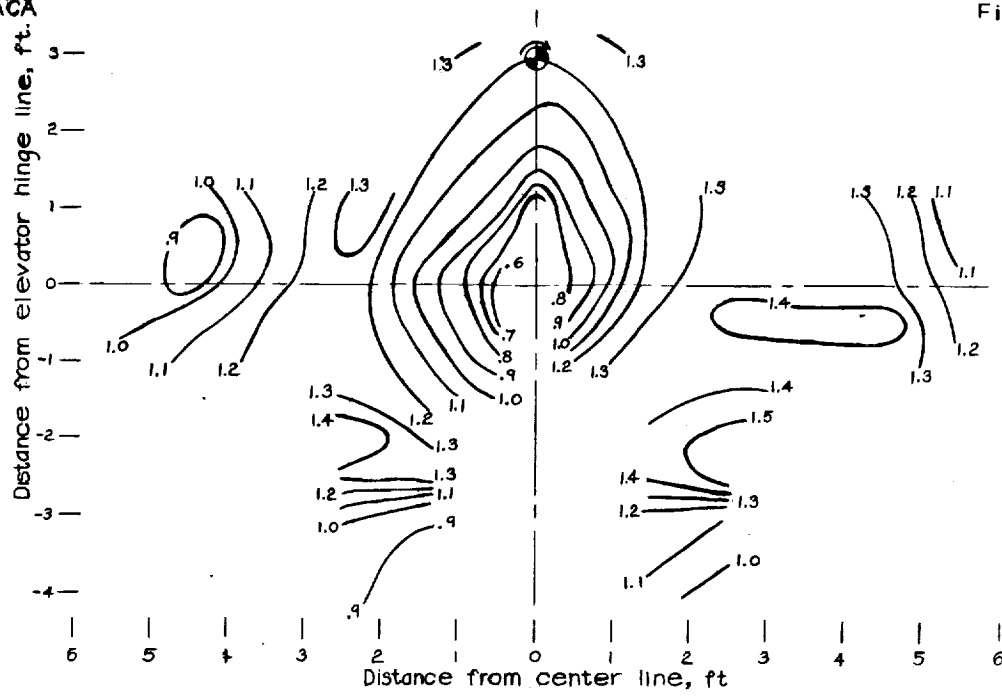
View looking forward; $\alpha_T, 6.8^\circ$;

$\alpha_f, 0^\circ$; $T_r, 0.18$.

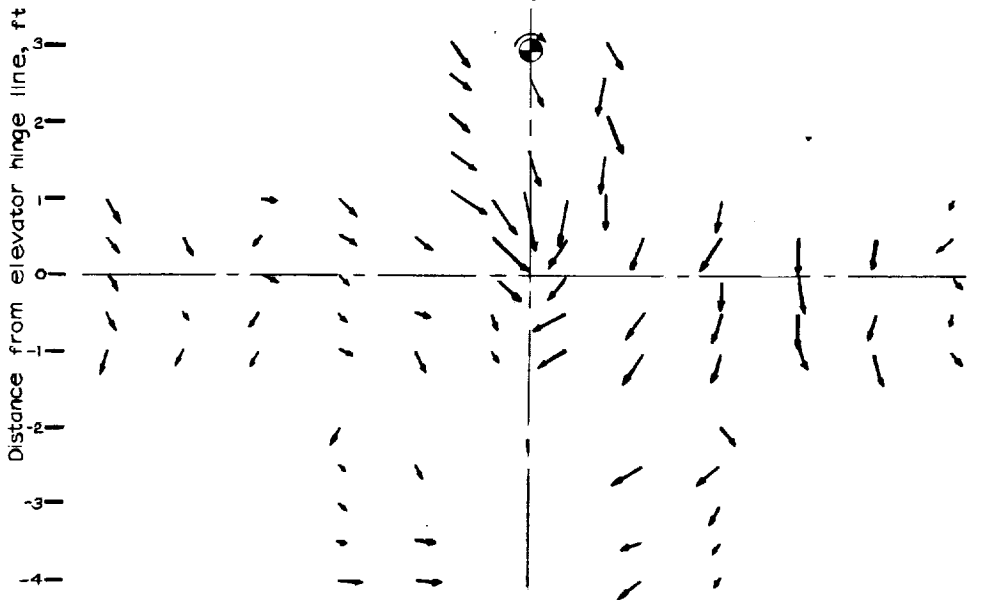


(b) Inclination of the air stream.
Figure 20. —Concluded.





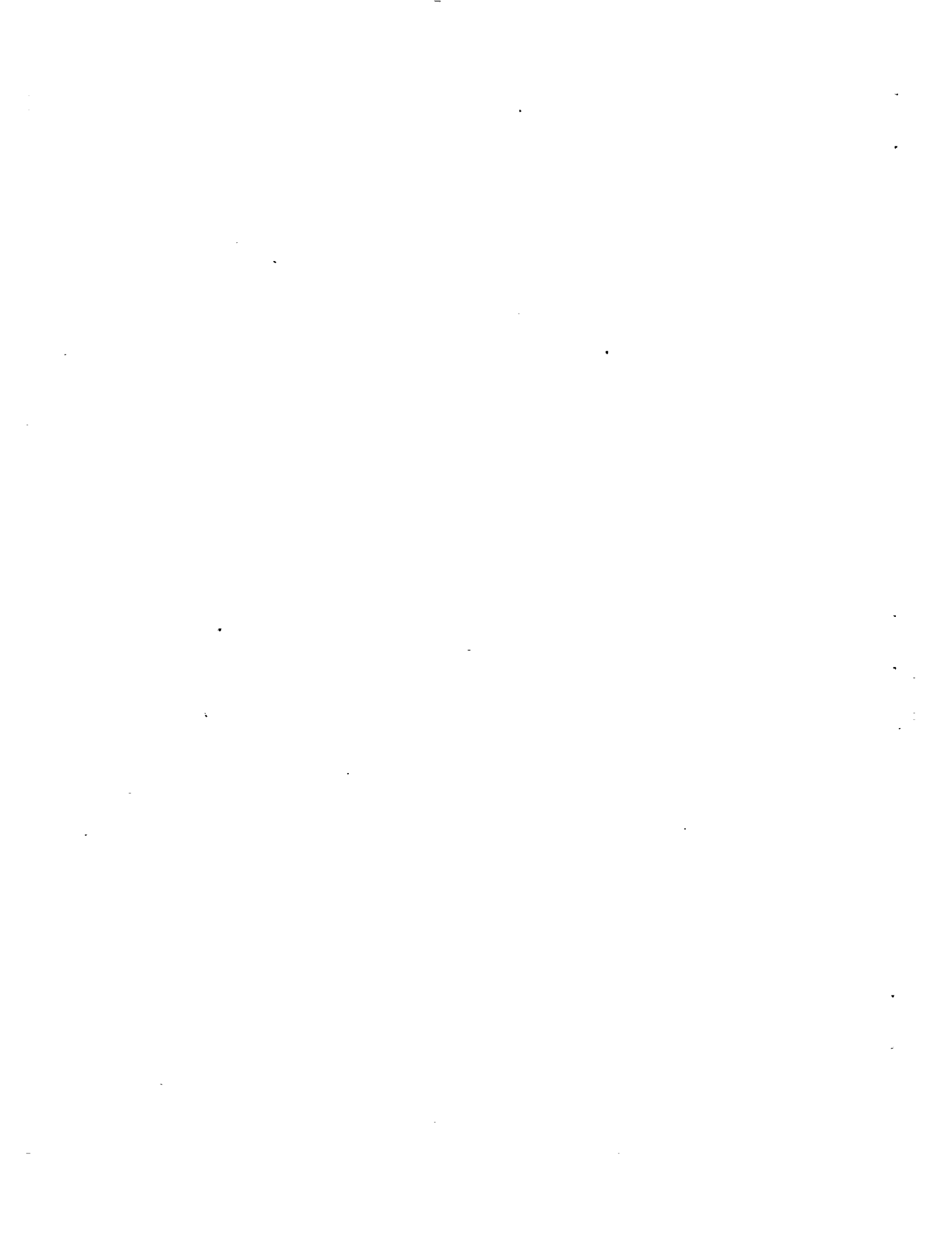
(a) Dynamic-pressure (q/q_0) contours.
 Figure 21. - Air flow in the plane of the elevator hinge line.
 View looking forward; $\alpha_T, 6.8^\circ$;
 $\delta_T, 0^\circ$; $T_c, 0.11$.

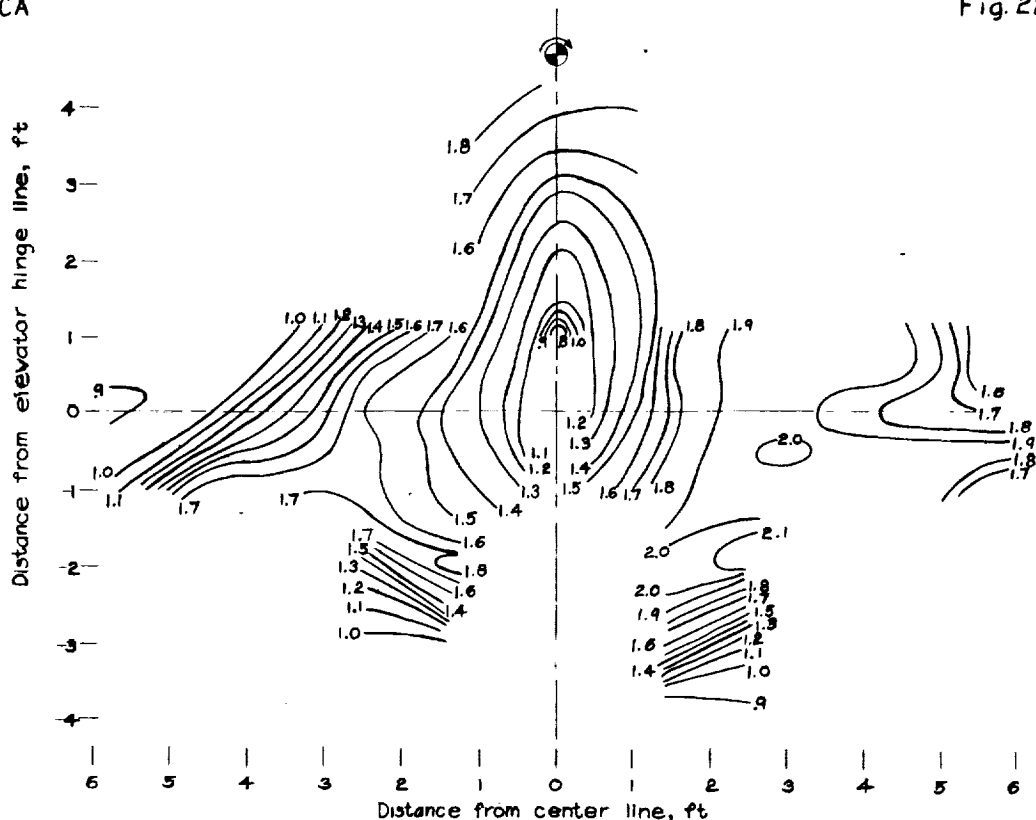


Scale of vectors
 0 10 20
 Deviation, deg

6 5 4 3 2 1 0 1 2 3 4 5 6
 Distance from center line, ft

(b) Inclination of the air stream.
 Figure 21. - Concluded.





(a) Dynamic-pressure (q/q_0) contours.
 Figure 22.- Airflow in the plane of the elevator hinge line. View looking forward;
 $\alpha_T, 10.7^\circ; \delta_f, 0^\circ; T_c, 0.31$.

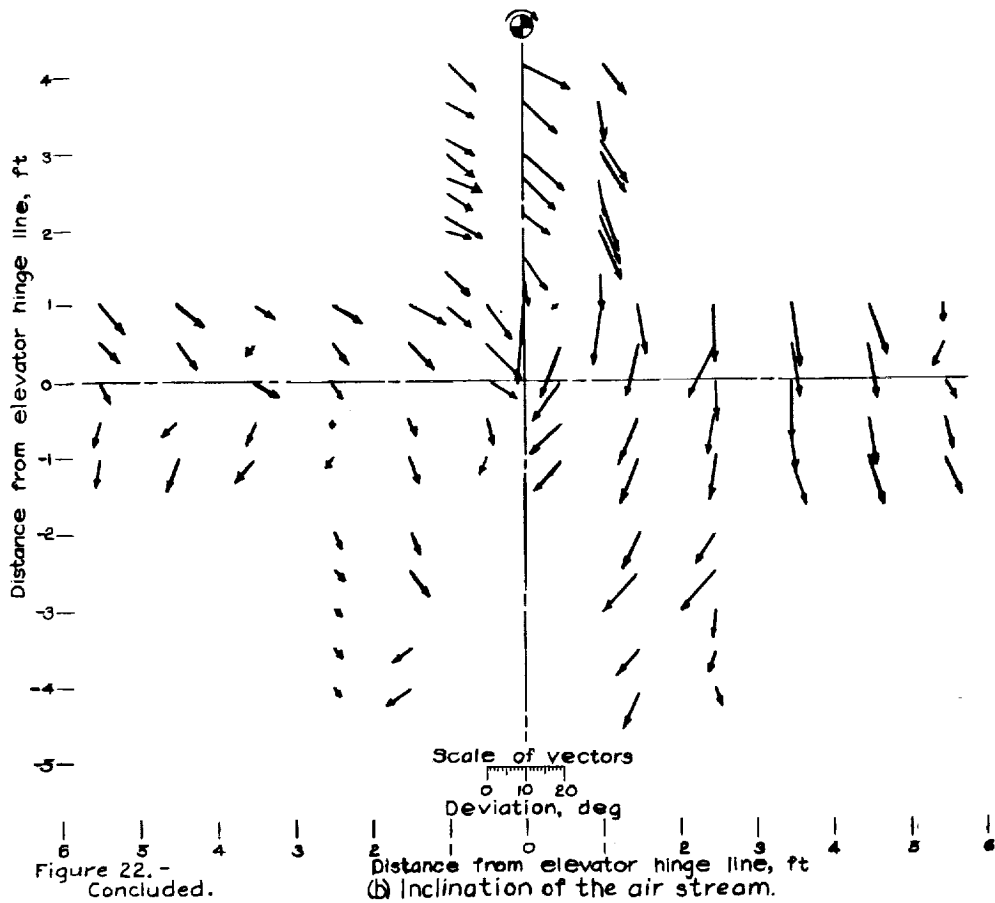
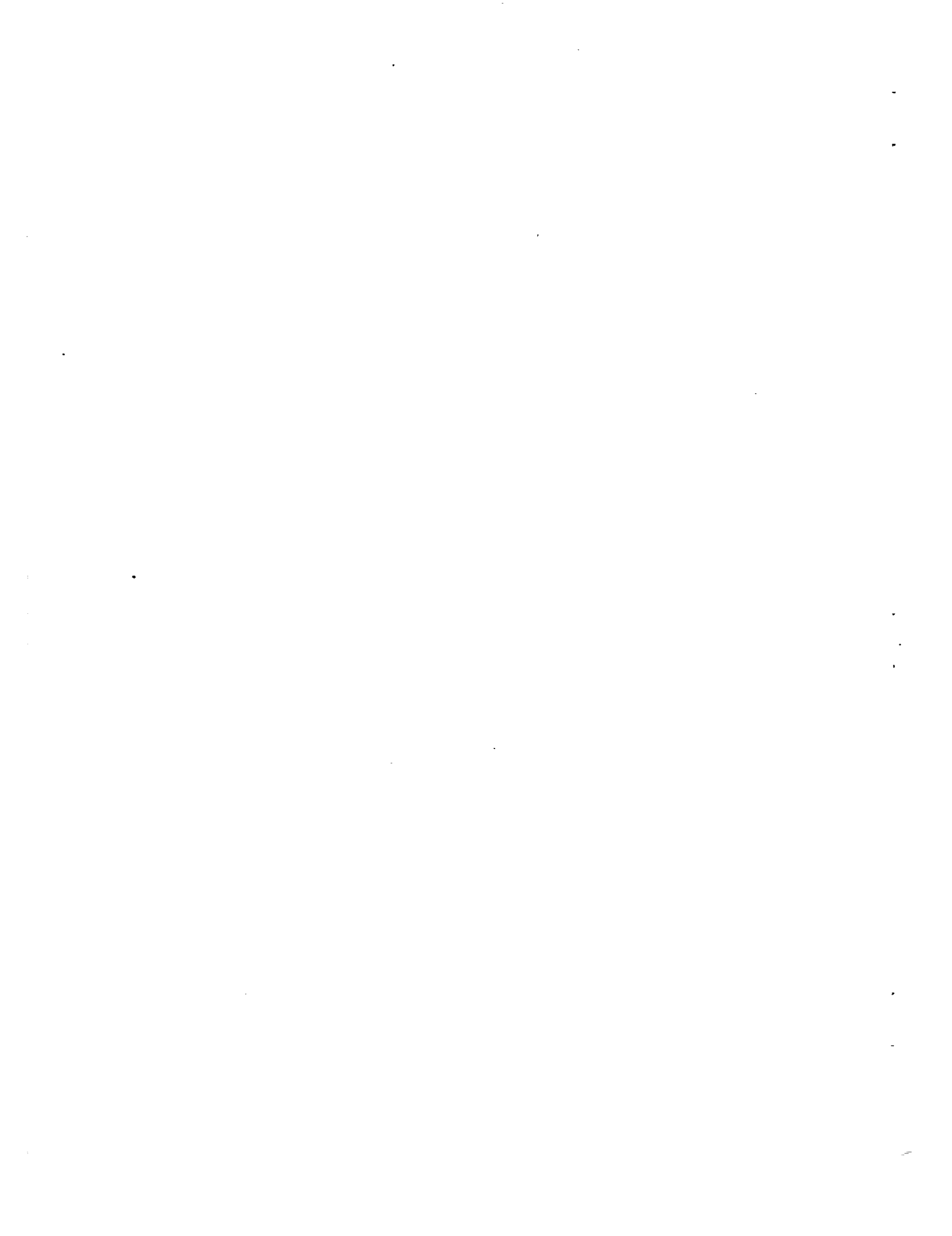
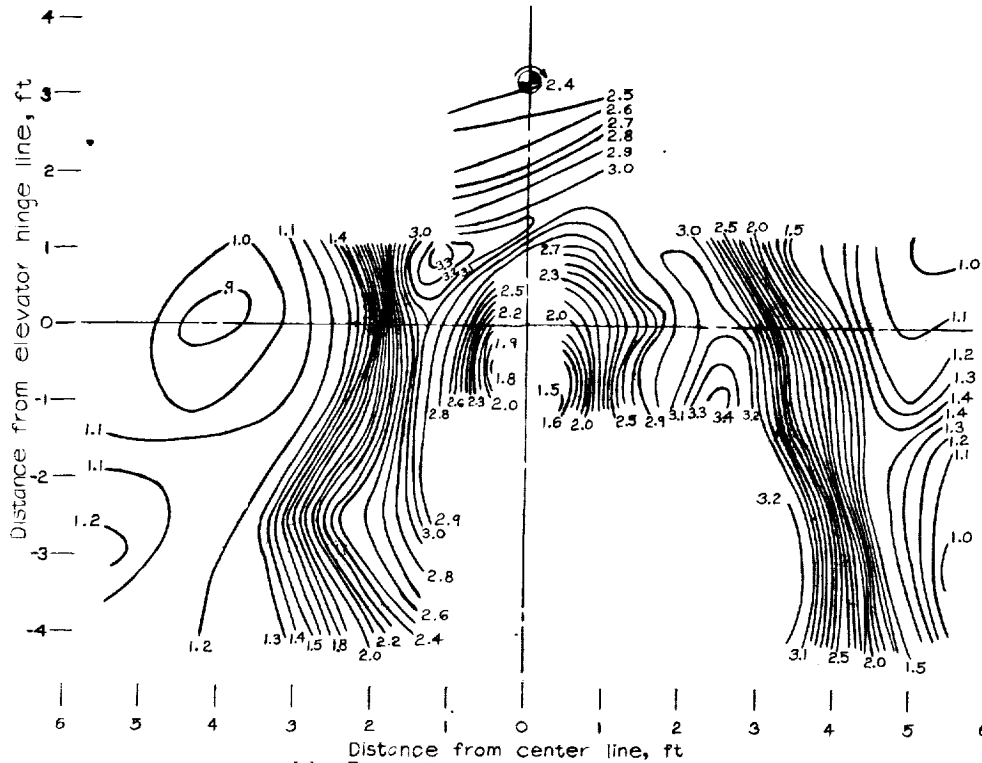


Figure 22.-
 Concluded.

(b) Inclination of the air stream.

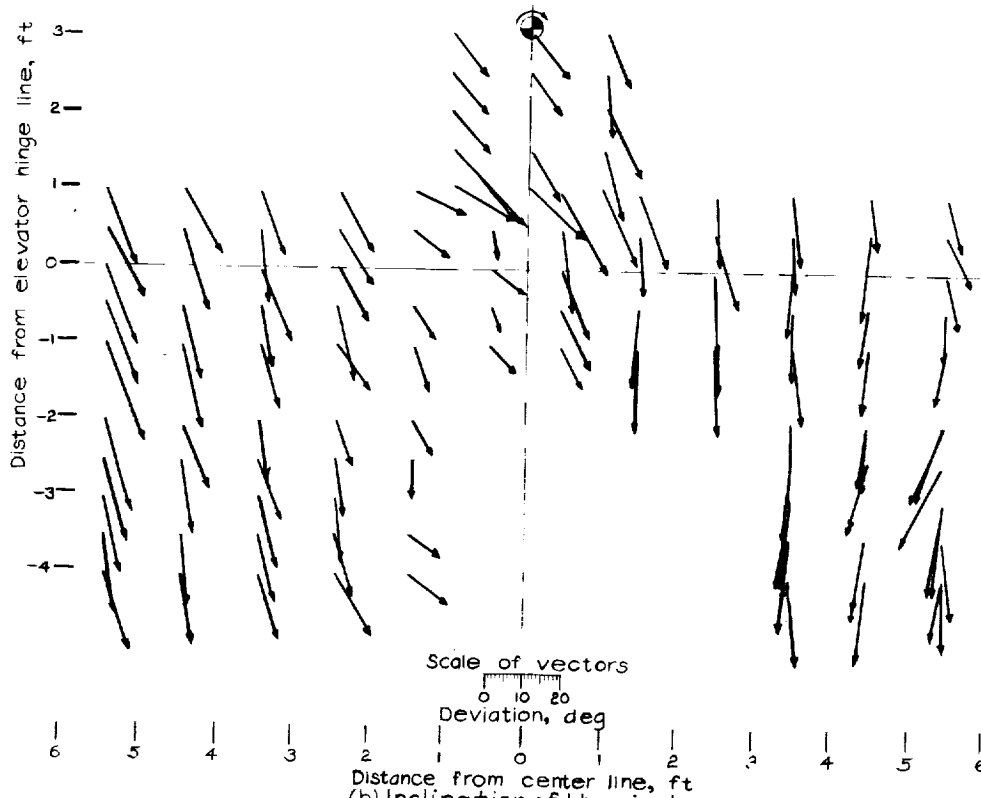
1-411





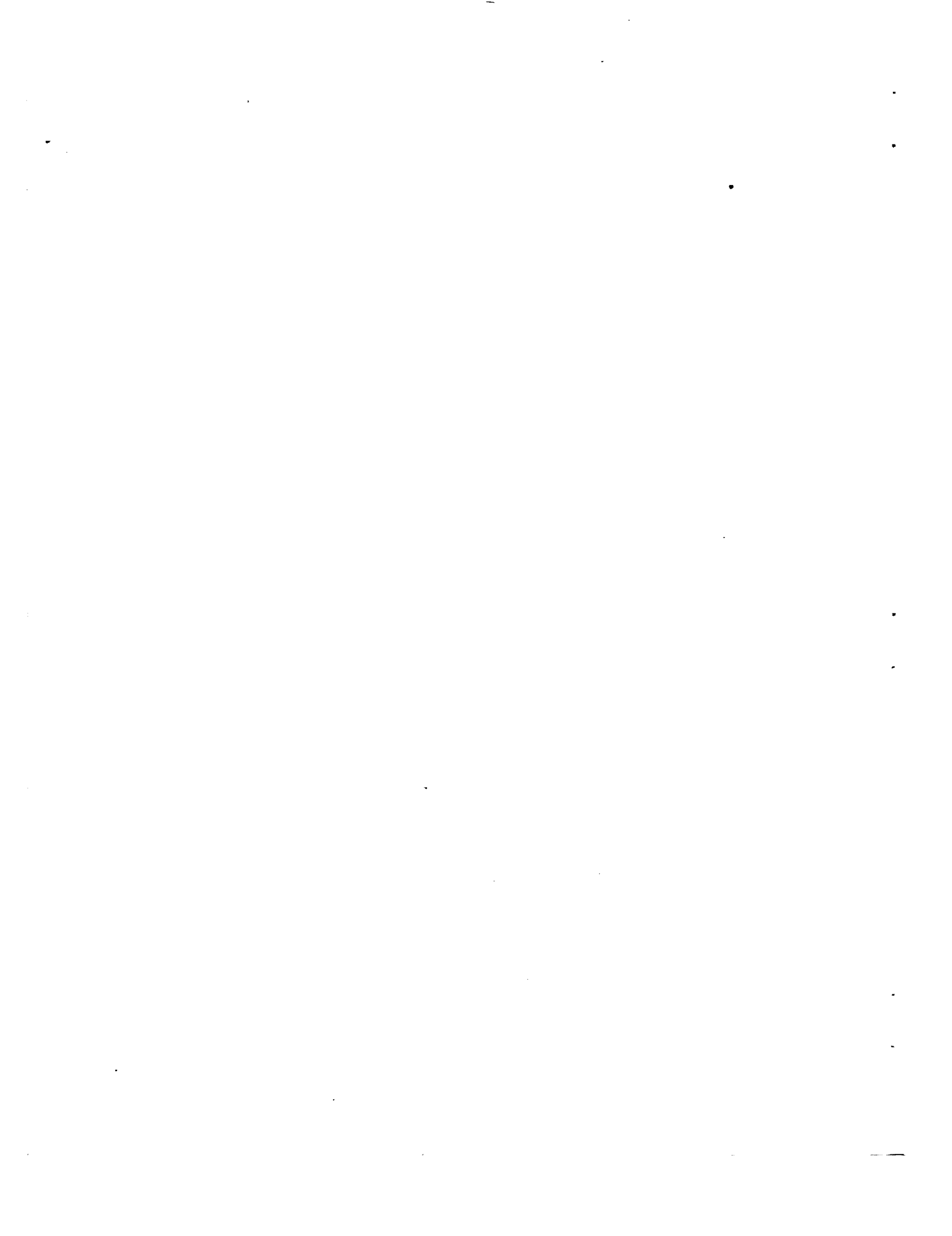
(a) Dynamic-pressure (q/q_0) contours.

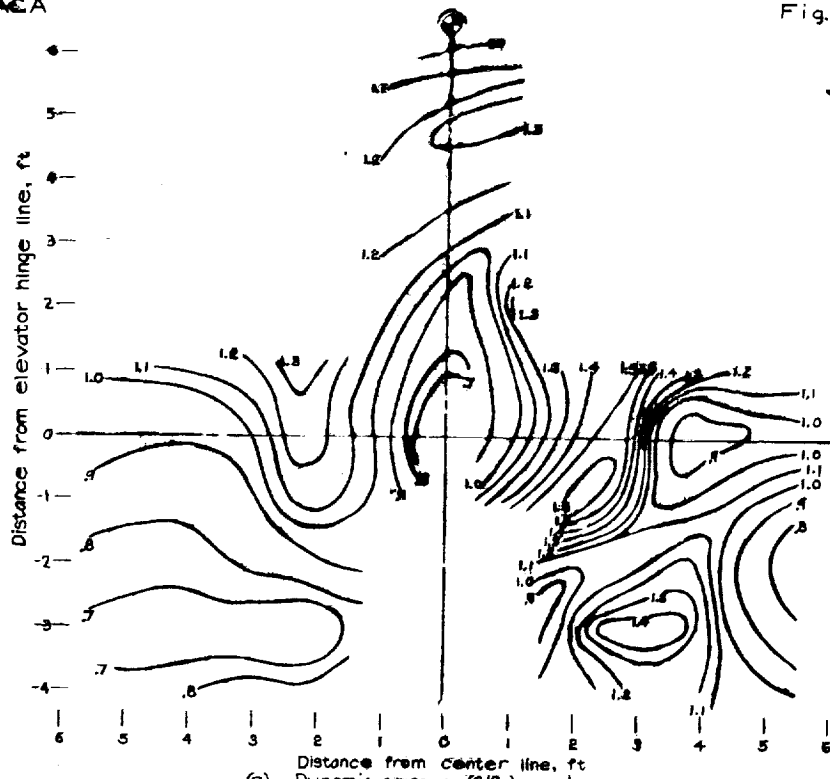
Figure 23.- Air flow in the elevator hinge line. View looking forward; α_T , 7.3° ; δ_f , 40° ; T_c , 0.52.



(b) Inclination of the airstream.

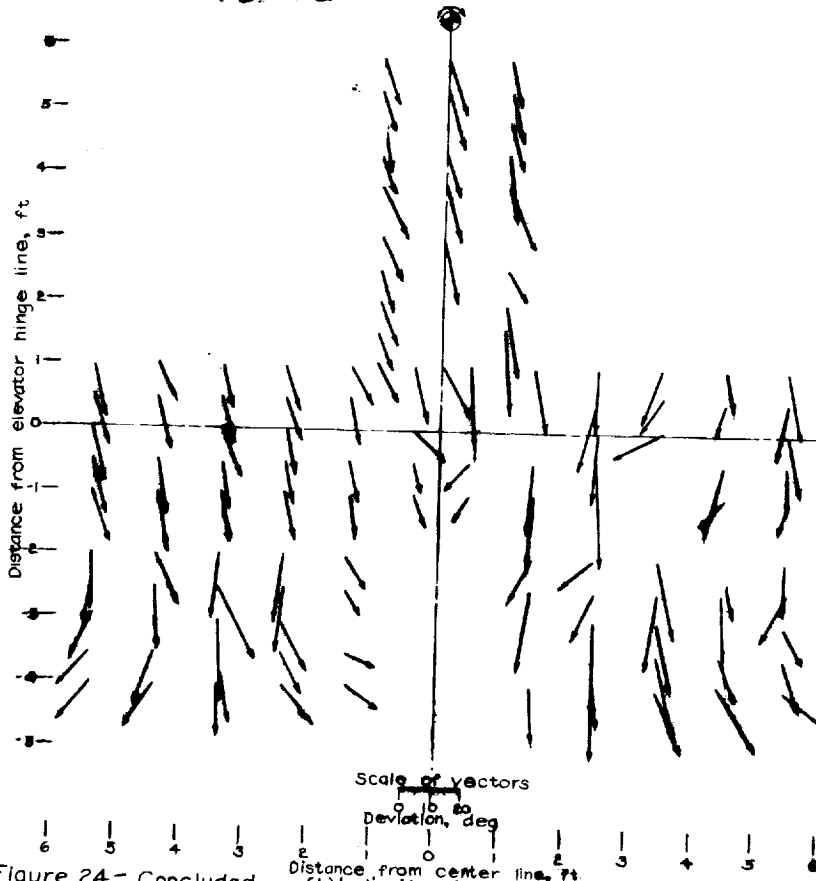
Figure 23.- Concluded.





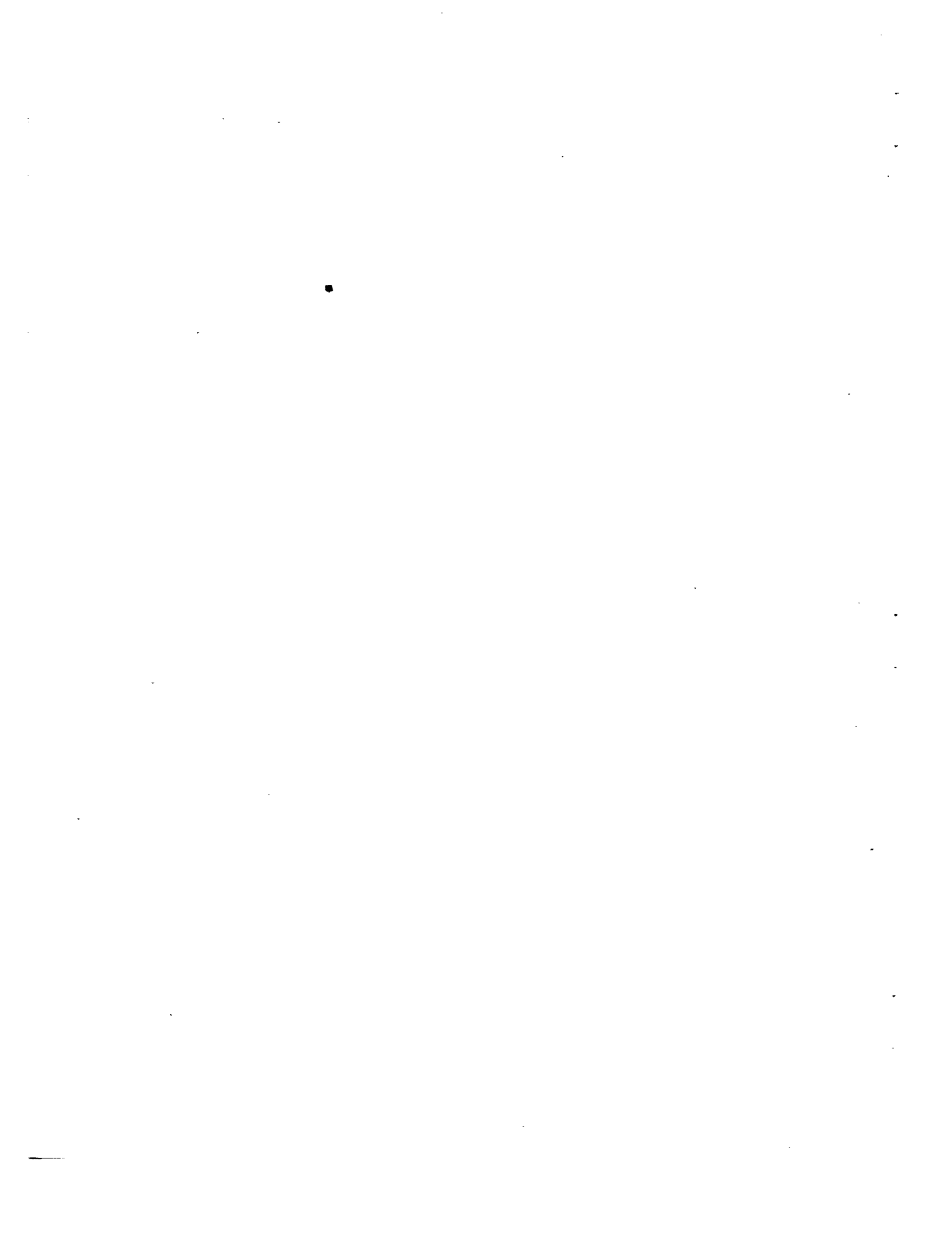
(a) Dynamic-pressure (q/q_0) contours.

Figure 24.- Air flow in the elevator hinge line. View looking forward; $\alpha_T, 15.0^\circ$; $\delta f, 4.0^\circ$; $\tau_e, 0.08$



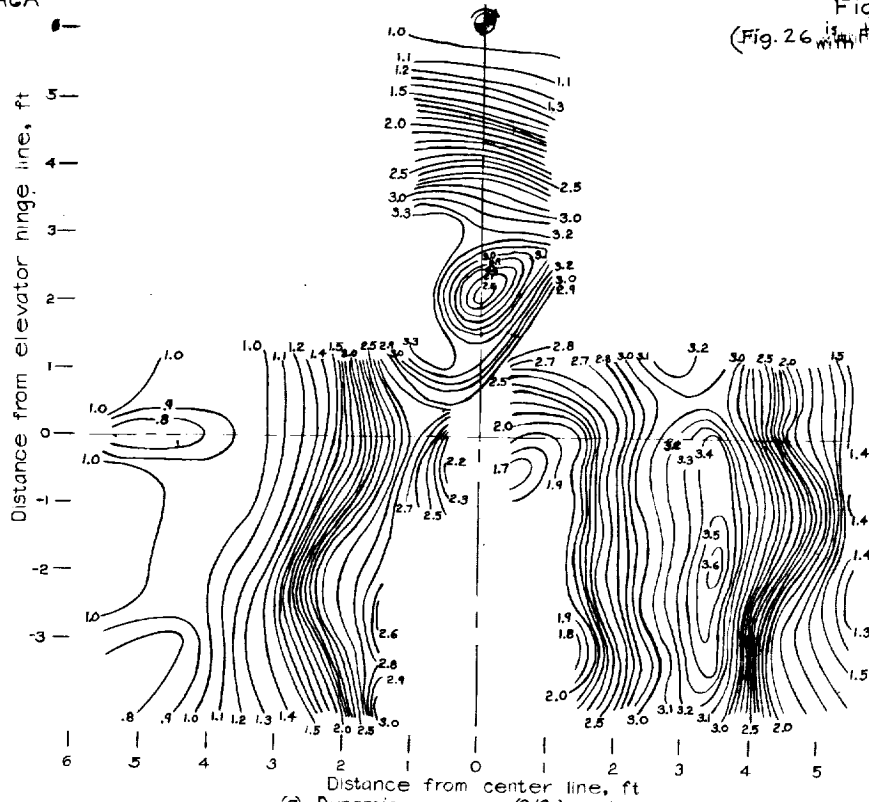
(b) Inclination of the air stream.

Figure 24.- Concluded.



NACA

Fig. 25
(Fig. 26 is in Fig. 9)



(a) Dynamic-pressure (q/q_0) contours.
Figure 25.-Air flow in the plane of the elevator hinge line. View looking forward; $\alpha_T, 14.2^\circ$; $\delta_f, 40^\circ$; $T_c, 0.58$.

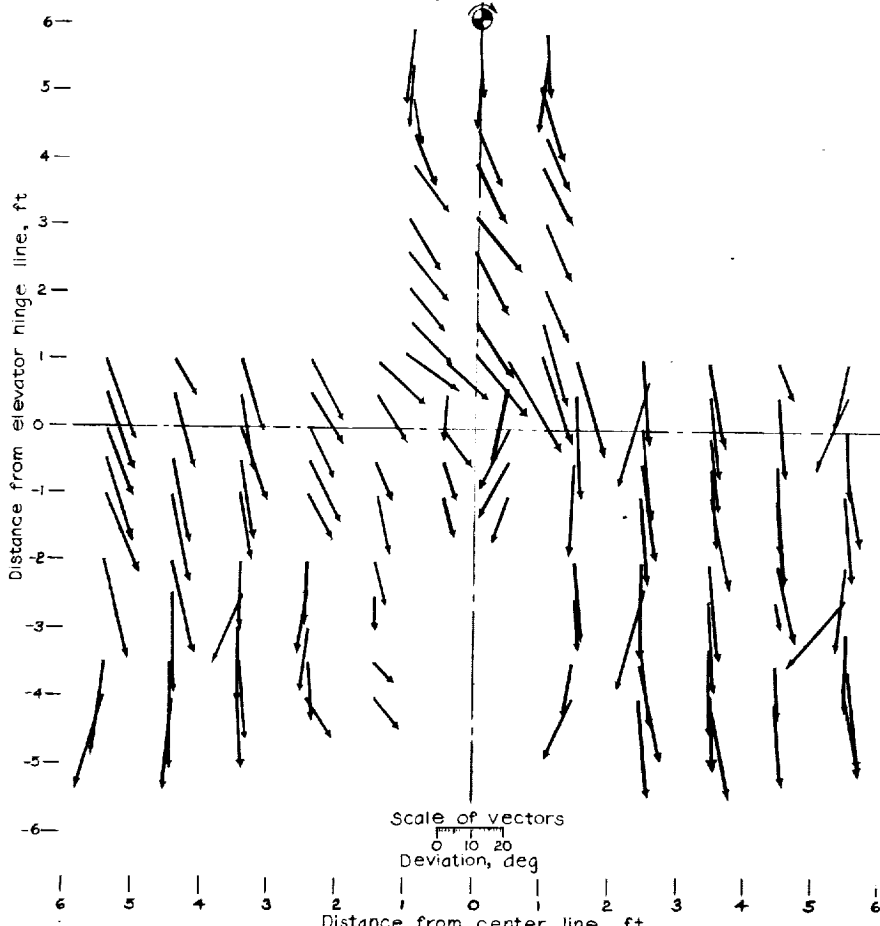
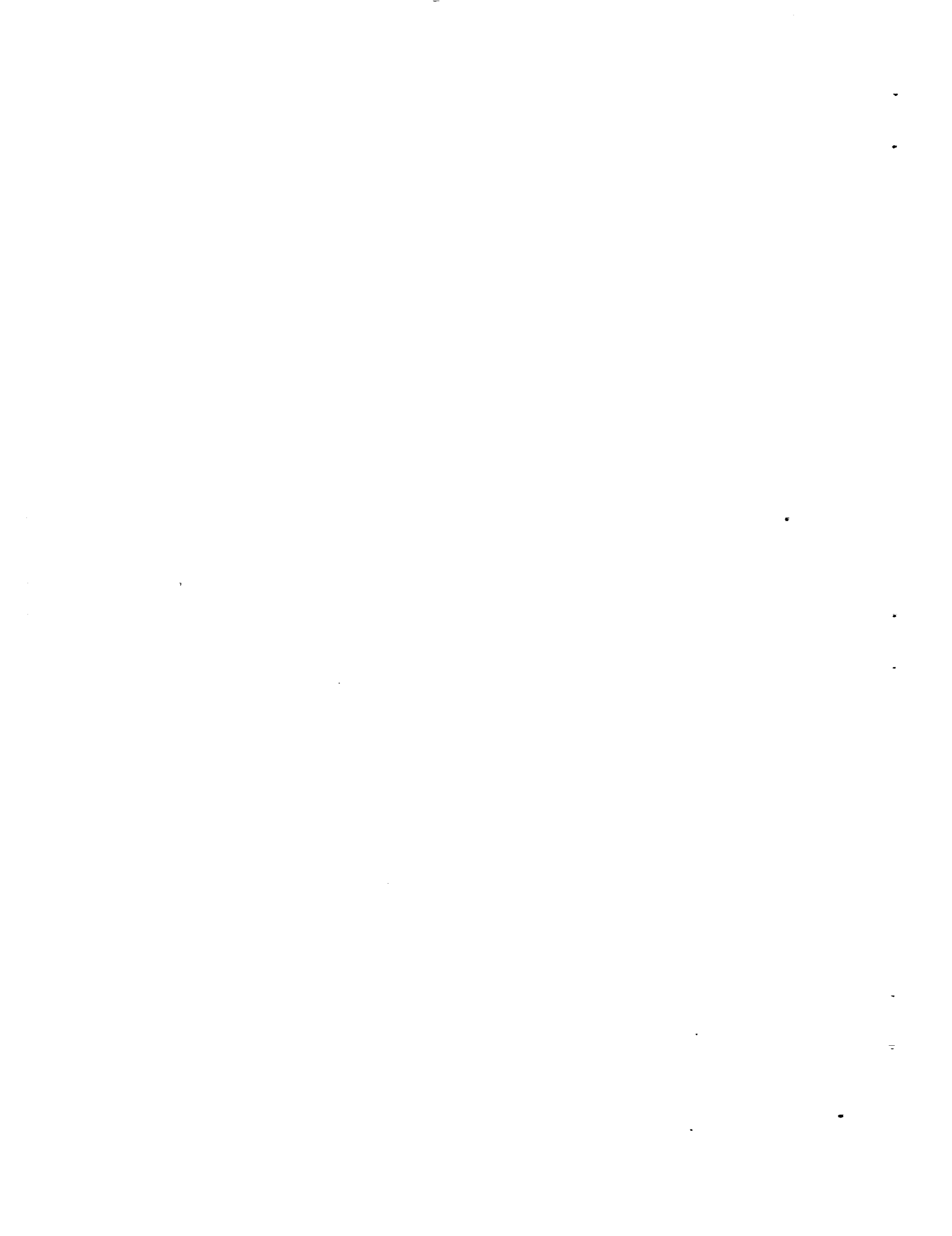


Figure 25.-Concluded.
(b) Inclination of the air stream.



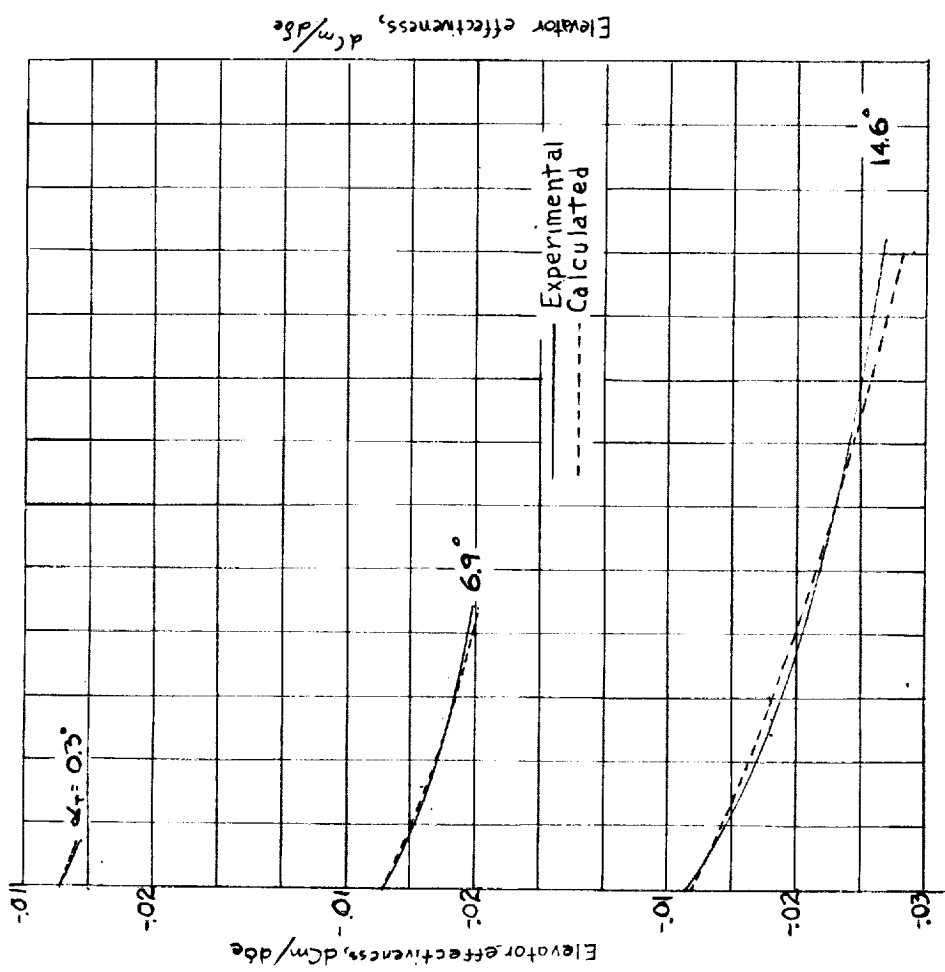


Figure 27.- Experimental and calculated effects of propeller operation on the elevator effectiveness, flaps retracted.

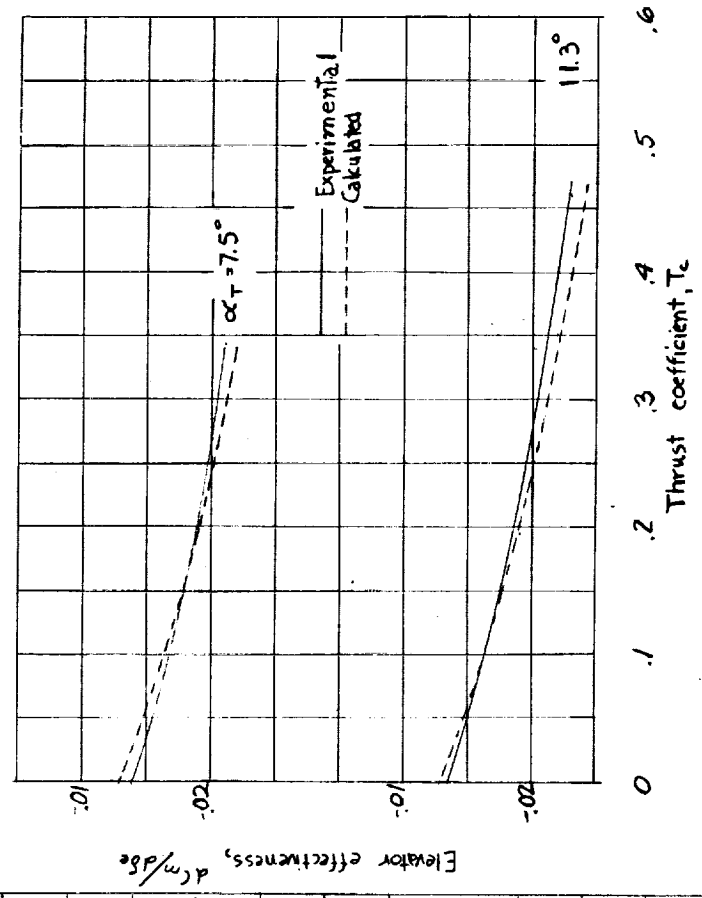
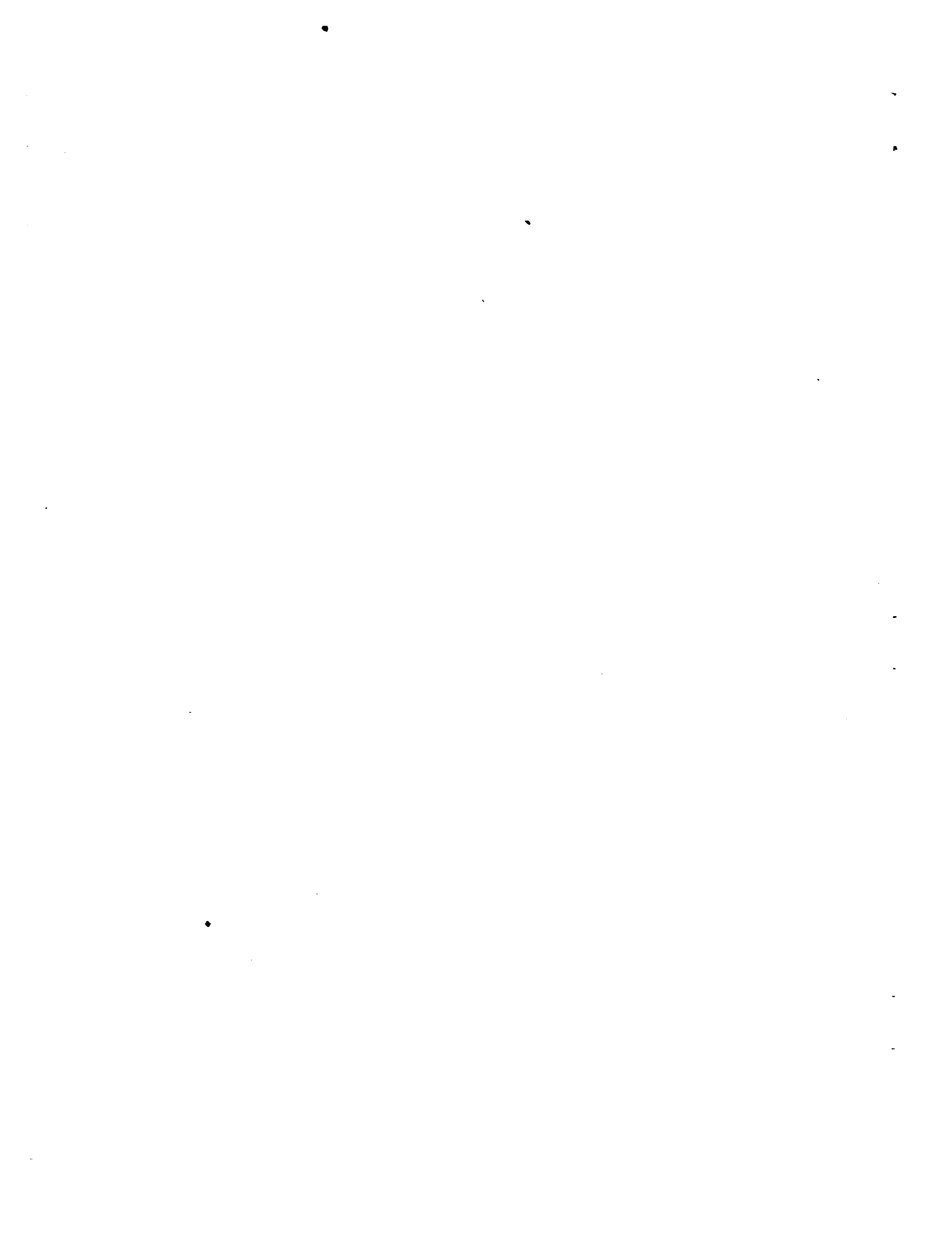


Figure 28.- Experimental and calculated effects of propeller operation on the elevator effectiveness, flaps deflected.



L-411

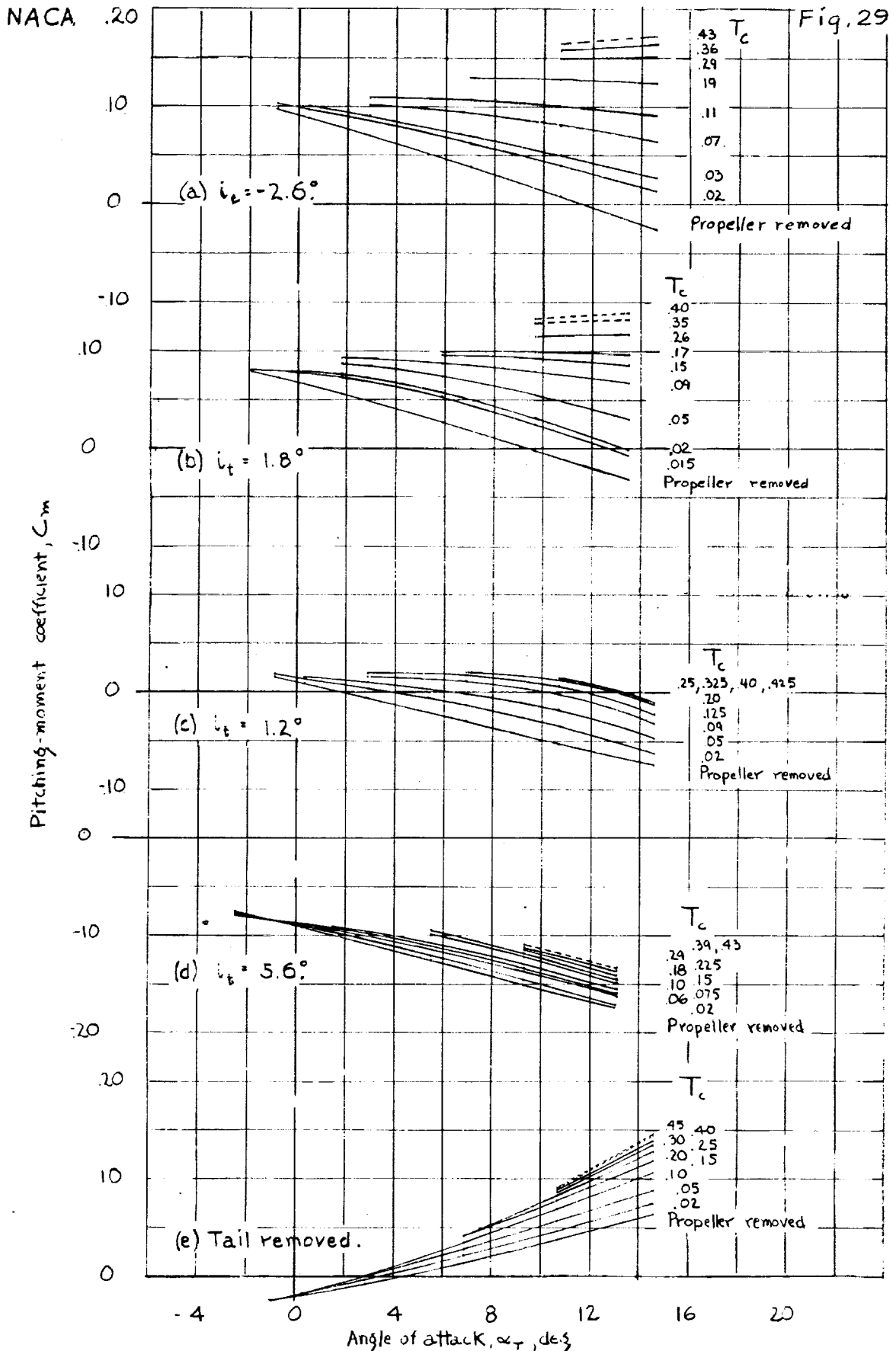
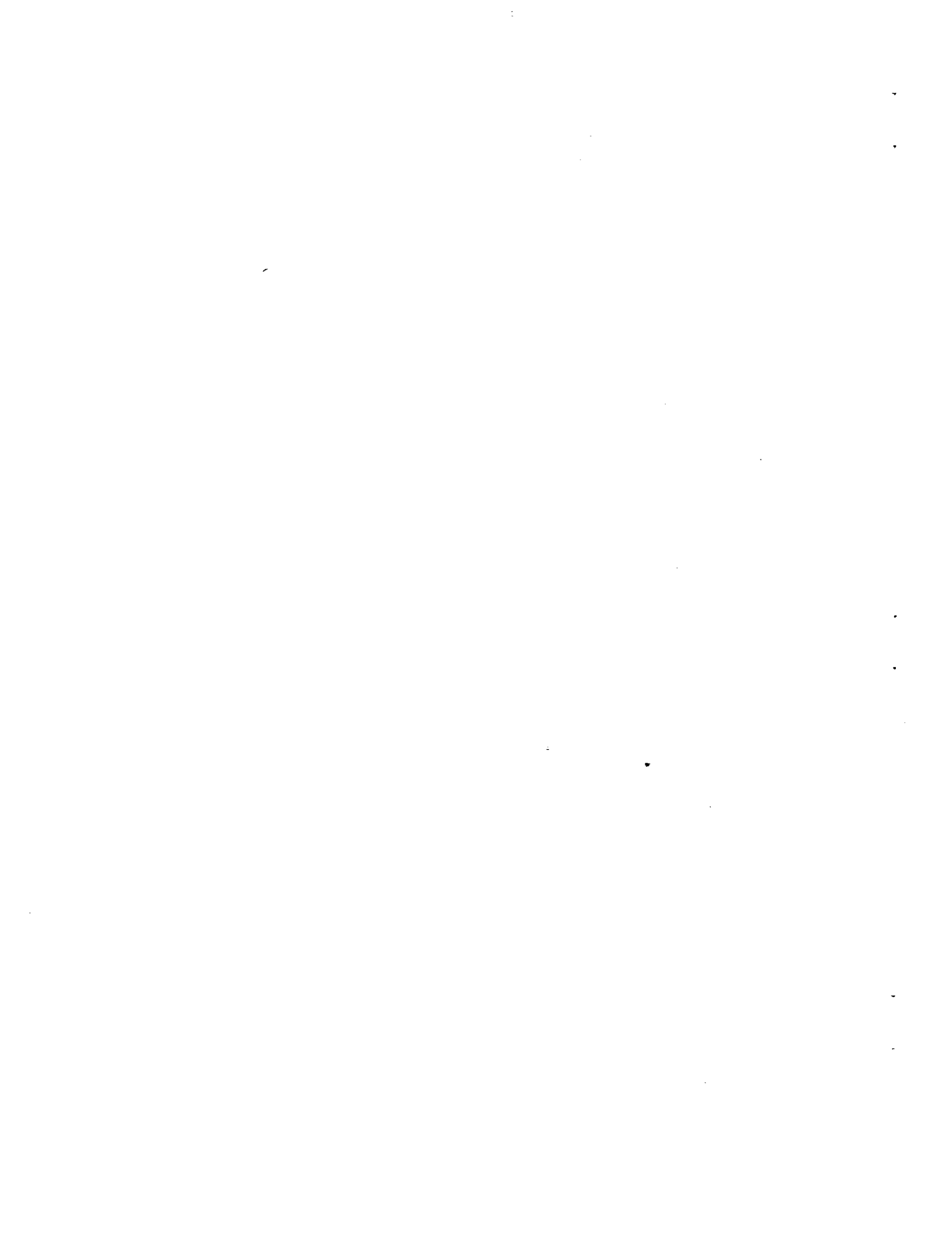


Figure 29. - Variation of pitching-moment coefficient with angle of attack and thrust coefficient for different tail settings; flaps retracted. Dotted curves are from extrapolated values



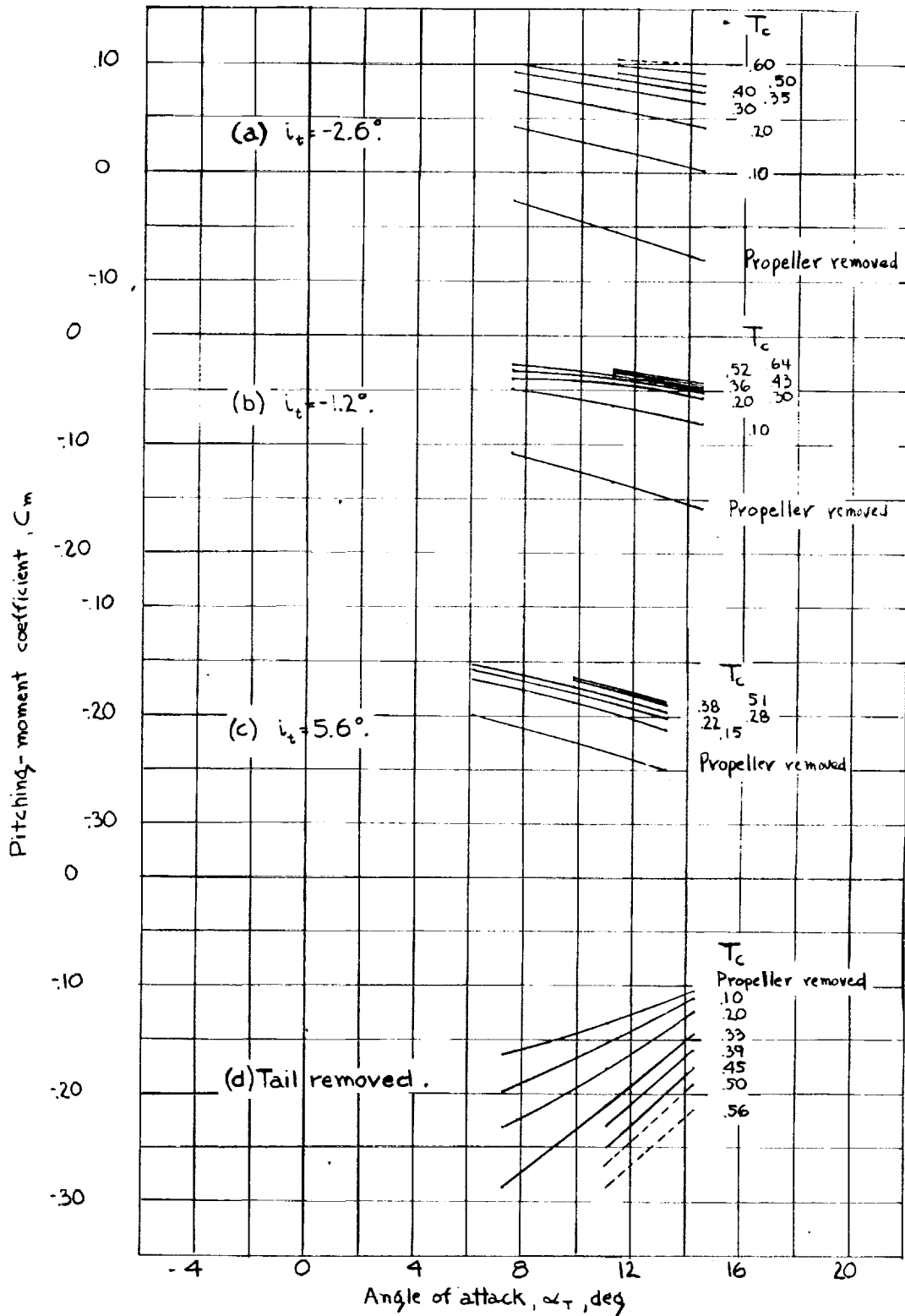
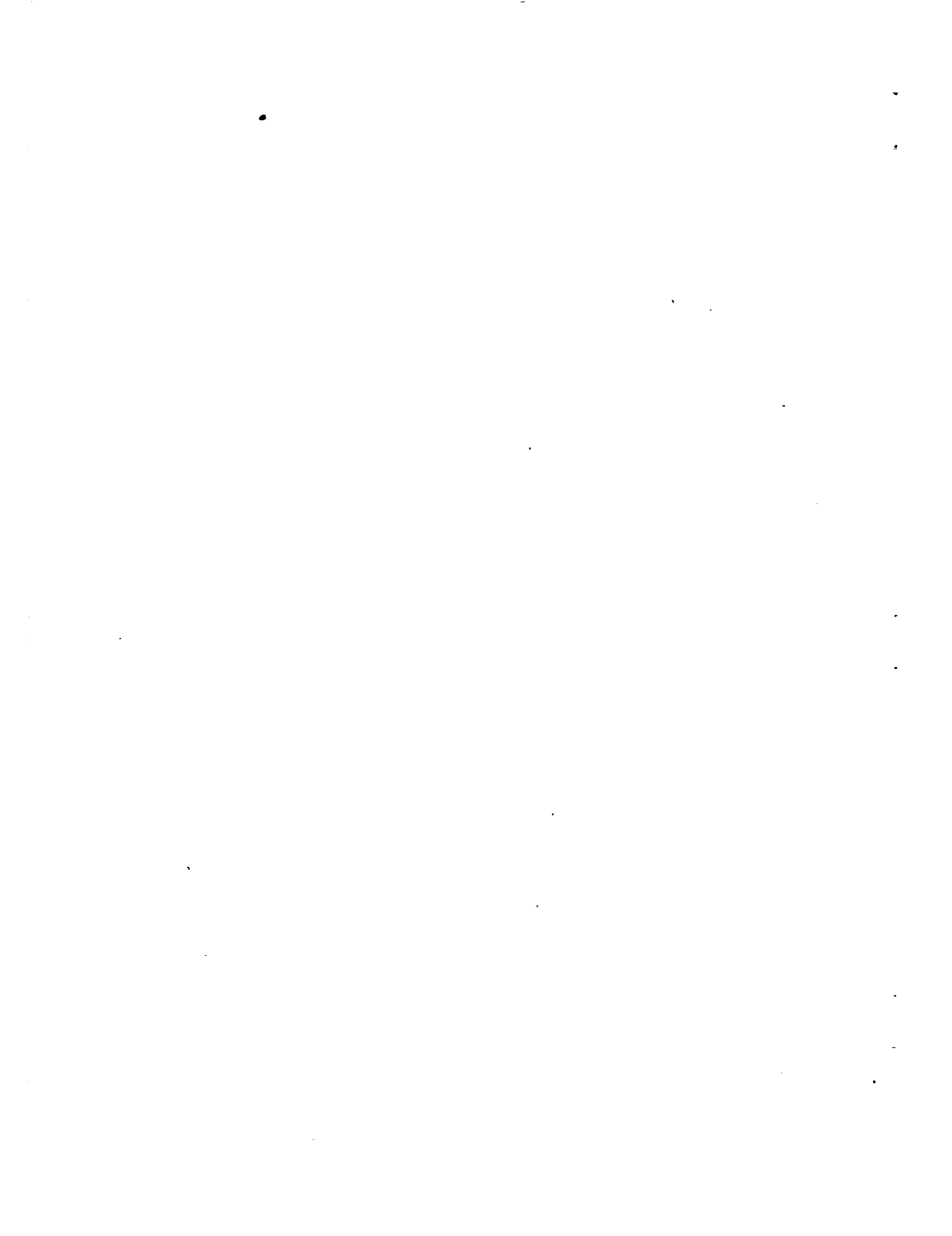


Figure 30. - Variation of pitching-moment coefficient with angle of attack and thrust coefficient for different tail settings, flaps deflected. Dotted curves are from extrapolated values.



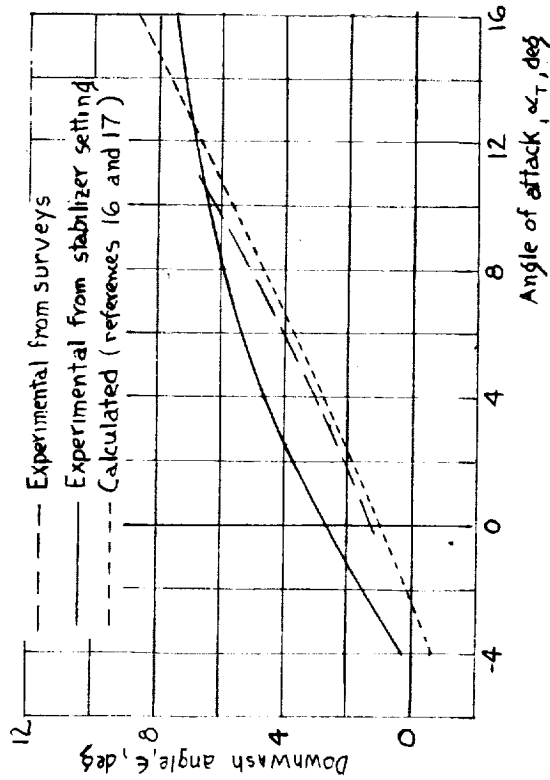


Figure 31. - Comparison of the experimental downwash angles, as obtained from surveys and stabilizer settings, with the calculated values. Propeller removed; flaps retracted.

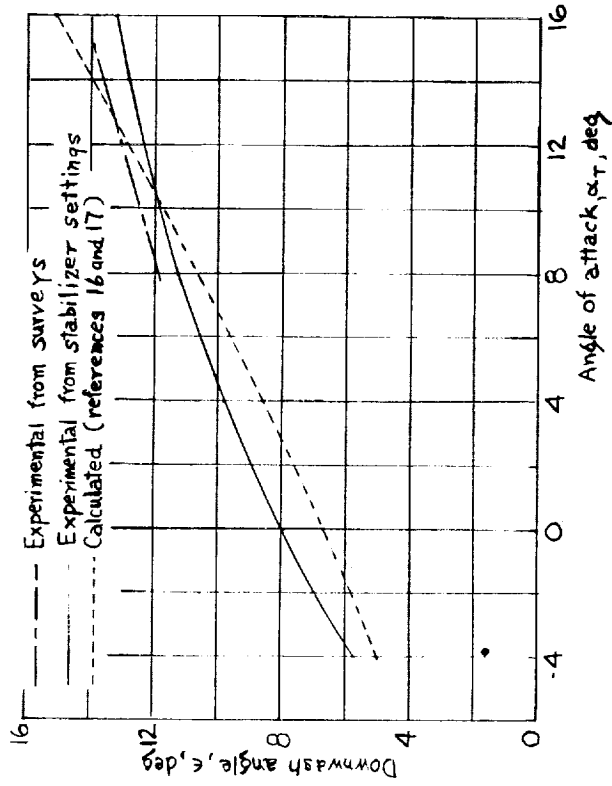
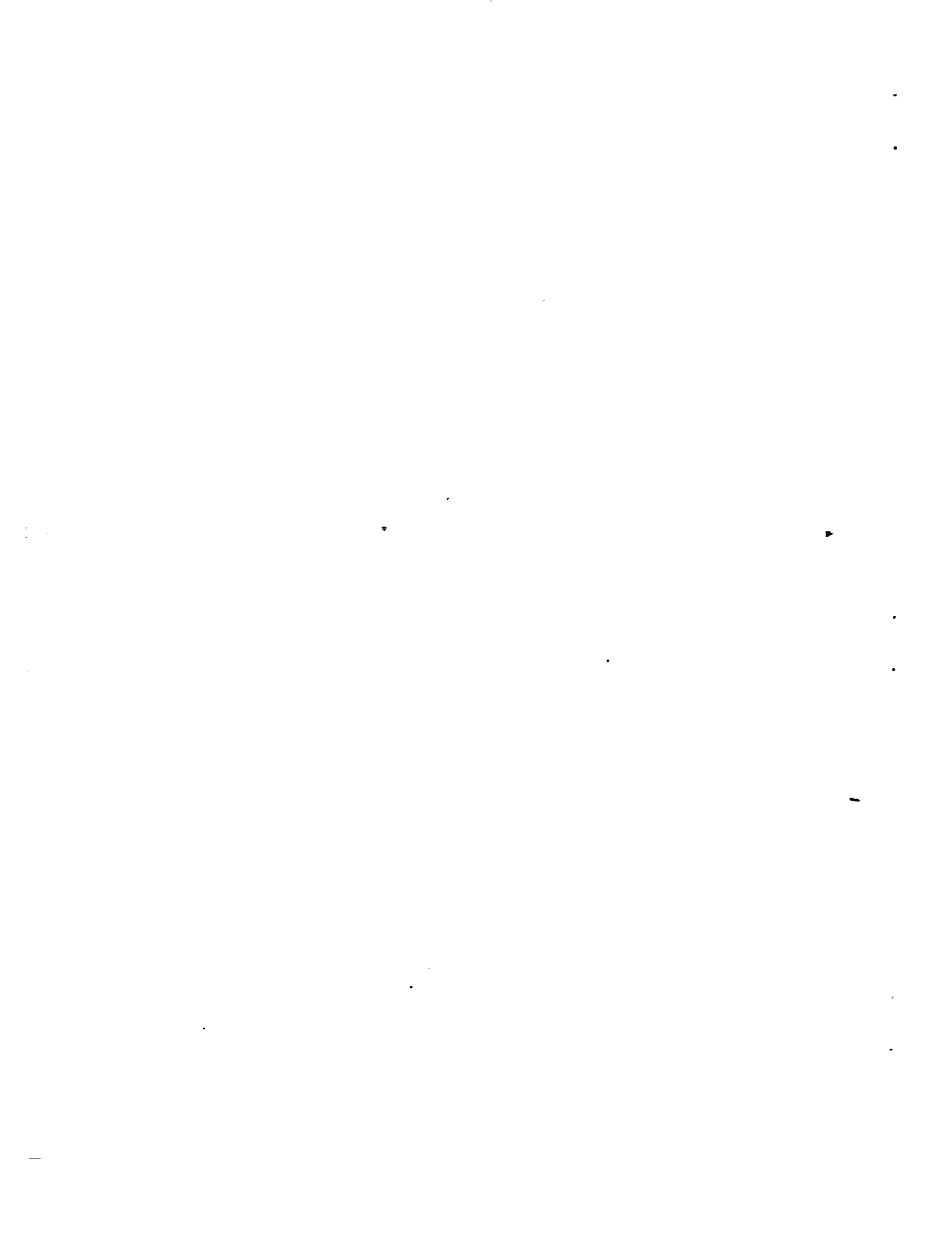


Figure 32. - Comparison of the experimental downwash angles, as obtained from surveys and stabilizer settings, with the calculated values. Propeller removed; flaps deflected.



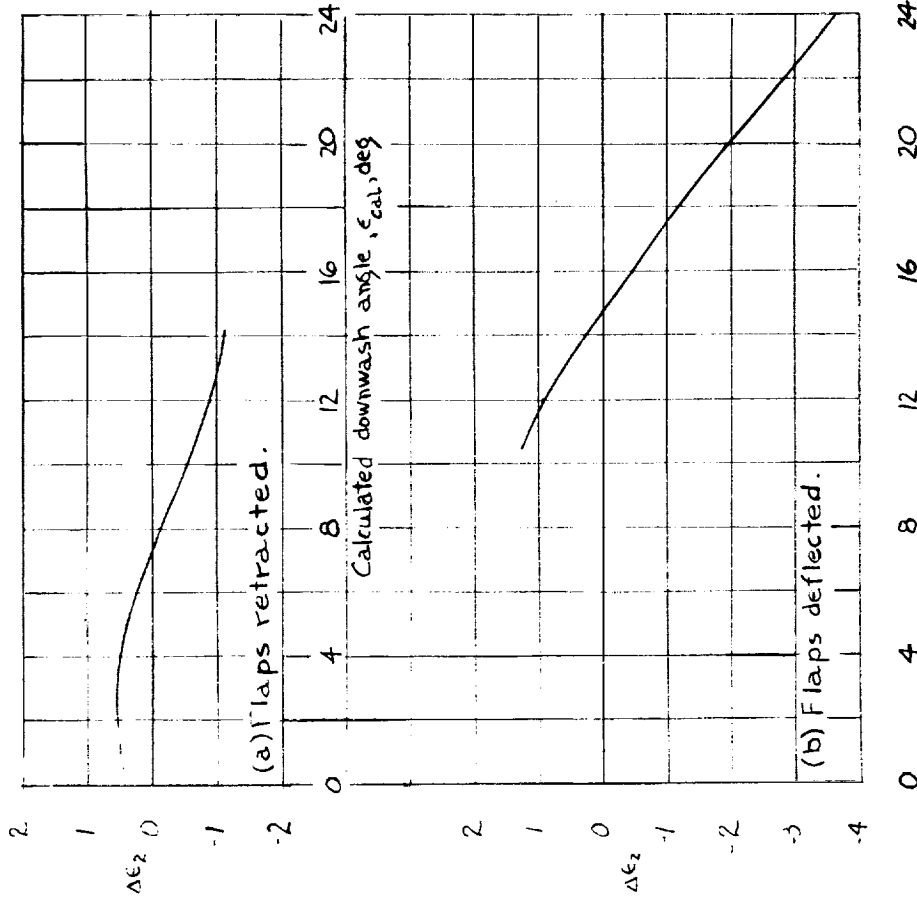


Figure 34. - Average variation of the correction factor $\Delta\epsilon_2$ with ϵ_{cal} for all propeller conditions.

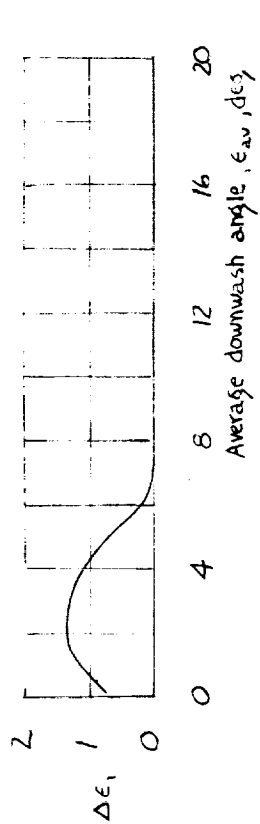


Figure 33. - Average variation of the empirical factor $\Delta\epsilon_1$ with ϵ_{av} for all flap and propeller conditions.



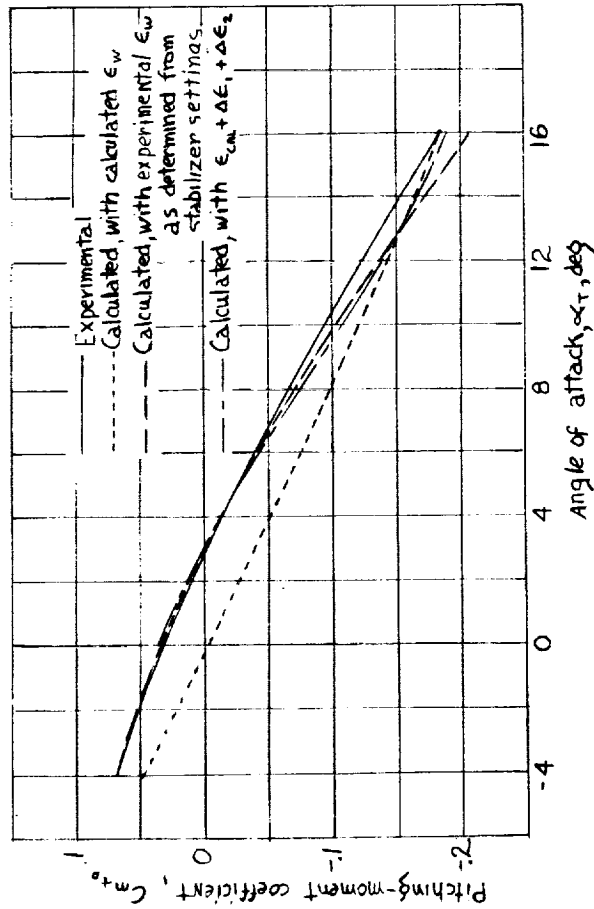


Figure 35. — Comparison of experimental and calculated tail contributions to the pitching moment. Propeller removed; flaps retracted; $\zeta_1 = 1.2^\circ$. Experimental values have been obtained from cross plots.

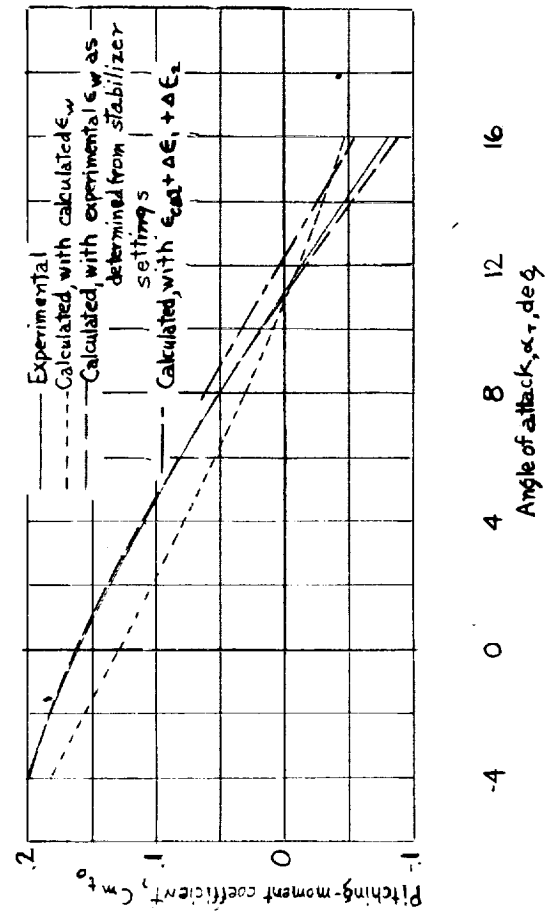
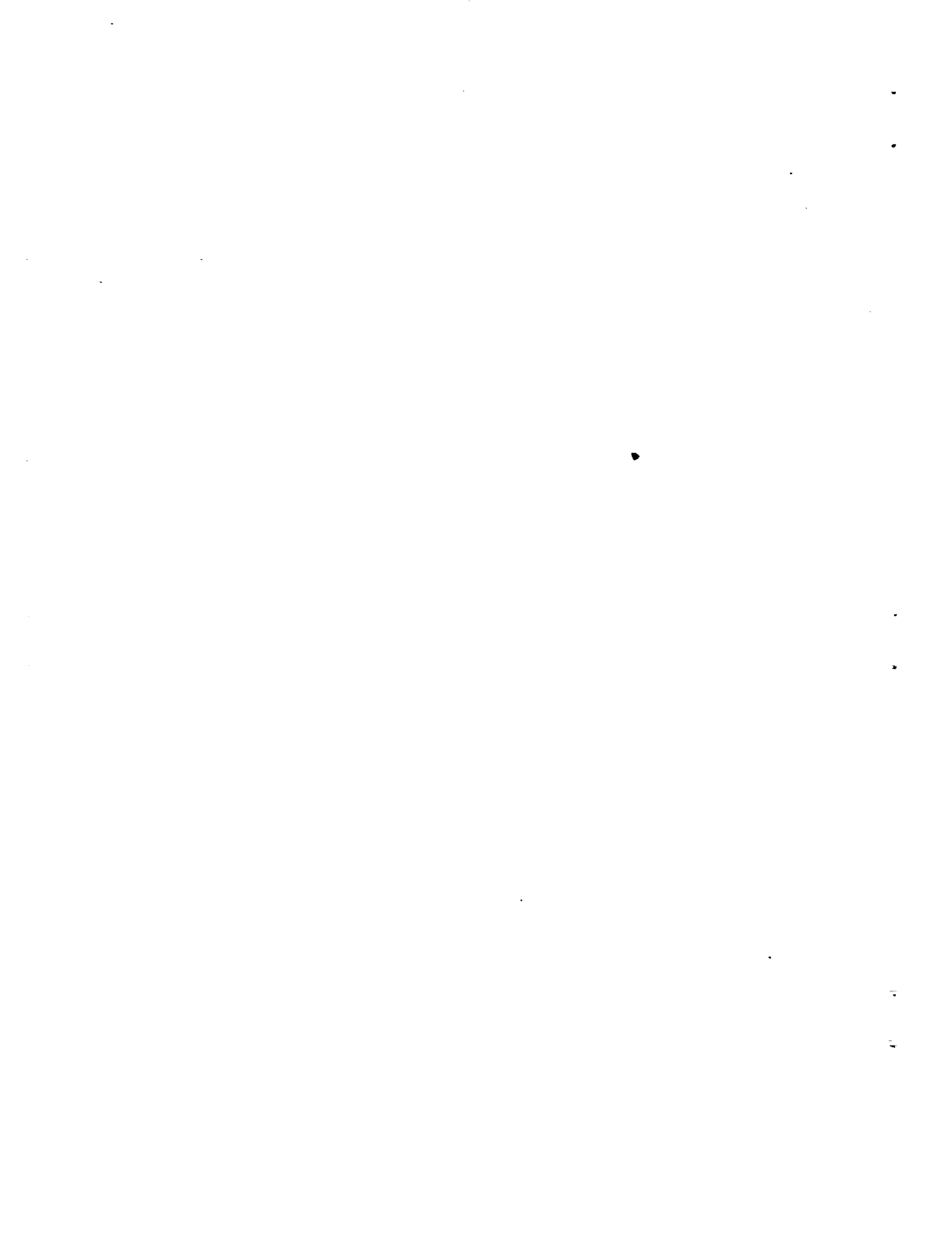


Figure 36. — Comparison of experimental and calculated tail contributions to the pitching moment. Propeller removed; flaps deflected; $\zeta_1 = 1.2^\circ$.



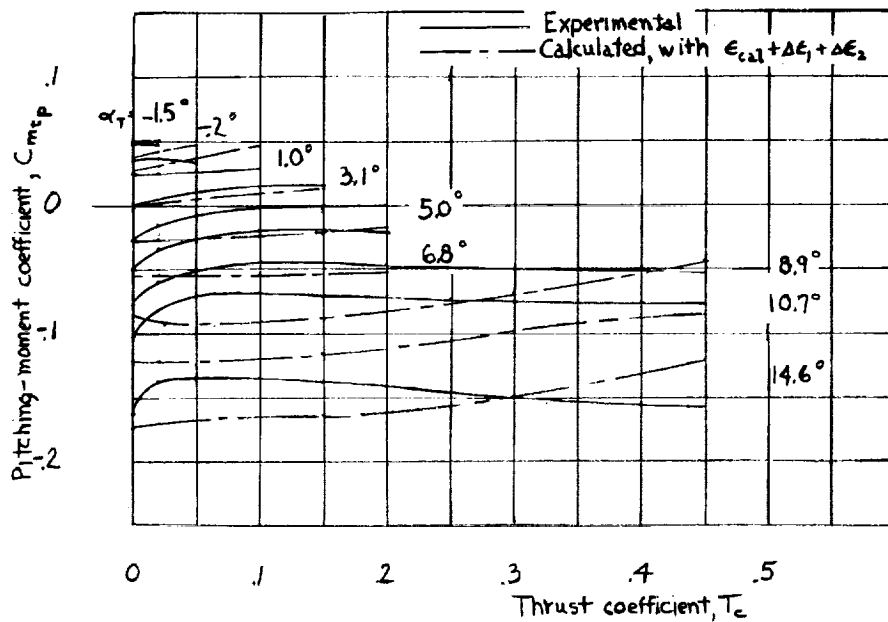


Figure 37 .- Comparison of experimental and calculated tail contributions to the pitching moment. Propeller operating; flaps retracted; $\alpha_f = 1.2^\circ$. Calculated values have been obtained with $\epsilon_{cal} + \Delta\epsilon_1 + \Delta\epsilon_2$.

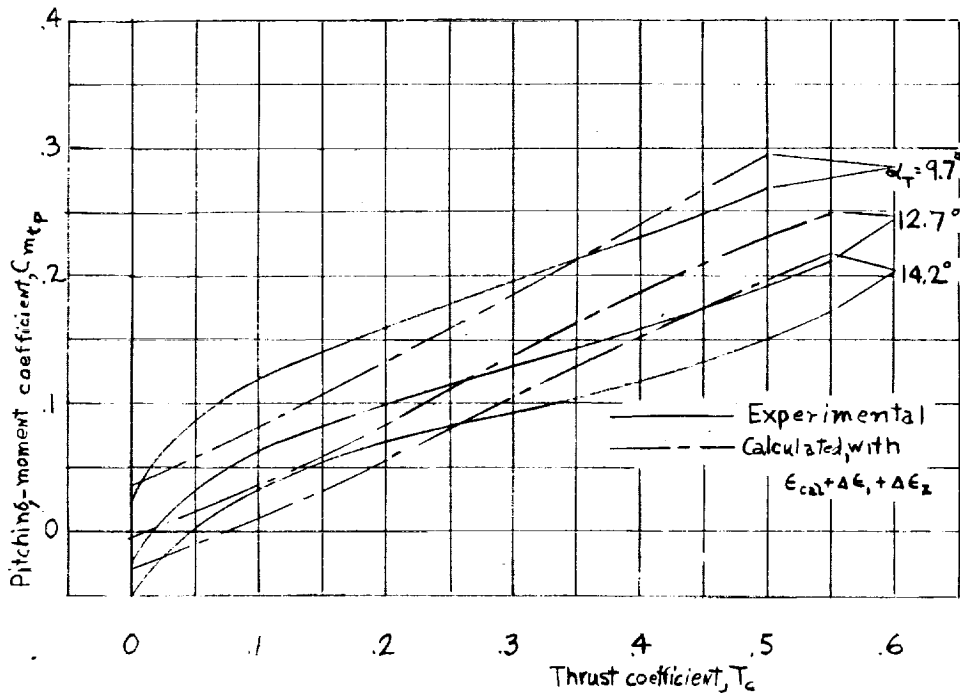
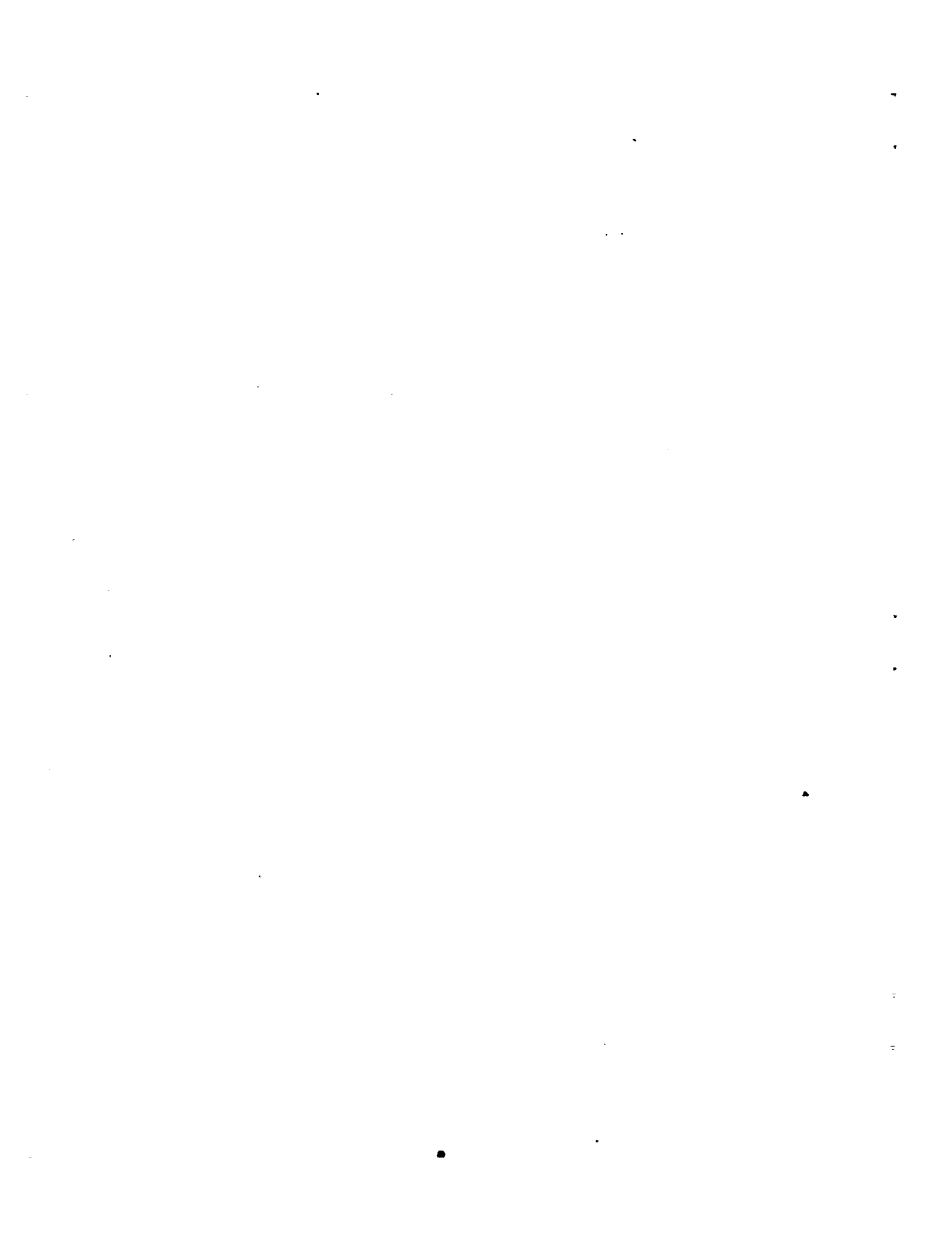


Figure 38 .- Comparison of experimental and calculated tail contributions to the pitching moment. Propeller operating; flaps deflected; $\alpha_f = 1.2^\circ$. Calculated values have been obtained with $\epsilon_{cal} + \Delta\epsilon_1 + \Delta\epsilon_2$.



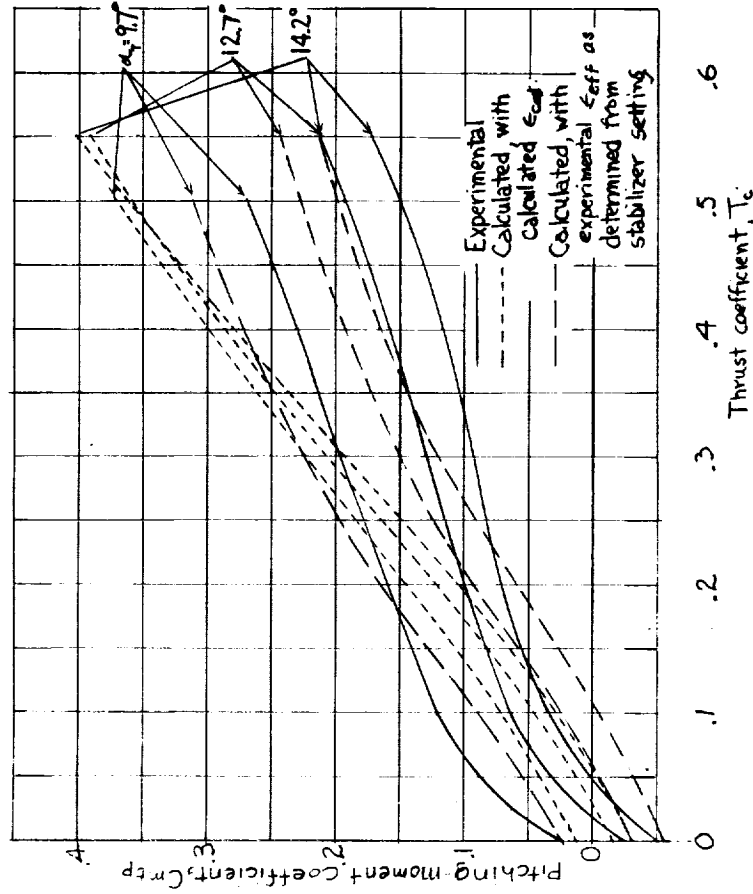


Figure 39.- Comparison of experimental and calculated tail contributions to the pitching moment. Propeller operating; flaps retracted; $i_4 = 1.2^\circ$. Calculated values have been obtained with ϵ_{eff} and ϵ_{cal} .

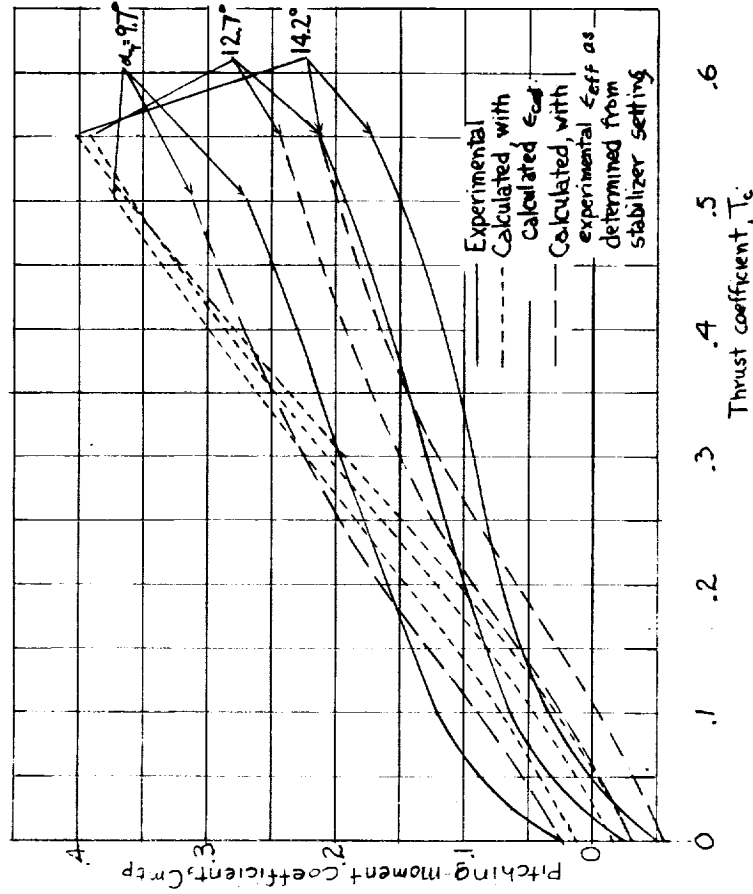
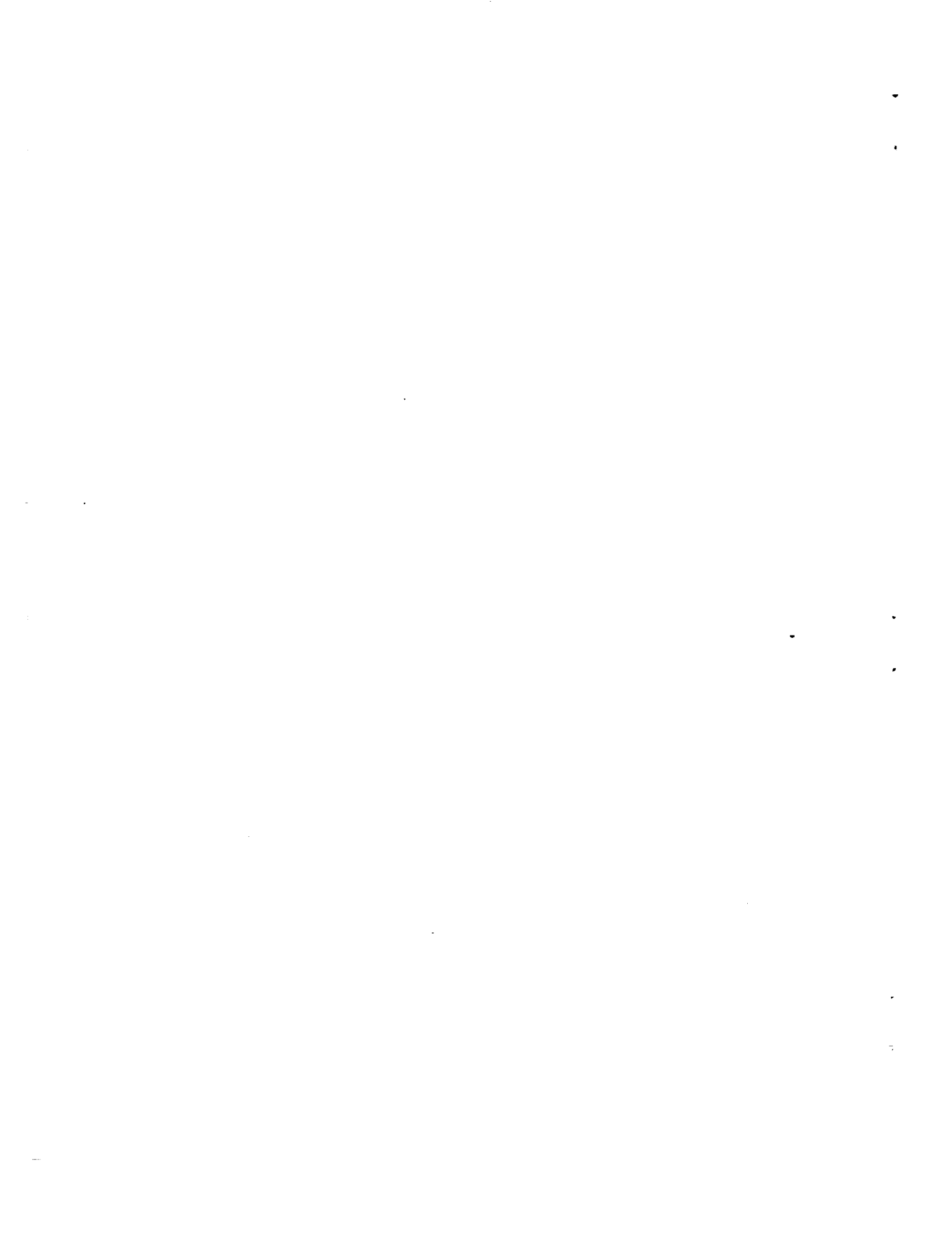


Figure 40.- Comparison of experimental and calculated tail contributions to the pitching moment. Propeller operating; flaps deflected; $i_4 = 1.2^\circ$. Calculated values have been obtained with ϵ_{eff} and ϵ_{cal} .



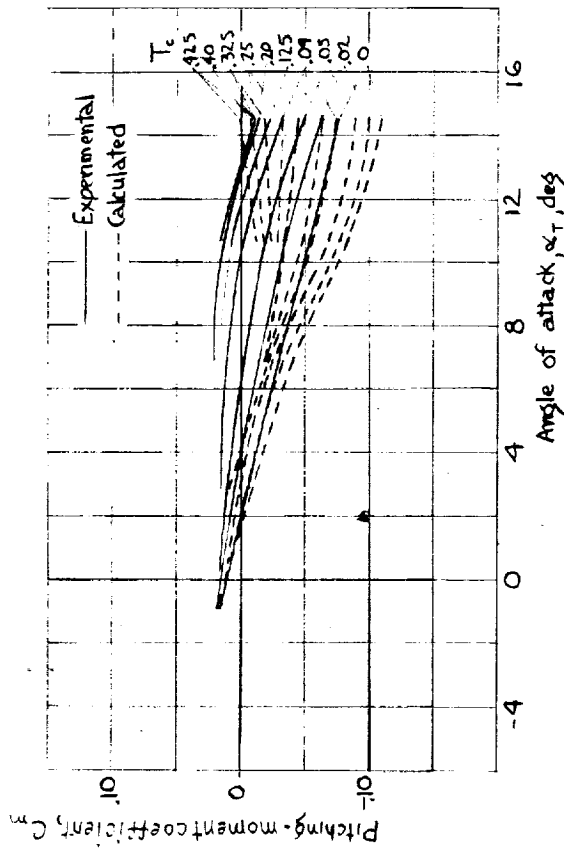


Figure 41. - Experimental and calculated pitching-moment curves for the complete mock-up. Propeller operating; flaps retracted; $i_f = 1.2^\circ$.

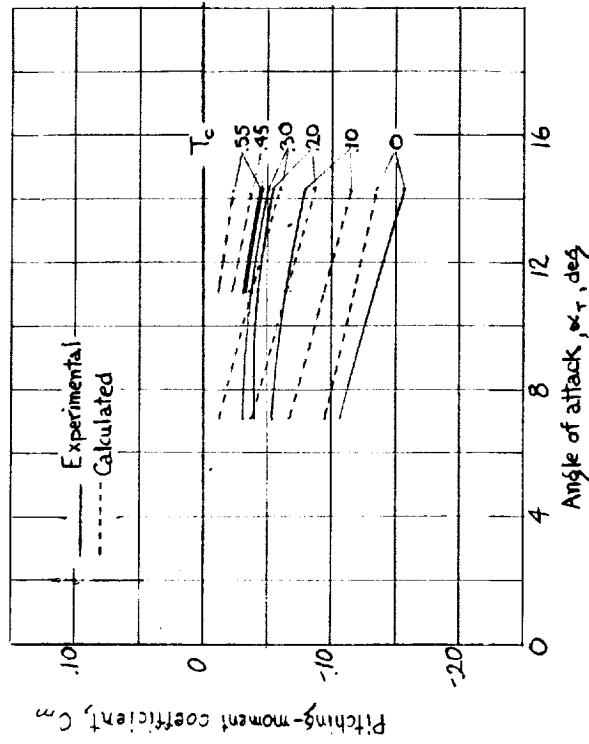
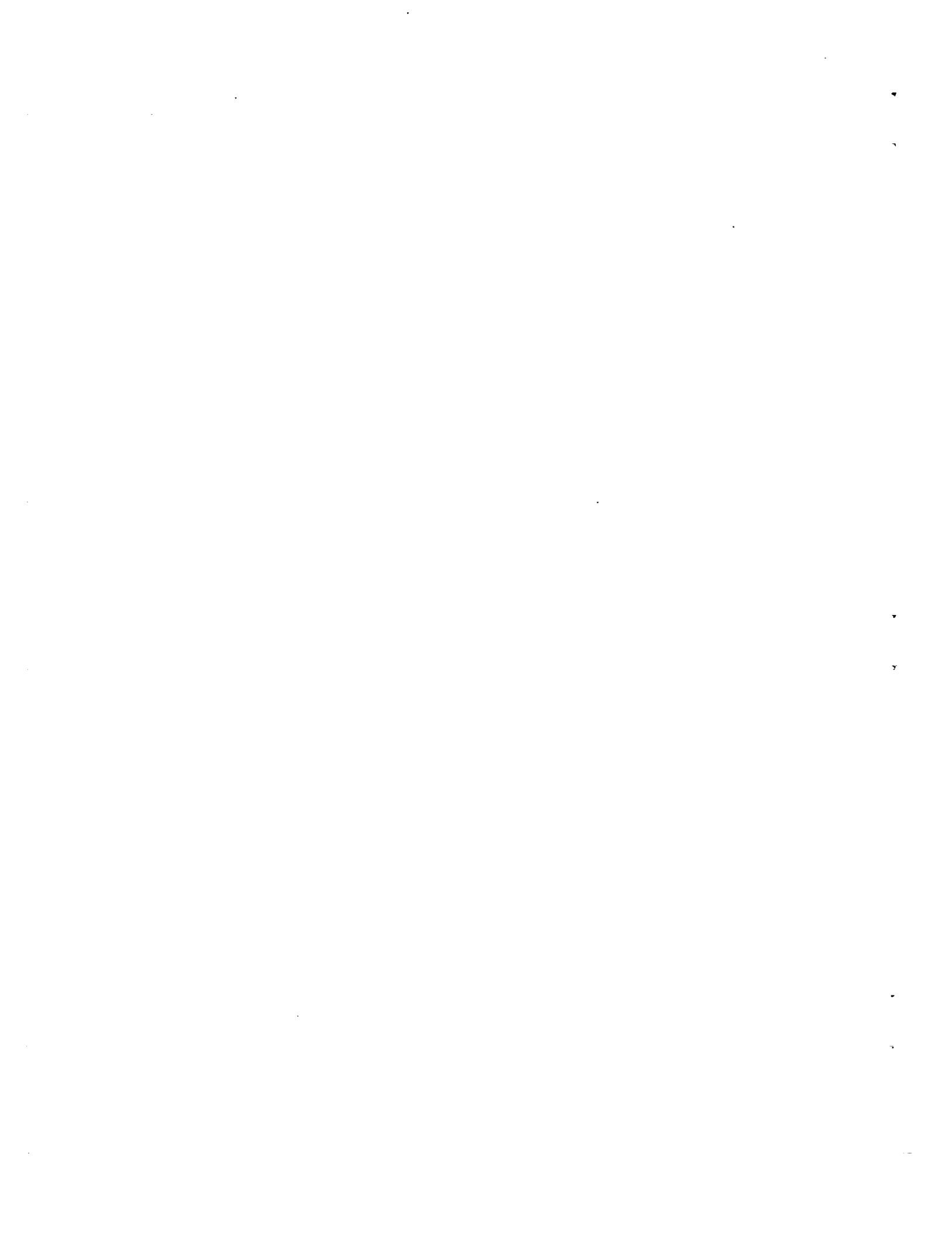


Figure 42. - Experimental and calculated pitching-moment curves for the complete mock-up. Propeller operating; flaps deflected; $i_f = 1.2^\circ$.



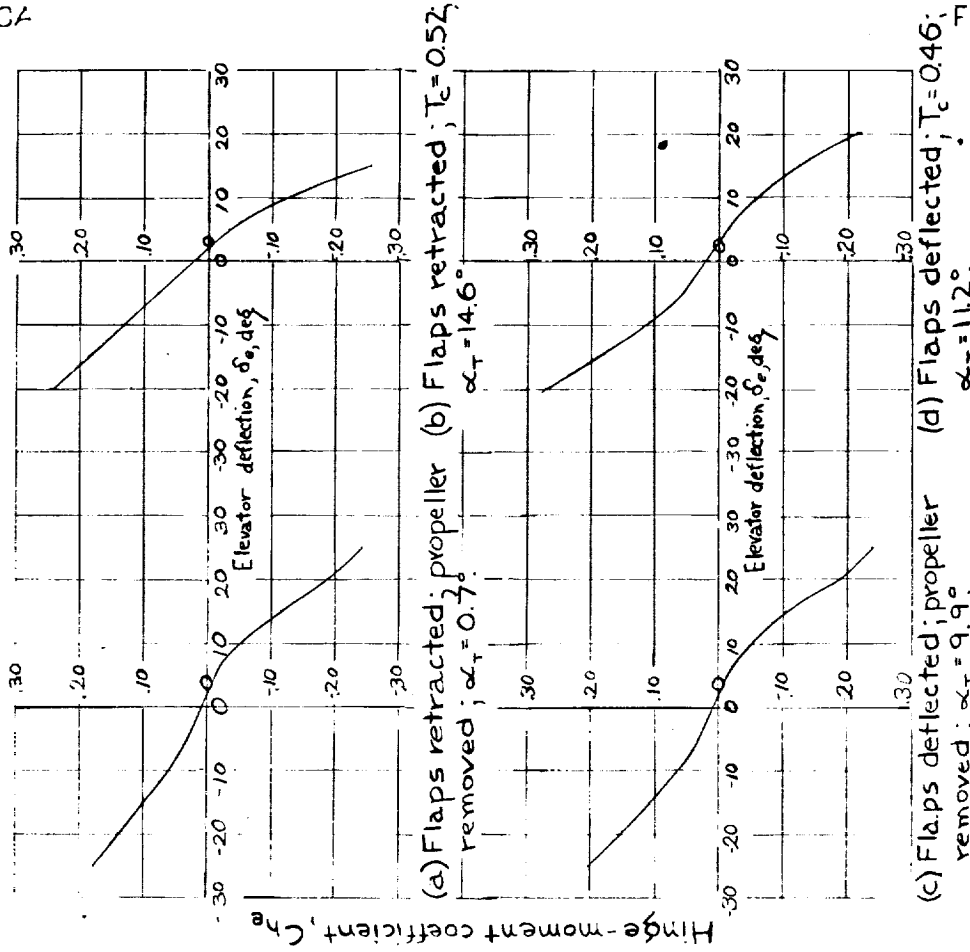


Figure 44. - Typical experimental curves showing variation of hinge-moment coefficient with elevator angle.

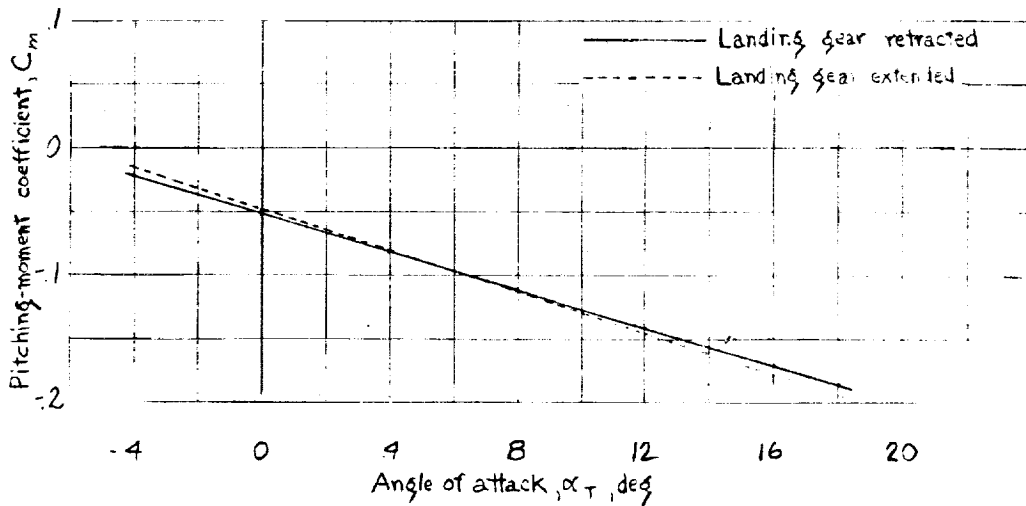
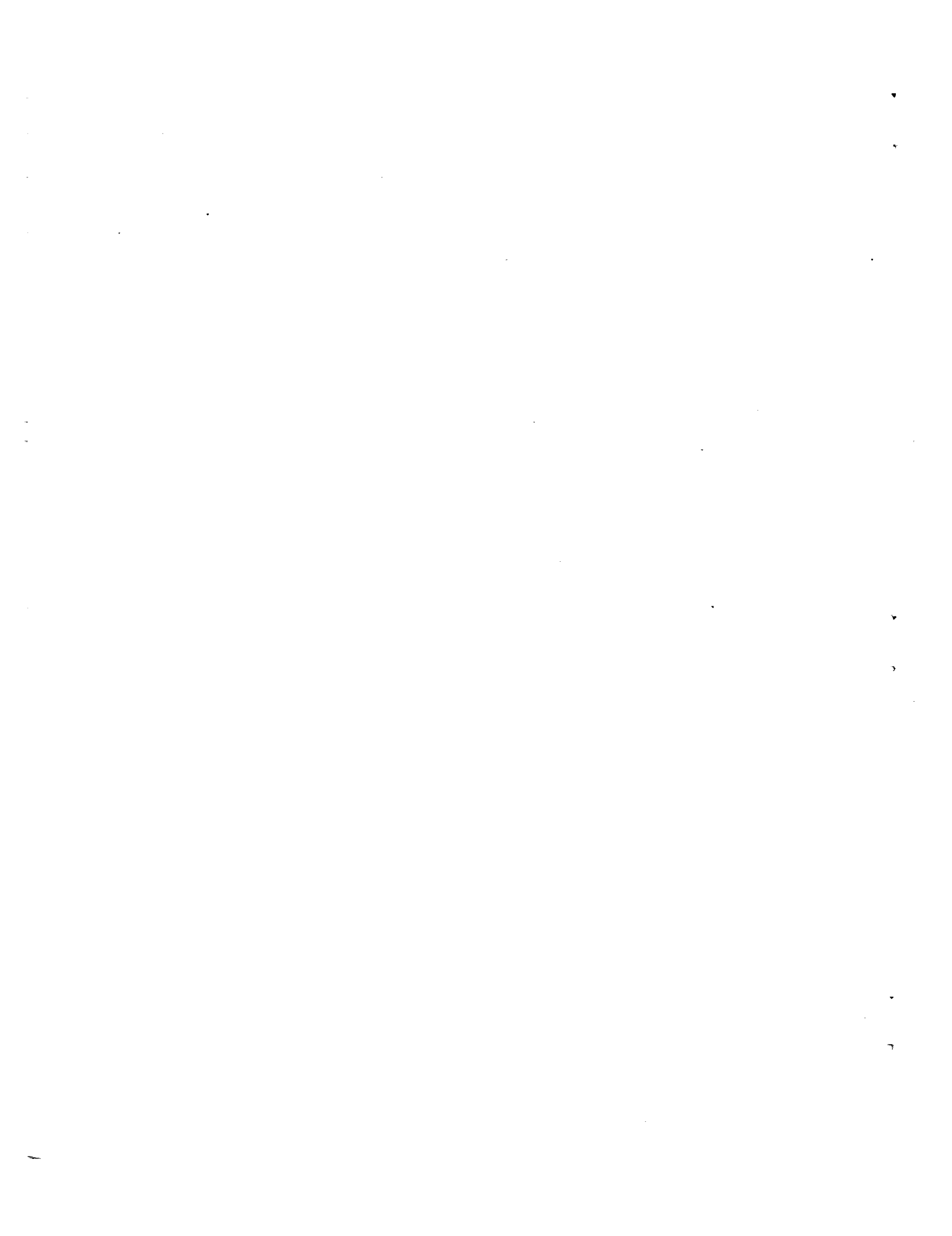


Figure 43. - Effect of landing-gear extension on the pitching moments. Propeller removed; constant center-of-gravity position.



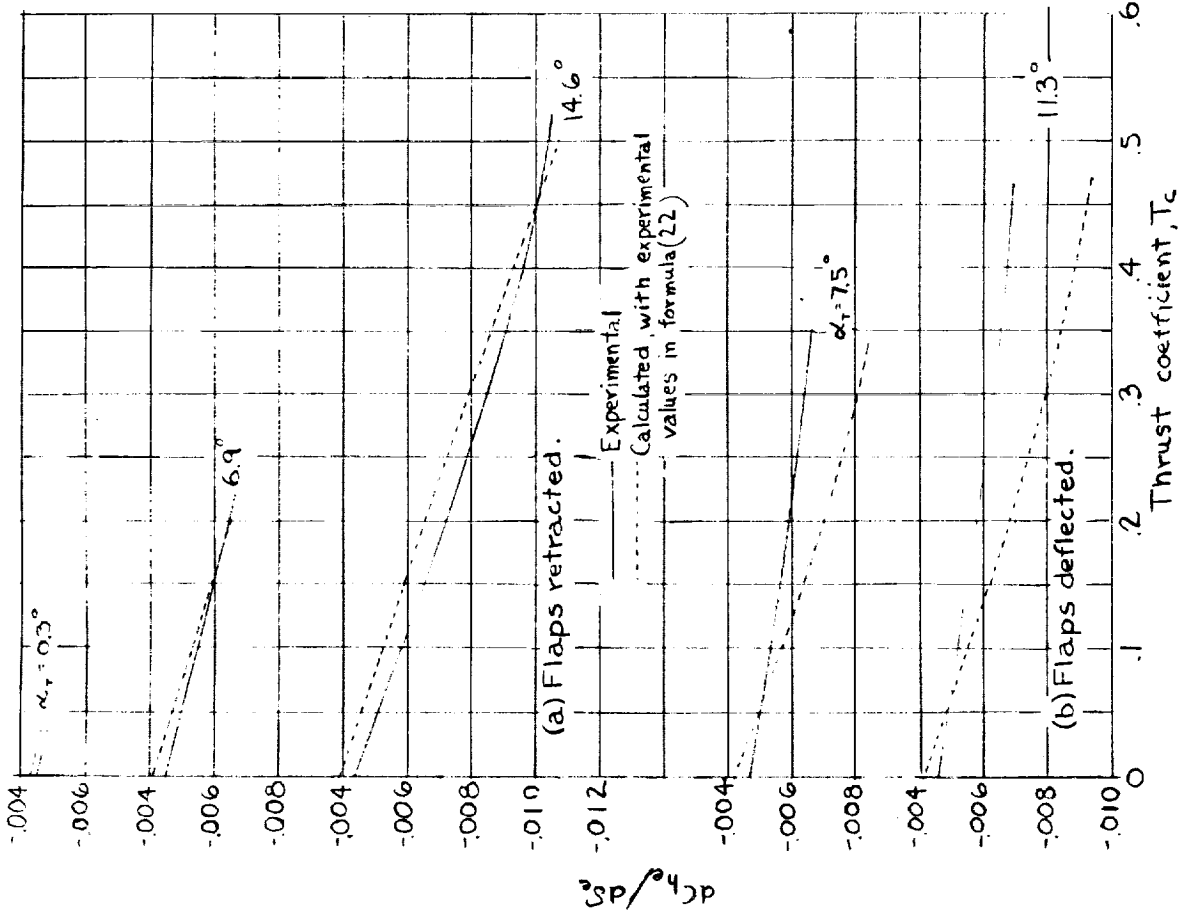


Figure 45 - Experimental and calculated rate of change of hinge-moment coefficient with elevator angle, propeller operating.

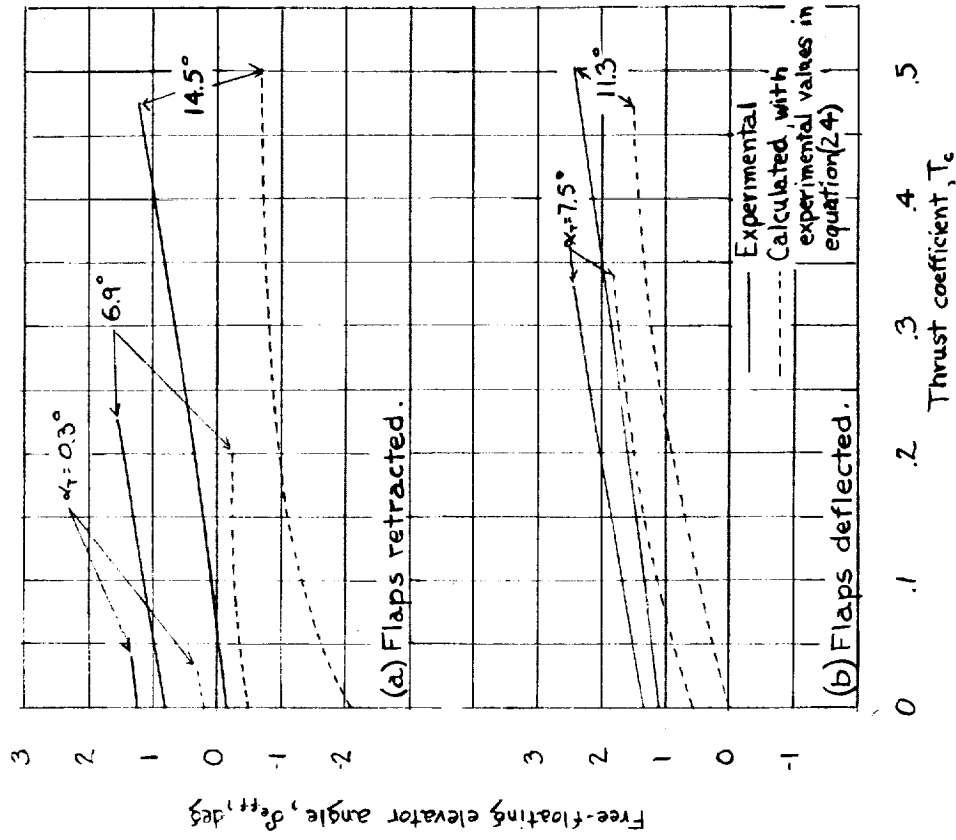


Figure 46 - Experimental and calculated elevator free-floating angles, propeller operating, $\zeta = 1.2$.



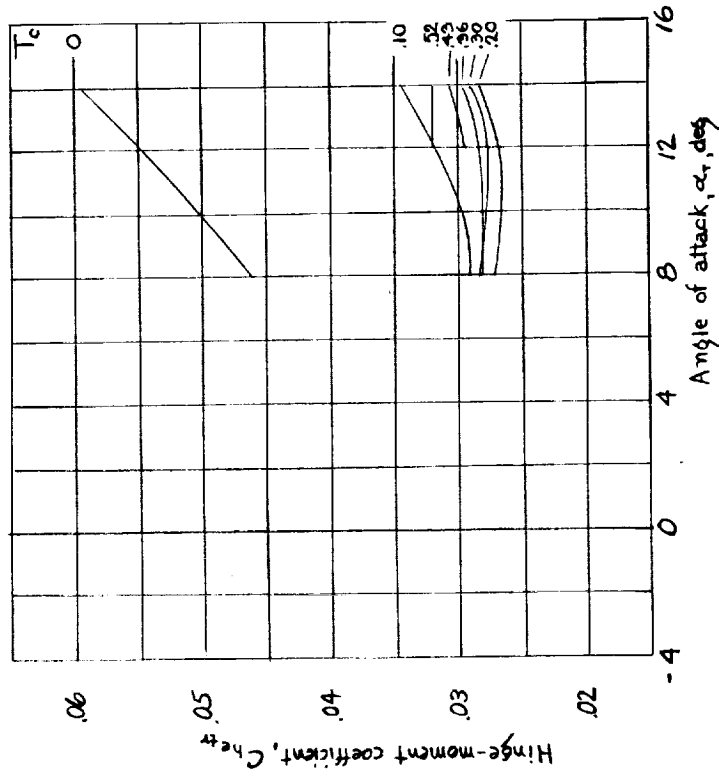


Figure 48. - Experimental variation of the hinge-moment coefficient at trim with angle of attack and thrust coefficient. Flaps deflected; $\alpha_t = 1.2^\circ$.

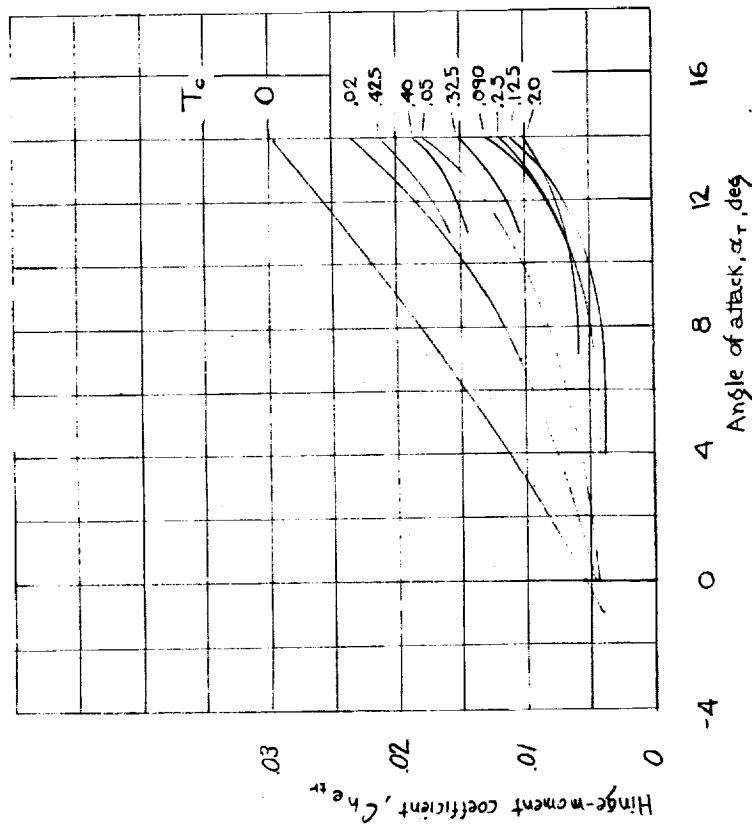


Figure 47. - Experimental variation of the hinge-moment coefficient at trim with angle of attack and thrust coefficient. Flaps retracted; $\alpha_t = 1.2^\circ$.

